INFORMATION TO USERS

This was produced from a copy of a document sent to us for microfilming. While the most advanced technological means to photograph and reproduce this document have been used, the quality is heavily dependent upon the quality of the material submitted.

The following explanation of techniques is provided to help you understand markings or notations which may appear on this reproduction.

1. The sign or "target" for pages apparently lacking from the document photographed is "Missing Page(s)". If it was possible to obtain the missing page(s) or section, they are spliced into the film along with adjacent pages. This may have necessitated cutting through an image and duplicating adjacent pages to assure you of complete continuity.

2. When an image on the film is obliterated with a round black mark it is an indication that the film inspector noticed either blurred copy because of movement during exposure, or duplicate copy. Unless we meant to delete copyrighted materials that should not have been filmed, you will find a good image of the page in the adjacent frame.

3. When a map, drawing or chart, etc., is part of the material being photographed the photographer has followed a definite method in "sectioning" the material. It is customary to begin filming at the upper left hand corner of a large sheet and to continue from left to right in equal sections with small overlaps. If necessary, sectioning is continued again—beginning below the first row and continuing on until complete.

4. For any illustrations that cannot be reproduced satisfactorily by xerography, photographic prints can be purchased at additional cost and tipped into your xerographic copy. Requests can be made to our Dissertations Customer Services Department.

5. Some pages in any document may have indistinct print. In all cases we have filmed the best available copy.

University
Microfilms
International

300 N. ZEEB ROAD, ANN ARBOR, MI 48106
18 BEDFORD ROW, LONDON WC1R 4EJ, ENGLAND

CALHOUN, PHILIP RAY

GEOMETRICALLY NONLINEAR FINITE-ELEMENT ANALYSIS OF CIRCULAR AND ARBITRARY ARCHES

The University of Arizona PH.D. 1980

GEOMETRICALLY NONLINEAR FINITE ELEMENT ANALYSIS OF CIRCULAR AND ARBITRARY ARCHES

by

Philip Ray Calhoun

A Dissertation Submitted to the Faculty of the

DEPARTMENT OF AEROSPACE AND MECHANICAL ENGINEERING

In Partial Fulfillment of the Requirements
For the Degree of

DOCTOR OF PHILOSOPHY
WITH A MAJOR IN MECHANICAL ENGINEERING

In The Graduate College

THE UNIVERSITY OF ARIZONA

1 9 8 0

THE UNIVERSITY OF ARIZONA
GRADUATE COLLEGE

As members of the Final Examination Committee, we certify that we have read the dissertation prepared by Philip Ray Calhoun

entitled Geometrically Nonlinear Finite Element Analysis of Circular and Arbitrary Arches

and recommend that it be accepted as fulfilling the dissertation requirement for the Degree of Doctor of Philosophy.

Donald A. DaDeppo	10-6-80 Date
Ralph M. Pickard	10-6-80 Date
Hans A. Ward	10/6/80 Date
	Date
	Date

Final approval and acceptance of this dissertation is contingent upon the candidate's submission of the final copy of the dissertation to the Graduate College.

I hereby certify that I have read this dissertation prepared under my direction and recommend that it be accepted as fulfilling the dissertation requirement.

Donald A DeDeppo	Oct 6, 1980
Dissertation Director	Date

STATEMENT BY AUTHOR

This dissertation has been submitted in partial fulfillment of requirements for an advanced degree at The University of Arizona and is deposited in the University Library to be made available to borrowers under rules of the Library.

Brief quotations from this dissertation are allowable without special permission, provided that accurate acknowledgment of source is made. Requests for permission for extended quotation from or reproduction of this manuscript in whole or in part may be granted by the head of the major department or the Dean of the Graduate College when in his judgment the proposed use of the material is in the interests of scholarship. In all other instances, however, permission must be obtained from the author.

SIGNED: Philip Ray Calhoun

ACKNOWLEDGMENTS

I wish to express my sincere appreciation to Dr. Donald DaDeppo of the Department of Civil Engineering for his guidance and encouragement which has led to the completion of this project. It was his interest and knowledge of continuum mechanics that has given me the motivation to pursue this field of study.

I also wish to express my gratitude to Dr. H. A. Kamel who was instrumental in my pursuing the field of finite element analysis. I also wish to express my appreciation to Dr. R. A. Richard for his advice and assistance throughout my course of study.

This work would not have been possible without the love and faith of the author's parents, Edna and Ramon. And finally, I wish to express my deepest appreciation to my wife, Georgia, who has shown extreme patience, kindness, and understanding during the past five years, and to our son, Christopher, who has given me the internal strength to finish this project.

TABLE OF CONTENTS

TABLE OF CONTENTS, Continued.

TABLE OF CONTENTS, Continued.

LIST OF ILLUSTRATIONS

LIST OF ILLUSTRATIONS, Continued.

LIST OF ILLUSTRATIONS, Continued.

LIST OF TABLES

ABSTRACT

A curved nonlinear finite element is developed in this work to observe the behavior of slender arches which undergo large deformations. The derivation of the strain equation is based upon the assumption that cross sections of the undeformed state remain undeformed and plane, but not necessarily normal to the centroidal axis during deformation. It is also assumed that the strain will be small and the rotations will be finite. The in-plane bending and the buckling modes for arches with fixed end and hinged end supports are analyzed. Deep circular arches and deep arches with arbitrary geometry of the centroidal axis are studied. Vertical concentrated loads, uniformly distributed loads, a combination of concentrated and distributed loads, and nonsymmetrical loads are considered. The governing differential equations are differentiated with respect to time to give a system of rate equations. Using these equations, the original nonlinear differential equations are solved using the Runge-Kutta scheme with Simpson's coefficients. If the solution drifts, a Newton-Raphson iteration scheme is used to return the solution to the equilibrium path.

CHAPTER 1

INTRODUCTION

Until the past two decades design and structural analysis of curved members were based primarily on classical linear elastic theory which assumed deformations and rotations to be small. Such analysis caused little difficulty and gave accurate results for almost all structures considered. However, with recent advancements in technology new materials have been developed which have led to the manufacturing of lighter and thinner structures. The analysis of such structures creates a need to represent complex behavior more accurately. Since the structures can undergo large deformations, deflection theories must be used and must make reference to the deformed geometry of the structure. When the use of deflection theories becomes necessary and large deformations are considered, the governing differential equations are nonlinear. Because of the nonlinear nature of these problems, it is very difficult to obtain an analytical solution; therefore, it becomes necessary to solve them numerically. With the recent advancements in computer technology, solutions to nonlinear problems have become more prevalent. Development of new computer hardware has offered faster systems with

greater computational and storage capabilities. Development of new computer software has offered more accurate and less computationally expensive algorithms.

The analysis of light and thin structures which undergo large deflections within the elastic range are considered to be geometrically nonlinear problems. Structural stability analysis deals with finding the point on the equilibrium path where instability occurs. The load level at which this occurs is the buckling load or the critical load. There are two types of buckling: (1) snap-through buckling in which the buckling mode is symmetric, (2) bifurcation buckling or sidesway buckling in which the buckling mode is antisymmetric. Snap-through buckling occurs when the load on the equilibrium path reaches a maximum; this maximum point is called the limit point. Figure 1.1 shows a typical load-deflection curve and the location of the limit point. Bifurcation buckling occurs when the primary equilibrium path intersects the secondary equilibrium path. The point of intersection between the two equilibrium paths is called the bifurcation point. A load-deflection curve representing bifurcation buckling is shown in Fig. 1.2.

In structural stability analysis the buckling load occurs at the instant when the stiffness of the structure goes to zero or from positive to negative. The calculation

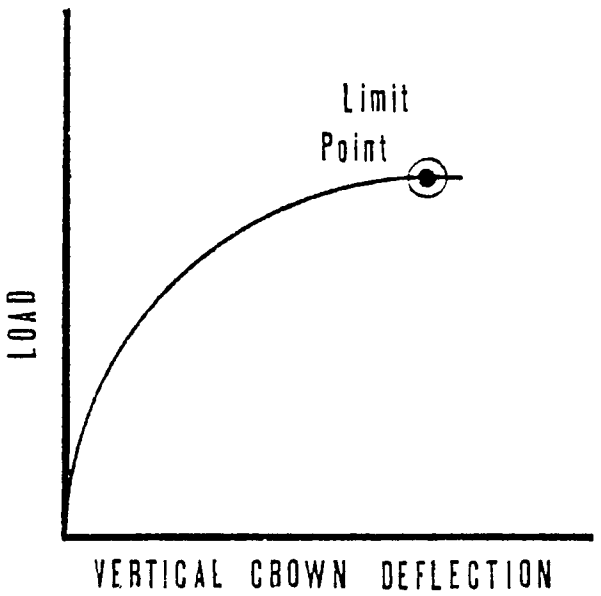

Fig. 1.1. Load-deflection curve showing limit point.

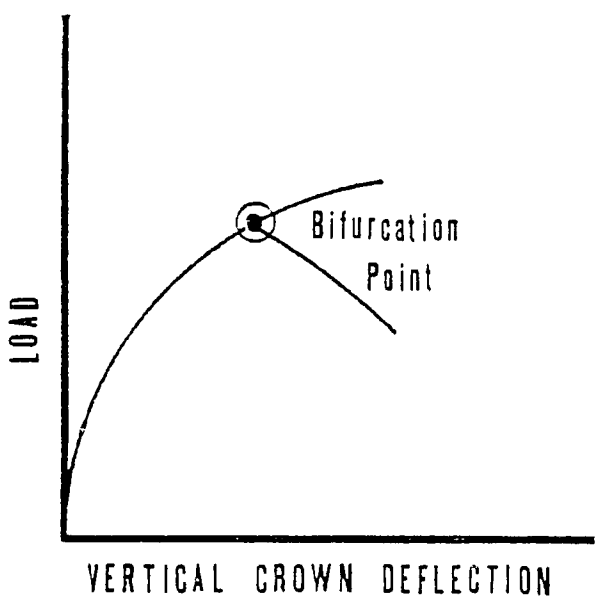

Fig. 1.2. Load-deflection curve showing bifurcation point.

of this point can be accomplished by plotting the determinant of the structural stiffness versus its deflection and the load-deflection curve on the same graph. The point at which the determinant intersects the horizontal axis is the deflection at which buckling occurs. The procedure for calculating the buckling load is shown in Fig. 1.3.

A powerful means by which to solve geometrically nonlinear problems is the finite element method, for it can geometrically represent almost any complex structure and its boundaries. The accuracy and the computational expense of the solution for nonlinear problems using the finite element method depends upon the interaction of the following factors: (1) the simplifying assumptions made in deriving the governing nonlinear differential equations, (2) the choice of which terms, if any, to neglect in the strain equation, (3) the choice of the assumed displacement field, (4) the method by which to represent the structure's geometry, i.e., exact equation, approximate equation based on a curve fitting scheme, or a mapping procedure, and (5) the solution scheme to be used in solving the nonlinear system of equations.

Purpose and Scope

It is the purpose of this study to develop a curved nonlinear finite element based upon the Winkler-Bach hypothesis with no restrictions placed on the magnitudes of the

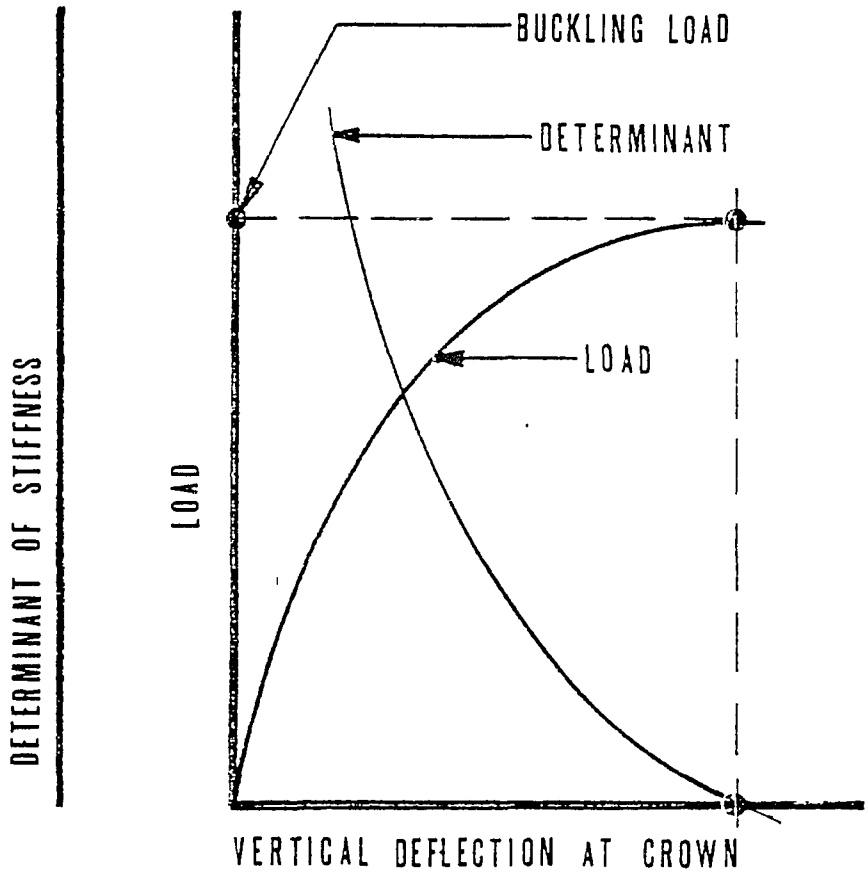

Fig. 1.3. Calculation of buckling load.

deformations. The strain equation is formulated on the basis of the reasonable assumption of small strain and finite rotations. All terms of the derived strain equation are retained. The curved nonlinear finite element is used to analyze in-plane bending and the buckling behavior of deep circular arches and deep arches in which the centroidal axis is of arbitrary geometry. Various loading conditions are considered. The solution scheme for solving the nonlinear system of equations is a Runge-Kutta scheme with Simpson's coefficients, and, if necessary, a Newton-Raphson iteration scheme is used to return to the equilibrium path.

CHAPTER 2

REVIEW OF LITERATURE

The purpose of this chapter is to discuss the state-of-the-art for the stability of slender arches which undergo large deflections and the state-of-the-art for finite element analysis of geometrically nonlinear problems.

The nonlinear theory of curved members was introduced by Euler (35). His work encompassed slender arches which neglected the extentional effect of the centroidal axis. The stability of shallow arches with a downward concentrated load at the crown were studied by Fung and Kaplan (19). Calculations and experiments for symmetrical circular arches which underwent large deflections were made by Langhaar, Boresi, Carver (26) and Lind (28). Their formulation was based on the Winkler-Bach hypothesis which states that plane sections normal to the undeformed centroidal line remain plane, unextended, and normal to the deformed centroidal line. The analytical and experimental results agreed favorably. Lind (28) extended this work to parabolic and catenary arches. The arches studied had hinged end supports with a downward concentrated load at the crown.

Using the Winkler-Bach hypothesis, Wempner and Kesti (42) developed a complete set of nonlinear algebraic equations

approximating the nonlinear differential equations. This work eventually led into the formulation of a finite element arch element (43). This will be discussed in detail later in the chapter.

From the exact inextensional theory of deep arches DaDeppo and Schmidt (9,12) analyzed two-hinged circular arches subjected to a downward concentrated load at the crown and a point load applied eccentrically near the crown. A comparison of critical loads for various subtending angles was made. The results revealed that Lind's work was accurate for arches having subtending angles of less than 90°. DaDeppo and Schmidt (11,14) also studied the stability of deep hinged arches under distributed and combined loads. DaDeppo and Schmidt (15) also investigated the stability of clamped arches which undergo large deflections with interacting loads. The loading condition was a combination of a downward concentrated load at the crown and the arches dead weight. It was found that the instability modes were dependent upon the intensity of the distributed load when there is no concentrated load. A snap through mode was observed for a high ratio. As the ratio decreased, a point was reached where bifurcation buckling occurred.

The studies that have been reviewed thus far have all dealt with structural nonlinearities. Very few analytical solutions can be obtained for such problems, therefore,

numerical solutions become necessary. In this work finite element analysis is used to solve geometrically nonlinear problems of curved structures. Gallagher (22) made a thorough and general investigation on the present finite element methods used to solve geometrically nonlinear problems. This study focused on three areas of interest: (1) the general procedure for the formulation of the finite element, (2) the choice of the assumed displacement field, and (3) the solution scheme for the global system of nonlinear equations. Since general finite element procedures are well established, the potential source of error for geometrically nonlinear problems depends primarily on the accuracy of the governing differential equations, the assumed displacement field, and the solution scheme. The constitutive equations are dependent upon the simplifying assumptions made. As for the choice of the displacement field, this is a complex issue and will be discussed in detail in the following paragraphs.

Within this study displacement fields for curved finite elements are the major concern. In reviewing the literature it was noticed that there were many publications on curved finite element models. Ashwell and Sabir (1) began the study of using independent interpolation polynomials as the finite element shape functions. Dawe (17, 18) continued such an investigation and included higher order polynomials. He analyzed both shallow and deep circular arches. The linear

displacement equations used were

$$\varepsilon = \frac{dU_t}{dS} - \frac{U_N}{R} \tag{1.1}$$

$$\beta = \frac{dU_N}{dS} + \frac{U_t}{R} \tag{1.2}$$

$$\chi = \frac{d^2U_N}{dS^2} + \frac{1}{R}\frac{dU_N}{dS} \tag{1.3}$$

where ε is the strain of the centroidal line

β is the rotation

R is the undeformed arch radius

S is arc length

χ is the change in curvature

U_N is the normal displacement component

U_t is the tangential displacement component.

The strain energy equation used was

$$U = \frac{E}{2}\int \left(\varepsilon^2 + \frac{t^2}{12}\chi^2\right) ds \ , \tag{1.4}$$

where E is Young's modulus

t is the arch thickness.

Five models were chosen,

1. A quintic-quintic model

$$U_N = A_1 + A_2S + A_3S^2 + A_4S^3 + A_5S^4 + A_6S^5 \tag{1.5}$$

$$U_t = A_7 + A_8S + A_9S^2 + A_{10}S^3 + A_{11}S^4 + A_{12}S^5 \tag{1.6}$$

2. A cubic-quintic model

$$U_N = A_1 + A_2 S + A_3 S^2 + A_4 S^3 \tag{1.7}$$

$$U_t = A_5 + A_6 S + A_7 S^2 + A_8 S^3 + A_9 S^4 + A_{10} S^5 \tag{1.8}$$

3. A quintic-cubic model

$$U_N = A_1 + A_2 S + A_3 S^2 + A_4 S^3 + A_5 S^4 + A_6 S^5 \tag{1.9}$$

$$U_t = A_7 + A_8 S + A_9 S^2 + A_{10} S^3 \tag{1.10}$$

4. A cubic-cubic model

$$U_N = A_1 + A_2 S + A_3 S^2 + A_4 S^3 \tag{1.11}$$

$$U_t = A_5 + A_6 S + A_7 S^2 + A_8 S^3 \tag{1.12}$$

5. A constraint strain, linear curvature element

$$U_N = A_1 \cos\left(\frac{S}{R}\right) + A_2 \sin\left(\frac{S}{R}\right) + A_3 + A_4 S \tag{1.13}$$

$$U_t = A_5 + A_6 \sin\left(\frac{S}{R}\right) - A_7 \cos\left(\frac{S}{R}\right) + A_8 S + \frac{A_9}{2} \frac{S^2}{R} \tag{1.14}$$

These models were tested on both semicircular and shallow (subtending angle of 30°) clamped arches for R/t of 17 and 272. It must be noted that Eqs. (1.1) - (1.3) are linear and the displacements must be small. For the problems tested the quintic-quintic model gave the best results in both cases. The moment distribution for all elements were erratic, however, the quintic-quintic model was the most accurate. All models gave accurate load-deflection results for the shallow arch problem.

Yamada and Ezawa (45) ran a similar study using the following models:

1. A cubic-linear model

$$U_N = A_1 + A_2S + A_3S^2 + A_4S^3 \quad (1.15)$$

$$U_t = A_5 + A_6S \quad (1.16)$$

2. A cubic-cubic model

$$U_N = A_1 + A_2S + A_3S^2 + A_4S^3 \quad (1.17)$$

$$U_t = A_5 + A_6S + A_7S^2 + A_8S^3 \quad (1.18)$$

3. A Kikuchi model

$$U_N = 1/2\ (U_{N_1} + U_{N_2}) \quad (1.19)$$

$$U_t = A_1 + A_2S \quad (1.20)$$

where U_{N_1} and U_{N_2} are the normal nodal displacements at nodal point 1 and 2, respectively.

4. A modified Kikuchi model

$$U_N = 1/2\ (U_{N_1} + U_{N_2}) + 1/6\ R(\beta_1-\beta_2) \quad (1.21)$$

$$U_t = A_1 + A_2S \quad (1.22)$$

where β_1 and β_2 are the nodal rotations at the nodal point 1 and 2, respectively.

5. A modified Kikuchi model

$$U_N = 1/2\ (U_{N_1} + U_{N_2}) + 1/2\ R\beta(\beta_1-\beta_2) + 1/6\beta(U_{t_1}-U_{t_2}) \quad (1.23)$$

$$U_t = A_1 + A_2S \quad (1.24)$$

where U_{t_1} and U_{t_2} are the tangential nodal displacements at nodal point 1 and 2, respectively.

6. Assembly of straight beam elements.

The arch equations used are (1.1)-(1.3). The strain energy equation used in (1.4). The same tests were made as in the study by Dawe (18). The results of these tests revealed that the cubic-cubic model was very accurate and tended to converge to the exact solution rapidly. The other models, except for the linear-cubic model, gave accurate results. However, the cubic-cubic model was considered to be the best.

A common requirement for finite elements is that their displacement functions and the angular rotations should be continuous on the interelement boundaries between adjacent elements. Also the displacement function should be able to give a satisfactory description of the rigid body motion. A great deal of emphasis has been placed on the explicit addition of rigid body modes. This procedure was introduced by Cantin and Clough (5). Matsui, Tetsuya, and Matsuoka (30) introduced explicitly the rigid body modes for a nonlinear finite element used in the stability analysis of shells. However, Haisler and Stricklin (24) and Membane and Stricklin (32) concluded that the explicit addition of rigid body modes is definitely not necessary.

Much discussion has also been made on the procedure for determining the existence of rigid body modes. The common method is to evaluate the eigenvalues of the elemental stiffness matrix. Fried (20,21) researched the need for energy error functions to account for the accuracy of the shape functions. Yamada and Ezawa (45) analyzed certain stability criteria of the flexibility matrix to account for rigid body modes.

After reviewing the literature, it becomes apparent that the effectiveness of the interpolation function is best demonstrated by the accuracy of the solution for the specific problem in which it is used. Therefore, an in-depth study of whether to include rigid body modes explicitly or implicitly is not necessary nor can it lead to any definite conclusions on the accuracy of the interpolation function.

At this point it is necessary to discuss the various nonlinear curved elements. Most nonlinear curved elements that exist were developed for the purpose of shell analysis. These elements were tested using simple arch problems, even though some of the assumptions used in their formulation differed from those of a general nonlinear arch problem. Since this work involves nonlinear arch analysis, the elements that will be discussed in the next few paragraphs were formulated primarily for arches.

Some nonlinear arch problems are solved using Eqs. (1.1)-(1.4). Since these equations represent linear theory, the nonlinear problems are solved by introducing small load increments and iterating at each load level. A detailed discussion of the various solution algorithms is discussed in Chapter 5.

Wempner and Patrick (43) developed a nonlinear arch finite element. This element was derived from a set of nonlinear algebriac equations based upon the Winkler-Bach theory. The behavior of the individual element is governed by a set of linear algebraic equations, whereas the nonlinearities arise from the differences between the rigid body rotations of adjacent elements. The solution of problems using this element require that the element length, the displacement increments, and the load increments be small. This is computationally expensive.

Wood and Zienkiewicz (44) developed a geometrically nonlinear finite element for the analysis of beams, frames, arches, and axisymmetric shells. This element is a paralinear isoparametric element (47) presented in a total Lagrangian coordinate system. Because of the numerical instability of the stiffness matrix, a reduced integration scheme was used. Such a scheme decreases the number of Gauss points needed for the numerical integration of the elemental stiffness. There were two test problems run using

this element that are of special interest: (1) a two-hinged deep arch with a vertical downward concentrated load at the crown, and (2) a deep clamped arch with a vertical downward concentrated load at the crown. The solution of the first problem using this nonlinear finite element compared favorably with the results obtained by DaDeppo and Schmidt (10) and Huddleston (25). In order to obtain the bifurcation point a small perturbing load was placed on the structure. This method was first employed by Batoz, Chattopadhyay, and Dhatt (3). As for the second problem the results using the nonlinear isoparametric element deviated by 3% from the results of DaDeppo and Schmidt (16).

This element was relatively impressive for the test problems chosen. However, it should be mentioned that the element has a large number of degrees of freedom which can be computationally expensive. Also it is effective for a formulation presented in the total Lagrangian state. For any other state such as the updated Lagrangian state it has no apparent advantage. Bathe and Boulourchi (2) ran some sample tests with this element and concluded that it demonstrated numerical instabilities and had definite limitations. One such limitation is the magnitude of the aspect ratio (length of element to height of element). As the aspect ratio increases the accuracy of the solution drops rapidly.

As mentioned in Chapter 1 the nonlinear arch element that is developed in this work can analyze arches with arbitrary geometry of the centroidal line. A spline curve fitting scheme is used to represent this arbitrary geometry. In reviewing the literature it was discovered that Liu (29) used a similar procedure to develop a quadrilateral shell finite element having arbitrary surface geometry. The curved surface geometry was based upon a bicubic spline patch representation. The piecewise continuity of patches was ensured by defining the patch boundaries as an intersecting network of parametric cubic spline curves. This element was used for linear analysis.

Even though nonlinear finite element analysis has made great advancements in the past decade, the complexities of the problems and the high cost of solving the problems still exist. Therefore, there is a need for alternative formulations and alternative solution schemes. The formulation of the curved finite element used in this work is new. The inclusion of an arch with arbitrary geometry and a different solution scheme add to the uniqueness of the study of stability analysis of geometrically nonlinear problems.

CHAPTER 3

FORMULATION OF ARCH EQUATIONS

The governing nonlinear differential equations for the nonshallow arches studied in this research were derived by Qaqish (35). This derivation was based on the assumptions that plane cross sections of the undeformed arch remain in plane, but not necessarily normal to the centroidal axis during deformation. It must also be noted that transverse shear was considered and no restrictions were placed on the magnitudes of the deformation.

An undeformed and deformed arch segment is shown in Fig. 3.1. For the undeformed geometry R, dS, and $d\phi$ represent the radius of curvature, element of arc length, and central angle respectively. Whereas for the deformed geometry the radius of curvature, the element of arc length, and the central angle are represented by R*, dS*, and $d\phi^*$.

The deformed length of the arch segment can be represented as

$$dS^* = dS\ (1 + \varepsilon_c)\ , \tag{3.1}$$

where ε_c is the strain of the centroidal line.

From the equation of the undeformed arc length

$$dS^* = R^*\ d\phi^* \tag{3.2}$$

where $$d\phi^* = d\beta + d\phi\ . \tag{3.3}$$

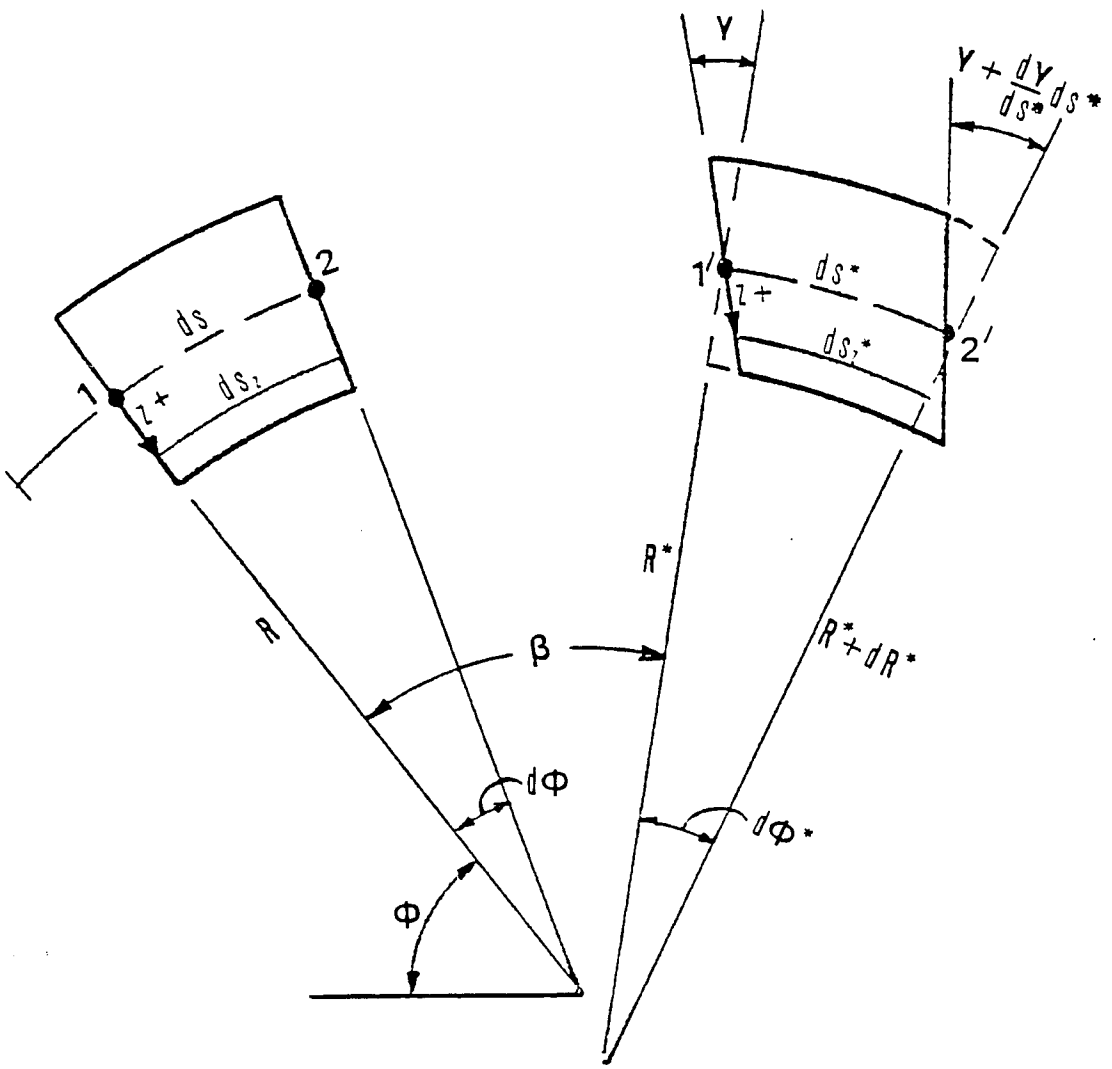

Fig. 3.1. An arch element in the deformed and undeformed configuration.

The curvature of the deformed arch segment is

$$K^* = \frac{1}{R^*} = \frac{d\phi^*}{dS^*} \tag{3.4}$$

Substituting Eqs. (3.1) and (3.3) into (3.4) gives

$$K^* = \frac{d\beta + d\phi}{dS(1+\varepsilon_c)} \quad . \tag{3.5}$$

Since the curvature in the undeformed state is

$$K = \frac{d\phi}{dS} \quad , \tag{3.6}$$

the curvature of the deformed element can be written as

$$K^* = \frac{1}{(1+\varepsilon_c)} \quad (\beta'+K) \tag{3.7}$$

where the prime term denotes differentiation with respect to the arc length, S.

Combining (3.1), (3.4) and (3.7) yields

$$\frac{d\phi^*}{dS} = K + \beta' \quad . \tag{3.8}$$

The deformed arc length at a distance z from the centroidal axis can be represented as

$$dS_z^* = (R^* - z\cos\gamma)d\phi^* - z\sin\gamma + z\sin(\gamma+d\gamma). \tag{3.9}$$

Since $d\gamma$ is considered to be small, the following approximations can be made,

$$\cos d\gamma = 1 \quad \text{and} \quad \sin d\gamma = d\gamma \cdot$$

Making use of the double angle formula,

$$\sin(\gamma+d\gamma) = \sin\gamma + \cos\gamma d\gamma \ . \qquad (3.10)$$

Substituting (3.10) into (3.9) yields

$$dS_z^* = (R^* - z\cos\gamma)d\phi^* + z\cos\gamma\, d\gamma. \qquad (3.11)$$

Since $dS_z^* = dS_z(1+\varepsilon_z)$

and $dS_z = dS - z\,d\phi$,

$$dS_z^* = \varepsilon_z\,(dS - zd\phi) + dS - zd\phi \ . \qquad (3.12)$$

Combining Eqs. (3.7), (3.12), and (3.11) gives

$$\varepsilon_z(dS - zd\phi) + dS - zd\phi =$$

$$\left[\frac{(1+\varepsilon_c)}{\beta' + K} - z\cos\gamma\right] d\phi^* + z\cos\gamma d\gamma \ . \qquad (3.13)$$

Dividing Eq. (3.13) by dS yields

$$\varepsilon_z - z\,K\varepsilon_z + 1 - z\,K = \left[\frac{(1+\varepsilon_c)}{\beta' + K} - z\cos\gamma\right] (K+\beta')$$

$$+ z\gamma'\cos\gamma \ . \qquad (3.14)$$

Rearranging (3.14) gives

$$\varepsilon_z = \frac{1}{1 - zK}\left[\left(\frac{(1+\varepsilon_c)}{\beta' + K} - z\cos\gamma\right)(K+\beta') + z\gamma'\cos\gamma\right.$$

$$\left. - 1 + zK\right] \ . \qquad (3.15)$$

If the transverse shear deformation is neglected,

$$\cos\gamma = 1 \quad \text{and} \quad \gamma' = 0 \ ;$$

therefore,

$$\varepsilon_z = \frac{1}{1 - Kz} \left(\varepsilon_c - z\beta'\right) . \tag{3.16}$$

This equation represents the strain in the arch at a distance z from the centroidal axis. It is also the basic equation that will be used in formulating the nonlinear arch finite element.

Formulation of the Strain Equation Using Normal and Tangential Displacement Components

With reference to Fig. 3.2, dS, $d\phi$, and R are the undeformed arc length, central angle, and radius of curvature, respectively. Whereas, for the deformed state, dS*, $d\phi$*, and R* are the arc length, the central angle, and the radius of curvature, respectively. The normal displacement component is U_N, and the tangential displacement component is U_t. Using the geometry of Fig. 3.2 and the fact that $d\phi$ is small, the following relationships were developed.

$$d_2 = U_N d\phi \tag{3.17}$$

$$d_1 = dS + U_t + dU_t - U_N d\phi . \tag{3.18}$$

Also,

$$d_1 = U_t + dS^* \cos\beta . \tag{3.19}$$

$$d_3 = U_N + dU_N + U_t d\phi \tag{3.20}$$

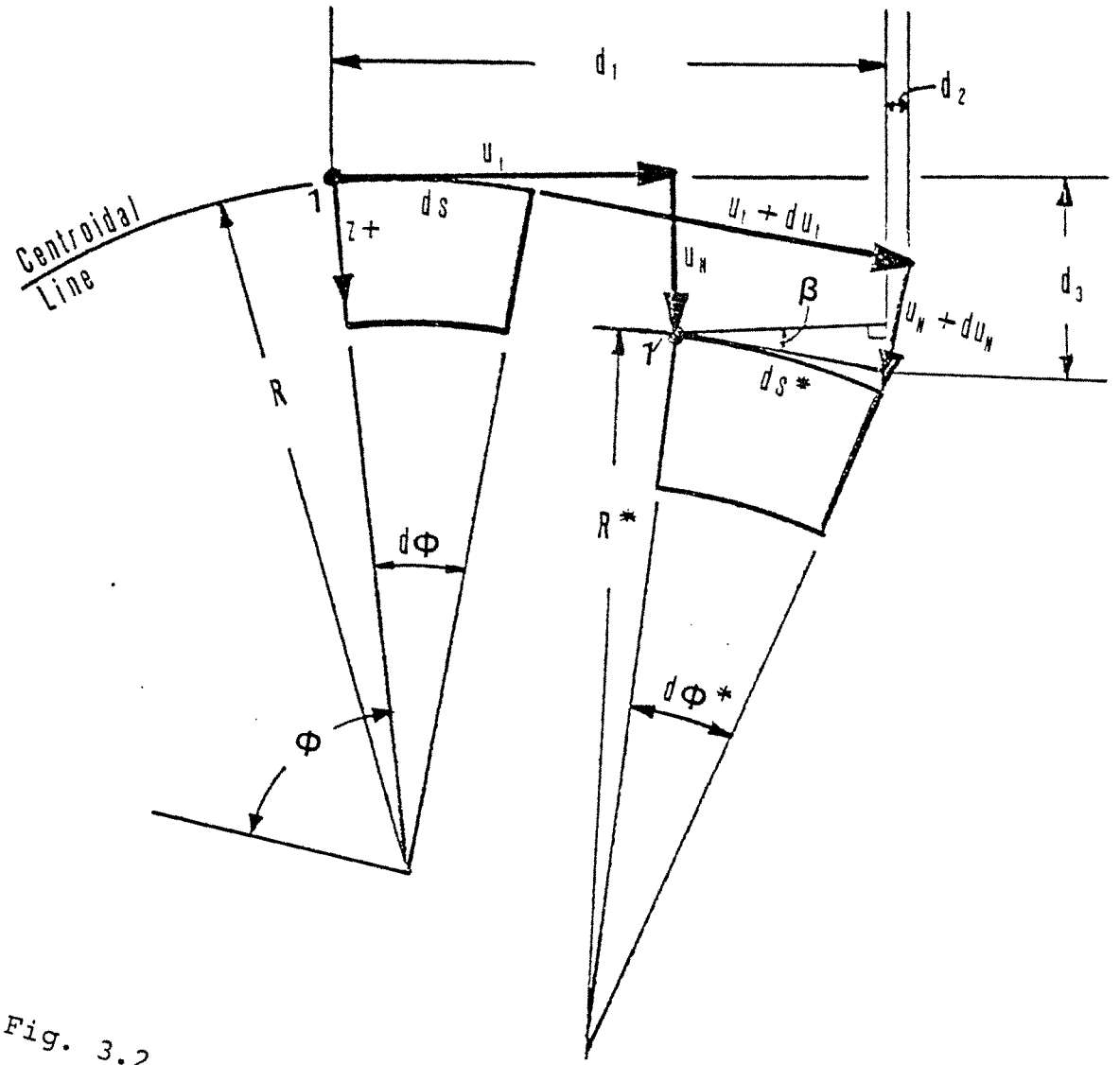

Fig. 3.2. Displaced arch segment.

Also,

$$d_3 = U_N + dS^* \sin\beta \ . \qquad (3.21)$$

Equating (3.18) and (3.19) yields

$$dS^* \cos\beta = dS + dU_t - U_N d\phi \ . \qquad (3.22)$$

Substituting (3.1) into (3.22) and dividing through (3.22) by dS gives

$$(1+\varepsilon_c) \cos\beta = 1 + U_t' - K U_N \ . \qquad (3.23)$$

Equating (3.20) and (3.21) yields

$$dS^* \sin\beta = dU_N + U_t d\phi \ . \qquad (3.24)$$

Substituting (3.1) into (3.24) and then dividing by dS gives

$$(1+\varepsilon_c) \sin\beta = U_N' + K U_t \ . \qquad (3.25)$$

Squaring (3.23) and (3.25) and adding the results yields

$$(1+2\varepsilon_c+\varepsilon_c^2) = (1+2U_t' - 2KU_NU_t' - 2KU_N + 2KU_N'U_t + U_N'^2 + K^2U_t^2 + U_t'^2 + K^2U_N^2) \qquad (3.26)$$

At this point a small strain assumption is made; that is the

$$\varepsilon_c << 1$$

therefore, ε_c^2 can be neglected as being small compared to ε_c. With this assumption Eq. (3.26) yields the following expression for ε_c

$$\varepsilon_c = 1/2(U_t'^2 + U_N'^2 + K^2U_N^2 + K^2U_t^2 + 2U_t' - 2 K U_N - 2 K U_NU_t' + 2 K U_tU_N') . \quad (3.27$$

In order to formulate an expression for β and β' in terms of the normal and tangential components of displacements and their derivatives, divide (3.25) by (3.23) to obtain expression

$$\tan\beta = \frac{(U_N' + K U_t)}{(1 + U_t' - K U_N)} . \quad (3.28)$$

Therefore, the rotation

$$\beta = \tan^{-1} \frac{(U_N' + K U_t)}{(1 + U_t' - K U_N)} \quad (3.29)$$

Let $a = U_N' + K U_t$

$b = 1 + U_t' - K U_N$.

Then,

$$\beta = \tan^{-1}\left(\frac{a}{b}\right) . \quad (3.30)$$

Differentiation of Eq. (3.30) with respect to S yields

$$\beta' = \frac{1}{1 + \left(\frac{a}{b}\right)^2} \frac{d\left(\frac{a}{b}\right)}{dS} .$$

or,

$$\beta' = \frac{ba' - ab'}{b^2 + a^2} \quad (3.31)$$

where,

$$a' = U_N'' + K'U_t + K U_t' \quad (3.32)$$

$$b' = U_t'' - K'U_N - K U_N' \quad (3.33)$$

Let $c = ba' - ab'$

$d = b^2 + a^2$

therefore,

$$\beta' = \frac{c}{d} \tag{3.34}$$

where,

$$c = (K'U_t + KU_t' + U_N'' + K'U_tU_t' + KU_t'^2 + U_t'U_N'' - K'KU_NU_t - K^2U_NU_t' - KU_NU_N'' - KU_tU_t'' + K'KU_NU_t + K^2U_tU_N' - U_N'U_t'' + K'U_NU_N' + KU_N'^2) \tag{3.35}$$

and

$$d = (1 + U_t'^2 + U_N'^2 + K^2U_N^2 + K^2U_t^2 + 2U_t' - 2KU_N - 2KU_NU_t' + 2KU_tU_N') \tag{3.36}$$

Substituting (3.27) and (3.34) into (3.16) will give the strain in the arch at a distance z from the centroidal axis in terms of the normal and tangential components of displacements of the centroidal line and their derivatives.

CHAPTER 4

FORMULATION OF THE NONLINEAR ARCH FINITE ELEMENT

The purpose of this chapter is to formulate a finite element which is used in the nonlinear structural analysis of arches with circular and arbitrary geometries. To begin it is advantageous to introduce the concept of virtual work, or even more specifically the concept of virtual displacements, which is essential to the fundamental study of the finite element method. In the principle of virtual displacements it is assumed that a body in equilibrium under body forces and surface forces is subjected to a virtual displacement state described at each point. The displacements must be "kinematically admissible"; that is, they are continuous functions and satisfy kinematic boundary conditions on the portion of the surface on which such conditions are prescribed (23).

Having satisfied the appropriate conditions, the principle of virtual displacements for conservative forces states that the sum of the potential of the applied loads (δW_e) and the variation of the strain energy (δU) during a virtual displacement δu is equal to zero, or

$$\delta U + \delta W_e = 0 \qquad (4.1)$$

The variation in strain energy term is represented as

$$\delta U = \int_{vol} \sigma \delta \varepsilon \, d\,vol \qquad (4.2)$$

where σ is the stress and $\delta\varepsilon$ is the virtual strain which is a function of a virtual displacement, δu. The potential of the applied loads can be expressed as

$$\delta W_e = \left(\int q(s) dS^* \right) \delta u \quad , \qquad (4.3)$$

where $q(s)$ = load intensity

dS^* = deformed arc length

δu = virtual displacement field.

Finite Element Stiffness Formulation

Since the finite element method is based on the approximation of a displacement field, interpolation functions must be used. These functions have an important effect on both the numerical stability and the accuracy of the solution for the structural problem. A discussion on such choices was found in the Review of Literature. Since the governing differential equations used on problems discussed in the Review of Literature varied greatly from the equations used in this formulation, no definite conclusions could be drawn as to the best form for the interpolation functions. Initially a cubic polynomial was chosen for this formulation. The actual functions used were independent cubic polynomials for both the normal and tangential displacement fields. There

were two primary reasons for this choice: (1) it had demonstrated highly accurate results for Yamada and Ezawa (45), and (2) the high degree of nonlinearity used in the governing differential equations may have made the application of a higher order or more complex interpolating function economically not feasible.

The independent interpolation functions used for both the normal displacement field, U_N, and the tangential displacement field, U_t, are:

$$U_N = A_1 + A_2S + A_3S^2 + A_4S^3 \tag{4.4}$$

$$U_t = A_5 + A_6S + A_7S^2 + A_8S^3 \tag{4.5}$$

where S is the arc length and is the independent variable.

Equations (4.4) and (4.5) can be represented in matrix form as

$$\begin{bmatrix} U_N \\ U_t \end{bmatrix} = \left[\begin{array}{c|c|c|c|c|c|c|c} 1 & S & S^2 & S^3 & 0 & 0 & 0 & 0 \\ 0 & 0 & 0 & 0 & 1 & S & S^2 & S^3 \end{array}\right] \begin{bmatrix} A_1 \\ A_2 \\ A_3 \\ A_4 \\ A_5 \\ A_6 \\ A_7 \\ A_8 \end{bmatrix}$$

or,

$$\underset{2x1}{\underset{\sim}{U}} = \underset{2x8}{\underset{\sim}{S}} \; \underset{8x1}{\underset{\sim}{A}} \quad . \tag{4.6}$$

Because of the interpolation functions chosen, the finite element model has four degrees of freedom at each node. Such an element and the degrees of freedom are shown in Fig. 4.1.

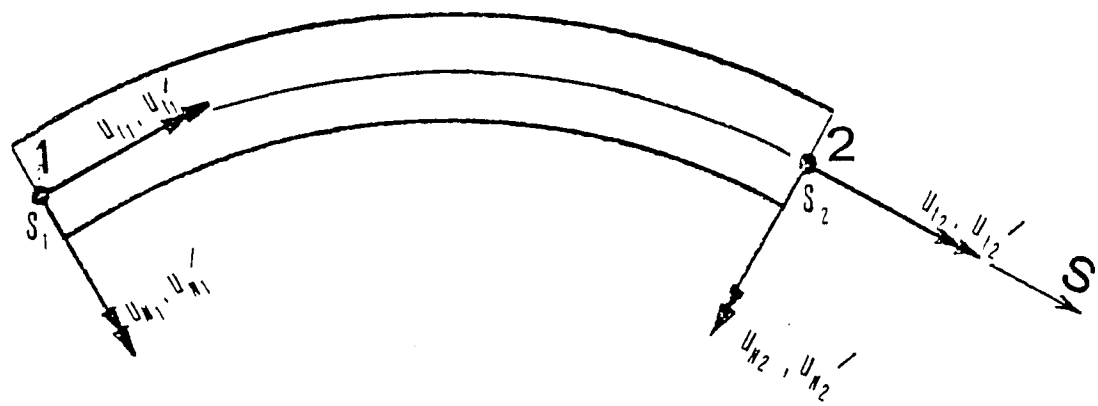

Fig. 4.1. Nonlinear arch finite element.

Since A has no obvious physical meaning, a series of matrix operations are carried out to express A in terms of p, the nodal degrees of freedom. To accomplish this, equations for U_N, U_N', U_t, and U_t' are needed. Equations (4.4) and (4.5) express U_N and U_t, respectively, and

$$U_N' = A_2 + 2 A_3 S + 3 A_4 S^2 \qquad (4.7)$$

$$U_t' = A_6 + 2 A_7 S + 3 A_8 S^2 \ . \qquad (4.8)$$

Applying the element constraints such as to assure compatibility at each node point the following system of equations evolved (S_1 and S_2 are the nodal point arc measurements).

$$\begin{bmatrix} U_{N_1} \\ U_{N_1}' \\ U_{t_1} \\ U_{t_1}' \\ U_{N_2} \\ U_{N_2}' \\ U_{t_2} \\ U_{t_2}' \end{bmatrix} = \left[\begin{array}{c|c|c|c|c|c|c|c} 1 & S_1 & S_1^2 & S_1^3 & 0 & 0 & 0 & 0 \\ 0 & 1 & 2S_1 & 3S_1^2 & 0 & 0 & 0 & 0 \\ 0 & 0 & 0 & 0 & 1 & S_1 & S_1^2 & S_1^3 \\ 0 & 0 & 0 & 0 & 0 & 1 & 2S_1 & 3S_1^2 \\ 1 & S_2 & S_2^2 & S_2^3 & 0 & 0 & 0 & 0 \\ 0 & 1 & 2S_2 & 3S_2^2 & 0 & 0 & 0 & 0 \\ 0 & 0 & 0 & 0 & 1 & S_2 & S_2^2 & S_2^3 \\ 0 & 0 & 0 & 0 & 0 & 1 & 2S_2 & 3S_2^2 \end{array}\right] \begin{bmatrix} A_1 \\ A_2 \\ A_3 \\ A_4 \\ A_5 \\ A_6 \\ A_7 \\ A_8 \end{bmatrix}$$

or $$\underset{8\times1}{\underset{\sim}{p}} = \underset{8\times8}{\underset{\sim}{C}}\ \underset{8\times1}{\underset{\sim}{A}} \qquad (4.9)$$

By taking the inverse of C and performing a matrix multiplication, the new expression for A is

$$\underset{8\times8}{\underset{\sim}{A}} = \underset{8\times8}{\underset{\sim}{C^{-1}}}\ \underset{8\times1}{\underset{\sim}{p}}$$

Let $B = C^{-1}$

Then,

$$\underset{8\times1}{\underset{\sim}{A}} = \underset{8\times8}{\underset{\sim}{B}}\ \underset{8\times1}{\underset{\sim}{p}} \; . \qquad (4.10)$$

Substituting (4.10) into (4.6) gives

$$\underset{2\tilde{x}1}{\underset{\sim}{u}} = \underset{2\tilde{x}8}{\underset{\sim}{S}} \; \underset{8\tilde{x}8}{\underset{\sim}{B}} \; \underset{8\tilde{x}1}{\underset{\sim}{p}} \; . \qquad (4.11)$$

This is an expression for the assumed displacement field in terms of the independent variable S and the nodal degrees of freedom p.

From Chapter 3 it can be seen that the strain equation is a function of U_N, U_N', U_N'', U_t, U_t', and U_t''. The normal and tangential displacements and their derivatives can be represented in matrix form as shown below:

$$U_N = \left\lfloor 1 \mid S \mid S^2 \mid S^3 \mid 0 \mid 0 \mid 0 \mid 0 \right\rfloor \underset{\sim}{B} \underset{\sim}{p} \qquad (4.12)$$

$$U_N' = \left\lfloor 0 \mid 1 \mid 2S \mid 3S^2 \mid 0 \mid 0 \mid 0 \mid 0 \right\rfloor \underset{\sim}{B} \underset{\sim}{p} \qquad (4.13)$$

$$U_N'' = \left\lfloor 0 \mid 0 \mid 2 \mid 6S \mid 0 \mid 0 \mid 0 \mid 0 \right\rfloor \underset{\sim}{B} \underset{\sim}{p} \qquad (4.14)$$

$$U_t = \left\lfloor 0 \mid 0 \mid 0 \mid 0 \mid 1 \mid S \mid S^2 \mid S^3 \right\rfloor \underset{\sim}{B} \underset{\sim}{p} \qquad (4.15)$$

$$U_t' = \left\lfloor 0 \mid 0 \mid 0 \mid 0 \mid 0 \mid 1 \mid 2S \mid 3S^2 \right\rfloor \underset{\sim}{B} \underset{\sim}{p} \qquad (4.16)$$

$$U_t'' = \left\lfloor 0 \mid 0 \mid 0 \mid 0 \mid 0 \mid 0 \mid 2 \mid 6S \right\rfloor \underset{\sim}{B} \underset{\sim}{p} \qquad (4.17)$$

By taking the second partial derivative of the strain energy function with respect to the nodal degrees of freedom, the elemental stiffness matrix can be obtained.

Since this work considers geometric nonlinearities, the structural stiffness calculated is the instantaneous stiffness and will differ for each displacement step.

The strain energy for a linear elastic solid is

$$U = 1/2 \int_{vol} \sigma\varepsilon \, d\,vol \quad .$$

With reference to Fig. 4.2, the linear elastic solid strain energy function for the arch in question can be expressed as

$$U = 1/2 \int_{y_1}^{y_2} \int_{z_1}^{z_2} \int_{S_1}^{S_2} \sigma(z,S)\varepsilon(z,S) \, dS \, dz \, dy. \qquad (4.18)$$

The material is considered to be linearly elastic and to obey the one dimensional form of Hooke's Law

$$\sigma = E\varepsilon \qquad (4.19)$$

where E = Young's modulus.

Considering an arch of constant cross-sectional width t, the new form of the strain energy function is

$$U = \frac{tE}{2} \int_{z_1}^{z_2} \int_{S_1}^{S_2} \left(\varepsilon(z,S)\right)^2 \, dSdz \quad . \qquad (4.20)$$

Substituting (3.16) into (4.13) yields

$$U = \frac{tE}{2} \int_{z_1}^{z_2} \int_{S_1}^{S_2} \left\{\frac{1}{1-Kz} \left(\varepsilon_c - z\beta'\right)\right\}^2 dSdz \quad . \qquad (4.21)$$

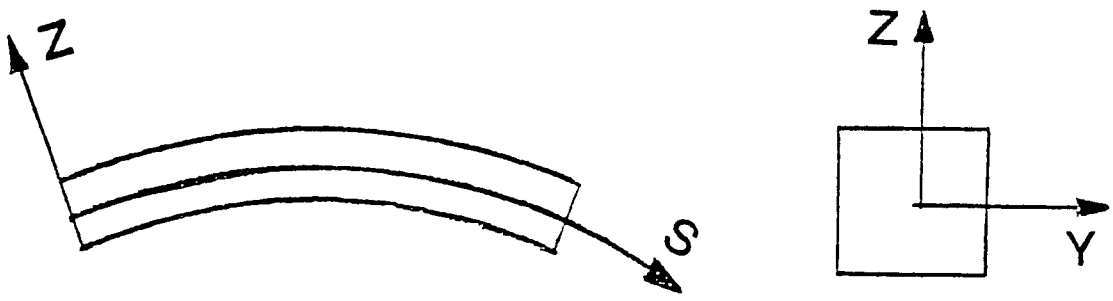

Fig. 4.2. Arch element coordinate system.

Expanding (4.21) gives

$$U = \frac{tE}{2}\left\{\int_{z_1}^{z_2}\int_{S_1}^{S_2}\left(\frac{1}{1 - 2Kz + K^2z^2}\right)\varepsilon_c^2\, dSdz\right.$$

$$- 2\int_{z_1}^{z_2}\int_{S_1}^{S_2}\left(\frac{1}{1 - 2Kz + K^2z^2}\right)\varepsilon_c\beta'\, dSdz$$

$$\left. + \int_{z_1}^{z_2}\int_{S_1}^{S_2}\left(\frac{z^2}{1 - 2Kz + K^2z^2}\right)\beta'^2 dSdz\right\} \quad . \quad (4.22)$$

The instantaneous stiffness is

$$K(p) = \frac{\partial^2 U}{\partial p_i \partial p_j} \quad . \quad (4.23)$$

Since ε_c and β' are the variables which include the p terms, it is necessary to take the following partial derivatives.

$$\frac{\partial(\varepsilon_c^2)}{p_i} = 2\,\varepsilon_c\,\frac{\partial\varepsilon_c}{\partial p_i} \tag{4.24}$$

$$\frac{\partial^2(\varepsilon_c^2)}{\partial p_i \partial p_j} = 2\left(\varepsilon_c\,\frac{\partial^2\varepsilon_c}{\partial p_i \partial p_j} + \frac{\partial\varepsilon_c}{\partial p_i}\,\frac{\partial\varepsilon_c}{\partial p_j}\right) \tag{4.25}$$

Using Equation (3.34),

$$\frac{\partial(\varepsilon_c\beta')}{\partial p_i} = \frac{\partial\left(\frac{\varepsilon_c c}{d}\right)}{\partial p_i}$$

also,

$$\frac{\partial(\varepsilon_c\beta')}{\partial p_i} = \frac{d\,\varepsilon_c\,\frac{\partial c}{\partial p_i} + c\,d\,\frac{\partial\varepsilon_c}{\partial p_i} - \varepsilon_c\,c\,\frac{\partial d}{\partial p_i}}{d^2} \tag{4.26}$$

$$\frac{\partial^2(\varepsilon_c\beta')}{\partial p_i \partial p_j} = \frac{1}{d^4}\left\{\frac{(d^4-d^3)}{2}\,\frac{\partial^2 c}{\partial p_i \partial p_j} + \frac{d^2}{2}\,\frac{\partial c}{\partial p_i}\,\frac{\partial d}{\partial p_j}\right.$$

$$\left. + \frac{d^2}{2}\,\frac{\partial d}{\partial p_i}\,\frac{\partial c}{\partial p_i} + \frac{cd^2}{2}\,\frac{\partial^2 d}{\partial p_i p_j} + cd\,\frac{\partial d}{\partial p_i}\,\frac{\partial d}{\partial p_j}\right\} \tag{4.27}$$

$$\frac{\partial(\ '^2)}{\partial p_i} = \frac{\partial\left(\frac{c^2}{d^2}\right)}{\partial p_i}$$

$$\frac{\partial(\beta'^2)}{\partial p_i} = 2\left(\frac{c}{d^2}\,\frac{\partial c}{\partial p_i} - \frac{c^2}{d^3}\,\frac{\partial d}{\partial p_i}\right) \tag{4.28}$$

$$\frac{\partial^2(\beta'^2)}{\partial p_i\, p_j} = \frac{2}{d^4}\left\{ d^2 \frac{\partial c}{\partial p_i}\frac{\partial c}{\partial p_j} - 2cd\frac{\partial c}{\partial p_i}\frac{\partial d}{\partial p_j} - 2cd\frac{\partial d}{\partial p_i}\frac{\partial c}{\partial p_j} + 3c^2\frac{\partial d}{\partial p_i}\frac{\partial d}{\partial p_j} - c^2 d\frac{\partial d}{\partial p_i \partial p_j} + cd^2\frac{\partial^2 c}{\partial p_i \partial p_j}\right\} \tag{4.29}$$

Combining (4.12)-(4.17) with (4.25), (4.27), (4.29), and (4.22) and performing a two-dimensional numerical integration on the resulting equations will give the general form of the instantaneous stiffness matrix. An example and summary of these operations are shown in Appendices A and B.

Formulation of Finite Element Consistent Loading

Putting matrix equations (4.11) into indicial form gives

$$U_N = \sum_{i=1}^{n} f_i(S)\, p_i \tag{4.30}$$

$$U_t = \sum_{i=1}^{n} g_i(S)\, p_i \quad . \tag{4.31}$$

Therefore, the virtual displacements can be represented as

$$\delta U_N = \sum_{i=1}^{n} f_i(S)\, \delta p_i \tag{4.32}$$

$$\delta U_t = \sum_{i=1}^{n} g_i(S)\, \delta p_i \tag{4.33}$$

With reference to Eq. (4.3), the following equation can be written:

$$\delta W_e = \left(\int q_n(S)\,dS^*\right)\delta U_N + \left(\int q_t(S)\,dS^*\right)\delta U_t \quad (4.34)$$

where $q_n(S)$ and $q_t(S)$ are the normal and tangential load intensities, respectively.

Since,

$$dS^* = (1+\varepsilon_c)\,dS$$

and with the aid of Eqns. (4.32) and (4.33), Eq. (4.34) can be rewritten in the form

$$\delta W_e = \int q_n(S)(1+\varepsilon_c) \sum_{i=1} f_i(S)\ \delta p_i\ dS + \int q_t(S)(1+\varepsilon_c) \sum_{i=1} g_i(S)\,\delta p_i\ dS\ ,$$

or

$$\delta W_e = \sum_{i=1}^{n}\left(\int q_n(S)(1+\varepsilon_c) f_i(S)\,dS\right)\delta p_i + \sum_{i=1}^{n}\left(\int q_t(S)(1+\varepsilon_c) g_i(S)\,dS\right)\delta p_i\ . \quad (4.35)$$

For small strains,

$$\delta W_e = \sum_{i=1}^{n}\left(\int q_n(S) f_i(S)\,dS\right)\delta p_i + \sum_{i=1}^{n}\left(\int q_t(S) g_i(S)\,dS\right)\delta p_i\ . \quad (4.36)$$

The external load is

$$Q_{e_i} = \int q_n(S) f_i(S) dS + \int q_t(S) g_i(S) dS \quad . \qquad (4.37)$$

In matrix form the external nodal load for an individual element is

$$\underset{8x1}{R_{NT}} = \int_{S_1}^{S_2} \underset{8x2}{T_{u,p}}^T \underset{2x1}{q(S)} \, dS \qquad (4.38)$$

where

$$\underset{2x8}{T_{u,p}} = \left[\begin{array}{c|c|c|c|c|c|c|c} 1 & S & S^2 & S^3 & 0 & 0 & 0 & 0 \\ 0 & 0 & 0 & 0 & 1 & S & S^2 & S^3 \end{array}\right] \underset{8x8}{B} \qquad (4.39)$$

and

$$\underset{2x1}{q(S)} = \begin{bmatrix} q_n(S) \\ q_t(S) \end{bmatrix} \quad . \qquad (4.40)$$

Transformation of the Arch Element from Curvilinear to Cartesian Coordinates

Thus far all formulations have dealt with a single element in a curvilinear coordinate system. In order to solve for the displacements of an entire structure the displacement of each nodal point must be referred to a common reference frame. Therefore it is imperative that for each element a transformation be made from the normal-tengential system to a global X-Y system.

Figure 4.3 shows the nodal transformations from the local curvilinear system to the global cartesian system. Figure 4.4 represents displacement vector transformations. From the geometry of this figure it can be seen that

$$a = \sin\theta\ U_y$$
$$c = \cos\theta\ U_y$$
$$b = \cos\theta\ U_x$$
$$d = \sin\theta\ U_x \quad .$$

Therefore,

$$u_t = \cos\theta\ u_x + \sin\theta\ U_y \tag{4.41}$$
$$U_N = -\sin\theta\ u_x + \cos\theta\ U_y \tag{4.42}$$

By differentiating (4.41) and (4.42) with respect to S and making use of the equation for the curvature

$$K = \frac{d\theta}{dS} \quad ,$$

the following matrix system of equations representing the transformation from the N-T system to the X-Y system can be derived.

$$\begin{bmatrix} U_N \\ U_N' \\ U_t \\ U_t' \end{bmatrix} = \left[\begin{array}{c|c|c|c} -\sin\theta & 0 & \cos\theta & 0 \\ -K\cos\theta & -\sin\theta & -K\sin\theta & \cos\theta \\ \cos\theta & 0 & \sin\theta & 0 \\ -K\sin\theta & \cos\theta & K\cos\theta & \sin\theta \end{array}\right] \begin{bmatrix} U_x \\ U_x' \\ U_y \\ U_y' \end{bmatrix}$$

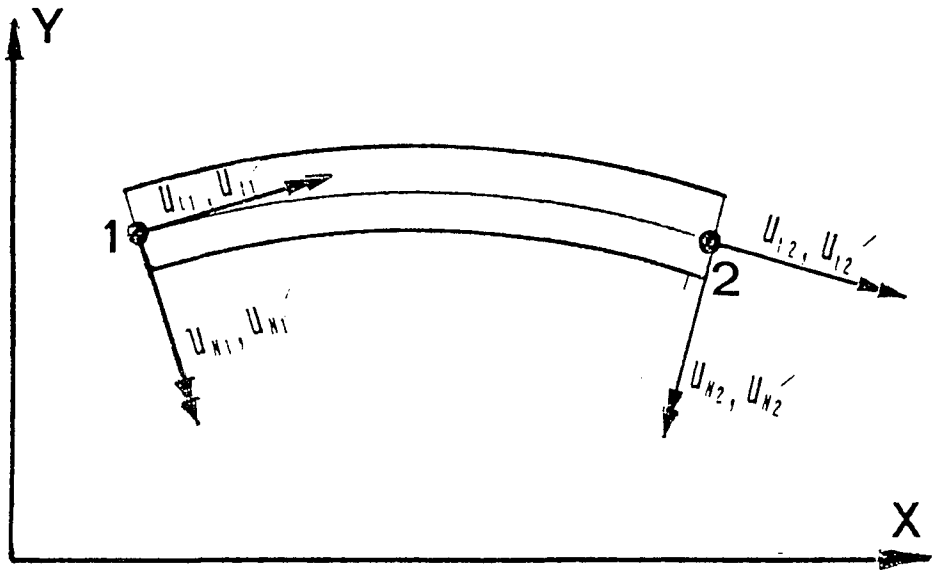

Curvilinear Displacements

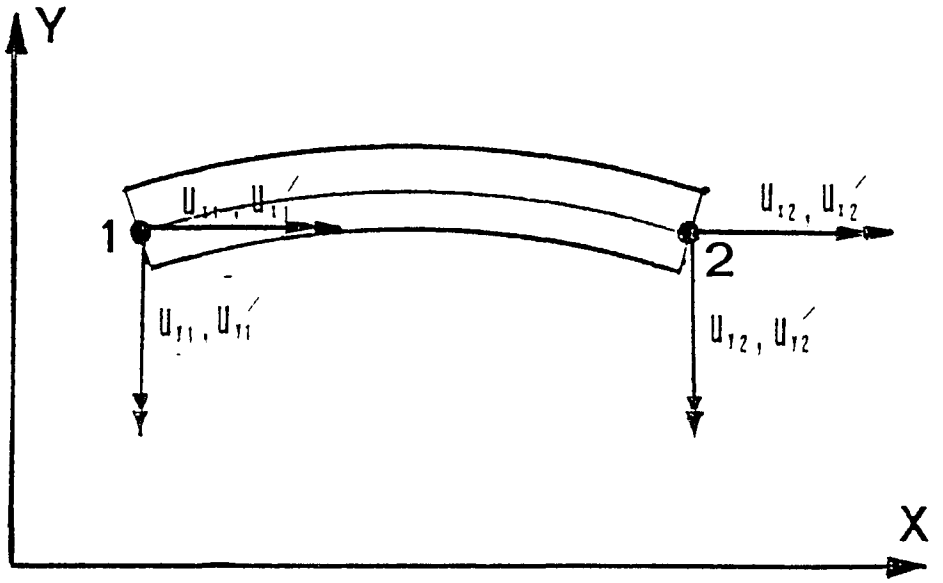

Cartesian Displacements

Fig. 4.3. Coordinate systems.

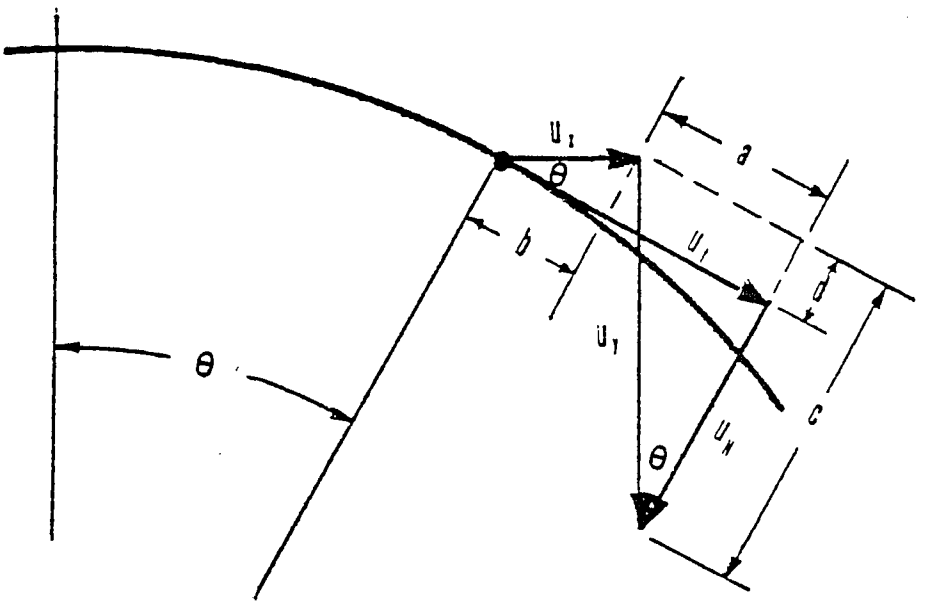

Fig. 4.4. Displacement vector transformations.

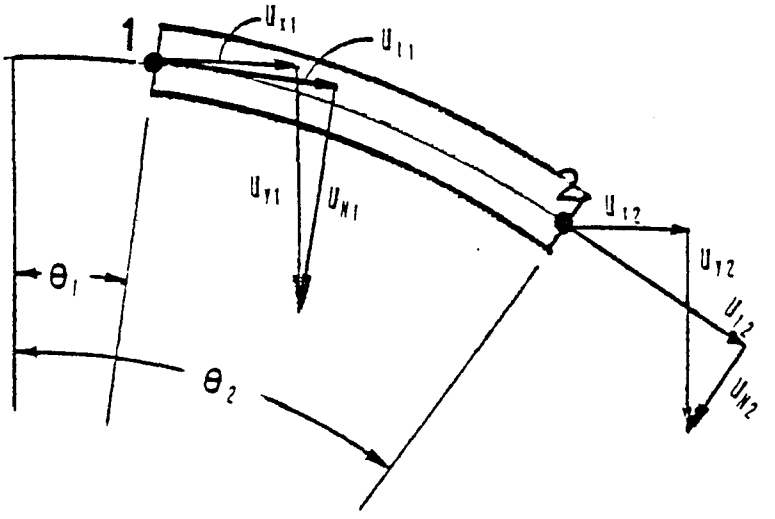

Fig. 4.5. Nodal point transformations.

Making use of these equations and Fig. 4.5, the transformation for the nodal point displacements will take the matrix form of

$$\underset{8\times1}{\underset{\sim}{p}_{NT}} = \underset{8\times8}{\underset{\sim}{T}} \; \underset{8\times1}{\underset{\sim}{p}_{xy}} \quad . \tag{4.43}$$

$$\underset{\sim}{p}_{NT} = \begin{bmatrix} U_{N_1} \\ U_{N_1}' \\ U_{t_1} \\ U_{t_1}' \\ U_{N_2} \\ U_{N_2}' \\ U_{t_2} \\ U_{t_2}' \end{bmatrix} \quad , \quad \underset{\sim}{p}_{xy} = \begin{bmatrix} U_{x_1} \\ U_{x_1}' \\ U_{y_1} \\ U_{y_1}' \\ U_{x_2} \\ U_{x_2}' \\ U_{y_2} \\ U_{y_2}' \end{bmatrix}$$

and

$$\underset{\sim}{T} = \left[\begin{array}{c|c|c|c|c|c|c|c} -\sin\theta_1 & 0 & \cos\theta_1 & 0 & 0 & 0 & 0 & 0 \\ -K_1\cos\theta_1 & -\sin\theta_1 & -K_1\sin\theta_1 & \cos\theta_1 & 0 & 0 & 0 & 0 \\ \cos\theta_1 & 0 & \sin\theta_1 & 0 & 0 & 0 & 0 & 0 \\ -K\sin\theta_1 & \cos\theta_1 & K_1\cos\theta_1 & \sin\theta_1 & 0 & 0 & 0 & 0 \\ 0 & 0 & 0 & 0 & -\sin\theta_2 & 0 & \cos\theta_2 & 0 \\ 0 & 0 & 0 & 0 & -K_2\cos\theta_2 & -\sin\theta_2 & -K_2\sin\theta_2 & \cos\theta_2 \\ 0 & 0 & 0 & 0 & \cos\theta_2 & 0 & \sin\theta_2 & 0 \\ 0 & 0 & 0 & 0 & -K_2\sin\theta_2 & \cos\theta_2 & K_2\cos\theta_2 & \sin\theta_2 \end{array}\right]$$

where $\underset{\sim}{T}$ is called the transformation matrix.

At this point it should be noted that if the arch is not circular then the values for $\cos\theta$ and $\sin\theta$ must be calculated using the equation of the curve and trigonometric identities. A discussion of this procedure is shown in Appendix C.

It is known that for one element in the normal-tangential system a structural system of equations can be expressed as

$$\underset{8\times8}{\underset{\sim}{K}_{NT}} \; \underset{8\times1}{\underset{\sim}{p}_{NT}} = \underset{8\times1}{\underset{\sim}{R}_{NT}} \tag{4.44}$$

where $\underset{\sim}{K}_{NT}$ = instantaneous stiffness

$\underset{\sim}{p}_{NT}$ = nodal degrees of freedom

$\underset{\sim}{R}_{NT}$ = externally applied loads

Substituting (4.43) into (4.44) yields

$$\underset{8\times8}{\underset{\sim}{K}_{NT}} \; \underset{8\times}{\underset{\sim}{T}} \; \underset{8\times1}{\underset{\sim}{p}_{xy}} = \underset{8\times1}{\underset{\sim}{R}_{NT}} \; . \tag{4.45}$$

In order to obtain a symmetric instantaneous stiffness matrix it is necessary to premultiply both sides of (4.45) by $\underset{\sim}{T}^T$.

$$\underset{8\times8}{\underset{\sim}{T}^T} \; \underset{8\times8}{\underset{\sim}{K}_{NT}} \; \underset{8\times8}{\underset{\sim}{T}} \; \underset{8\times1}{\underset{\sim}{p}_{xy}} = \underset{8\times8}{\underset{\sim}{T}^T} \; \underset{8\times1}{\underset{\sim}{R}_{NT}} \; .$$

Let

$$\underset{8\times8}{K_{xy}} = \underset{8\times8}{T^T}\ \underset{8\times8}{K_{NT}}\ \underset{8\times8}{T} \tag{4.46}$$

$$\underset{8\times1}{R_{xy}} = \underset{8\times8}{T^T}\ \underset{8\times1}{R_{NT}}\ , \tag{4.47}$$

Then, the structural system of equations in terms of the global cartesian coordinates is

$$\underset{8\times8}{K_{xy}}\ \underset{8\times1}{p_{xy}} = \underset{8\times1}{R_{xy}}\ . \tag{4.48}$$

Since the structure is a combination of many elements, each element stiffness must be placed into its proper location in the master stiffness matrix. Also the applied load for the element must be positioned into a master load vector. This will give a structural system of equations for the assembled structure. Because of the time consuming and repetitious nature of all of the processes discussed in this chapter, the actual procedure must be done on a digital computer.

Spline Curve Fitting

As mentioned in Chapter 1 the purpose of this study is to investigate arches with both circular and arbitrary geometries which are defined by discrete points on the centroidal line. No problems arise when dealing with circular segments, for they are considered exact; however,

the best method to represent an arbitrary geometrical slope does cause some concern. It is not exact, therefore, it must be represented by mathematical approximations. Within this work the geometry is found by analytically generating a curve between interpolation points. The actual form of curve fitting used is that of spline fitting. This is the analytical counterpart of the draftsman's spline, a tool that cannot only draw smooth curves but also can show the slope and curvature of the curve as continuous functions. A very good explanation of spline curve fitting is given by Pennington (34).

Given a set of interpolation points, i.e., (x_1,y_1), (x_2,y_2), (x_3,y_3),...,(x_n,y_n), a spline fit can be made between two successive points with a cubic polynomial. The curve segments must be matched up such that the first and second derivatives are continuous at each interpolation point. The second derivative of any line segment can be represented by

$$\frac{d^2y}{dx^2} = y'' = F_K \frac{x_{K+1} - x}{d_K} + F_{K+1} \frac{x - x_K}{d_K} \qquad (4.49)$$

where K is the number of the line segment, F_K and F_{K+1} are the second derivatives at the points x_K and x_{K+1}, respectively.

When referring to spline equations the prime term denotes differentiation with respect to x. Also,

$$d_K = x_{K+1} - x_K .$$

The cubic spline equation for each line segment is

$$y = C_{1,K}(x_{K+1}-x)^3 + C_{2,K}(x-x_K)^3 + C_{3,K}(x_{K+1}-x) + C_{4,K}(x_K-x) \qquad (4.50)$$

where $C_{1,K}$, $C_{2,K}$, $C_{3,K}$, and $C_{4,K}$ are the cubic constants and must be determined for each line segment.

An example on the use of this equation is shown in Appendix D.

The cubic constants are calculated using these equations:

$$C_{1,K} = F_K/6d_K$$

$$C_{2,K} = F_{K+1}/6d_K$$

$$C_{3,K} = (y_K/d_K) - F_K(d_K/6)$$

$$C_{4,K} = (y_{K+1}/d_K) - F_{K+1}(d_K/6) .$$

The F's are determined from

$$\underset{nxn}{\tilde{A}} \; \underset{nx1}{\tilde{F}} = \underset{nx1}{\tilde{B}} \qquad (4.51)$$

where n is the number of interpolation points and

$$B_1 = 0$$

$$B_n = 0$$

$$B_K = e_{K+1} - e_K$$

$$z_K = d_K/6$$

$$e_K = (y_K - y_{K-1})/d_{K-1} \quad .$$

Matrix $\underset{\sim}{A}$ is expressed as

$$\underset{\sim}{A} = \left[\begin{array}{c|c|c|c|c|c|c} -1/d_1 & 1/d_1+1/d_2 & -1/d_2 & 0 & \cdots & 0 & 0 \\ z & 2(z_1+z_2) & z & 0 & \cdots & 0 & 0 \\ 0 & z & 2(z_2+z_3) & z_3 & \cdots & 0 & 0 \\ 0 & \vdots & \vdots & \vdots & \vdots & \vdots & \vdots \\ \vdots & \vdots & \vdots & \vdots & \vdots & \vdots & \vdots \\ \vdots & \vdots & \vdots & \vdots & \vdots & \vdots & \vdots \\ 0 & 0 & \cdots & \cdots & z_{n-2} & 2(z_{n-2}+z_{n-1}) & z_{n-1} \\ 0 & 0 & \cdots & \cdots & -1/d_{n-2} & 1/d_{n-2}+1/d_{n-1} & -1/d_{n-1} \end{array}\right]$$

The system of equations in (4.51) is solved using a tri-diagonal equation solver.

In order to apply the spline fit to this particular study, the values of y' and y" are needed. The general expressions for y' and y" are easily obtained by differentiating (4.50) with respect to x. This gives

$$y' = -3C_{1,K}(x_{K+1}-x)^2 + 3C_{2,K}(x-x_K)^2 - C_{3,K} + C_{4,K} \quad (4.52)$$

and

$$y'' = 6C_{1,K}(x_{K+1}-x) + 6C_{2,K}(x-x_K) \quad (4.53)$$

With (4.52) and (4.53) the curvature at any point can be determined by

$$K = \frac{y''}{(1+y'^2)^{3/2}} \quad (4.54)$$

The value of K' can also be calculated at any point with the following equations for y', y", and y'" where

$$y''' = -6C_{1,K} + 6C_{2,K} \quad (4.55)$$

and

$$K' = \frac{(y''' - 3K(1+y'^2)^2 y')}{(1+y'^2)^2} \quad . \quad (4.56)$$

The derivations for K and K' can be found in Appendix E. Having obtained the cubic constants for each line segment, knowing the x value for all interpolation points and nodal points, and using (4.52)-(4.56), the transformation matrix, $\underset{\sim}{T}$, can be determined for each element.

Arc Length Measurement for Each Nodal Point

There are two types of arc length measurements which may be applied. The first is when each nodal point is an interpolation point. This indicates that each

element may differ in arc length. The scheme for each nodal point is

$$S_{n+1} = S_n + \Delta S \quad . \tag{4.57}$$

The initial value of S is given and

$$\Delta S = \int_{x_n}^{x_{n+1}} (1+y'^2)^{1/2} dx \quad . \tag{4.58}$$

The second procedure and by far the more computationally time consuming is by forming n number of elements between interpolation points. The elements with each line segment will have equal arc lengths.

With reference to Fig. 4.6, ΔS can be determined by using (4.58). The equal arc length increment can be calculated using the condition that

$$s = \frac{\Delta S}{n} \tag{4.59}$$

where s = arc length increment

n = number of subdivisions .

Therefore, the general expression for the arc length measurements using equal arc increments between interpolation points is

$$S_{n+1} = S_n + ms \tag{4.60}$$

where the initial value of S is known and

m = 1,2,3,...,n .

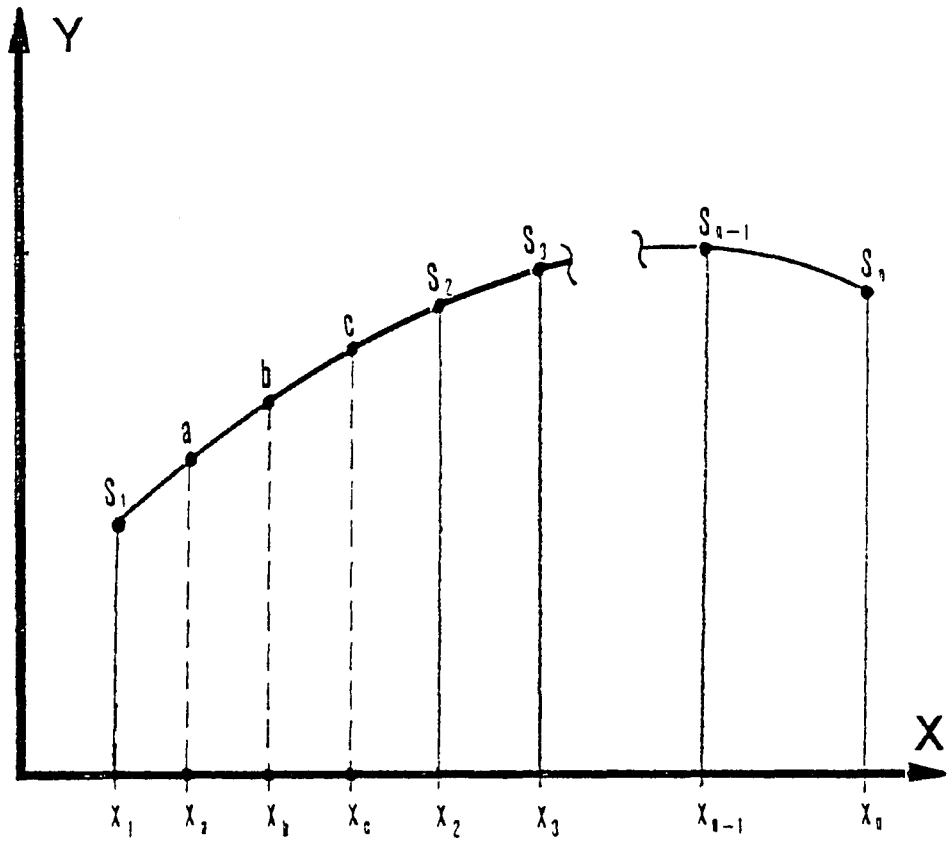

Fig. 4.6. Arc length which has equal subdivisions between interpolation points.

The primary problem with this method is in calculating the x values for the nodal points between the interpolation points. These values can be calculated using the following Newton-Raphson scheme. If it is desired to calculate the x value for point a (Fig. 4.6), the approach would be:

1. x_1, S_1, and S_a are known,
2. x_a must be determined using a Newton-Raphson scheme.

$$x_{i+1} = x_i - \frac{f(x_i)}{f'(x_i)} \tag{4.61}$$

where

$$f(x_i) = S_a - (S_1+I) \tag{4.62}$$

$$I = \int_{x_1}^{x_i} (1+y'^2)^{1/2} dx \tag{4.63}$$

$$f'(x_i) = (1+y'^2)^{1/2} \quad . \tag{4.64}$$

This iteration process will yield x_a. The same procedure would be used to calculate x_b and x_c. Since the method is an approximate scheme, the x values of the nodal points will not be exact. This will insert another approximation which could cause a decrease in accuracy of the solution scheme.

CHAPTER 5

SOLUTION SCHEMES

Stability of arches which undergo large deflections indicates that the structural problem is nonlinear. There are two major types of structural nonlinearities, material and geometric. Material nonlinear analysis is based upon an experimental stress-strain curve. Because of the possible randomness of experimental data, the solution of such problems cannot be exact and depends primarily on the accuracy of the data. Whereas geometrically nonlinear problems are based upon a mathematical equation, the accuracy of such problems depends upon the accuracy of the governing equations. In both types of nonlinear problems approximations may lead to solution errors. In an effort to avoid an increase in these errors an appropriate solution scheme is needed.

Solution Algorithms for Geometrically Nonlinear Problems

The structural problems discussed in this study are geometrically nonlinear finite element problems. Within this section the state-of-the-art for solving such problems will be reviewed.

The first algorithm to be explained is the Newton-Raphson scheme. The method itself is, of course, not new,

however, its application to nonlinear finite element problems was investigated by Stricklin, Haisler, and Von Riesemann (39). The equations of equilibrium for the entire system can be obtained as an application of Castigliano's Theorem which states that

$$\frac{\partial U}{\partial \underset{\sim}{p}} = \underset{\sim}{R} \quad , \tag{5.1}$$

where $\underset{\sim}{R}$ is independent of $\underset{\sim}{p}$,

U = strain energy function

$\underset{\sim}{p}$ = nodal degrees of freedom

$\underset{\sim}{R}$ = generalized applied forces

Equation (5.1) can be written as a function of p,

$$f(\underset{\sim}{p}) = \frac{\partial U}{\partial \underset{\sim}{p}} - \underset{\sim}{R} = \underset{\sim}{0} \quad . \tag{5.2}$$

Using the Taylor Series expansion,

$$f(\underset{\sim}{p}+\Delta\underset{\sim}{p}) = f(\underset{\sim}{p}) + \Delta\underset{\sim}{p} f'(\underset{\sim}{p}) + \frac{1}{2!} \Delta\underset{\sim}{p}^T \Delta\underset{\sim}{p} f''(\underset{\sim}{p}) + \ldots \tag{5.3}$$

Neglecting the higher order terms of (5.3), and acknowleging the fact that at an equilibrium configuration $f(p+\Delta p)$ vanishes if the proper correction, Δp, is used, the following expression can be derived

$$f(\underset{\sim}{p}) + \Delta\underset{\sim}{p} f'(\underset{\sim}{p}) = \underset{\sim}{0} \quad . \tag{5.4}$$

Since,

$$f'(\underset{\sim}{p}) = \frac{\partial^2 U}{\partial \underset{\sim}{p}^2} \quad . \tag{5.5}$$

Substituting (5.5) and (5.2) into (5.4), yields the following system of equations:

$$\frac{\partial^2 U}{\partial \underset{\sim}{p}^2} \underset{\sim}{\Delta p} = \underset{\sim}{R} - \frac{\partial U}{\partial \underset{\sim}{p}} \tag{5.6}$$

where $\frac{\partial^2 U}{\partial \underset{\sim}{p}^2}$ is the instantaneous stiffness matrix,

$\underset{\sim}{\Delta p}$ is the Newton-Raphson displacement correction, and

$\underset{\sim}{R} - \frac{\partial U}{\partial \underset{\sim}{p}}$ is the load residual .

The displacement incrementing scheme is

$$\underset{\sim}{p}_{i+1} = \underset{\sim}{p}_i + \underset{\sim}{\Delta p} \; . \tag{5.7}$$

The process continues until some convergence criteria is met. The scheme begins by

$$\frac{\partial^2 U}{\partial \underset{\sim}{p}^2} (\underset{\sim}{p}_o) \; \underset{\sim}{\Delta p} = \underset{\sim}{R} \quad . \tag{5.8}$$

If the entire load is applied initially, the method will most likely diverge. Therefore, it is recommended to break the load into various steps and have the solution converge at each step. The selection of the magnitude of the load step is vital and will be discussed later. A graphical representation of this solution scheme is shown in Fig. 5.1.

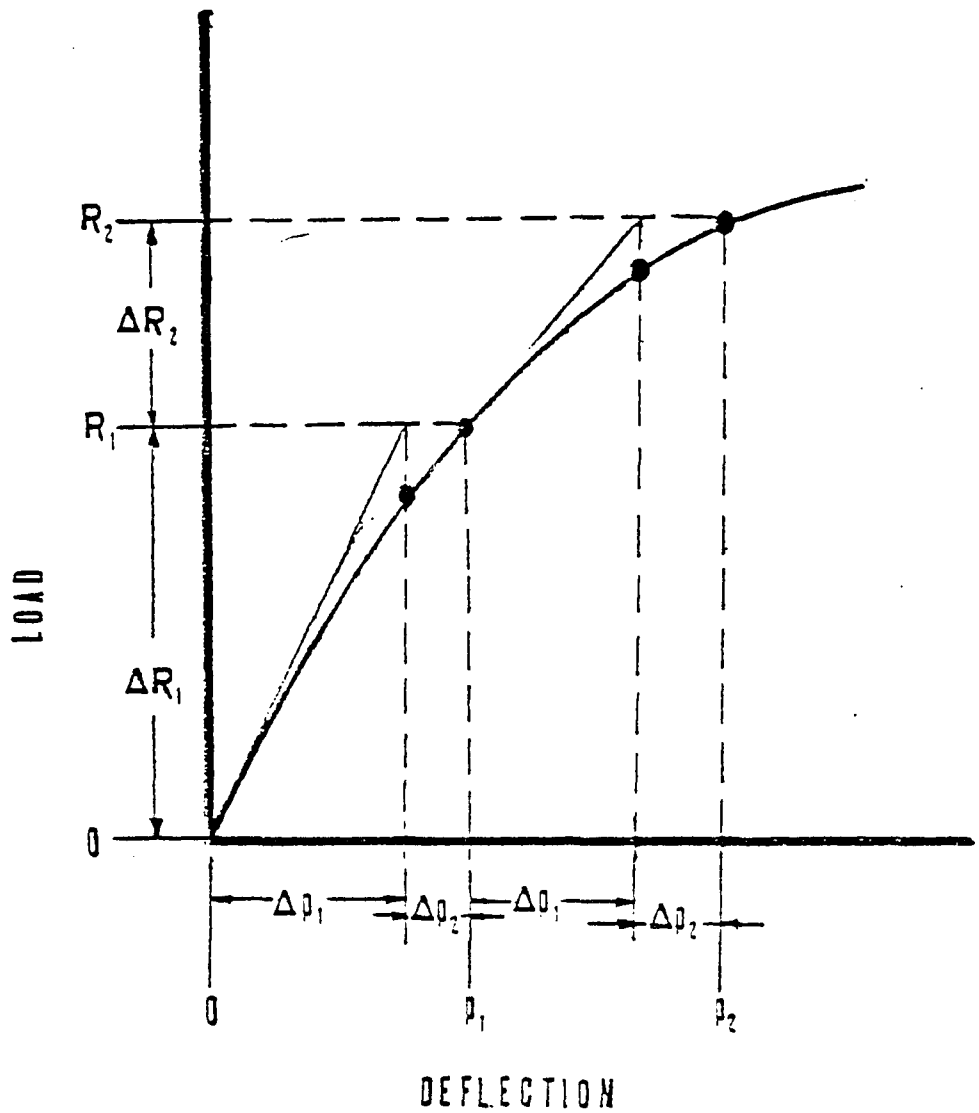

Fig. 5.1. Newton-Raphson iteration scheme.

Another area of concern is in the calculation of the master stiffness matrix. This process is very costly. Therefore, it may be possible to update the stiffness matrix at selected points rather than updating it at each iteration. This is called the Modified Newton-Raphson form. How often the updating occurs depends upon the nonlinear nature of the problem and the experience of the user.

The next solution scheme to be examined is a form of the perturbation method. This method was used by Walker (41), Connor and Morin (6), and Yokoo, Nakamura, and Uetani (46). The purpose of this method is to obtain "path parameters" which are assigned values to aid in the determining of the stepsize along the equilibrium path. It is actually a form of the predictor corrector type methods. It is excessively expensive and has no apparent advantage in general nonlinear analysis. However, it has shown some promise in postbuckling analysis.

The final scheme to be discussed is an initial value formulation where the generalized forces can be expressed as

$$\underset{\sim}{R} = \lambda \underset{\sim}{\bar{R}} \quad , \tag{5.9}$$

λ is a normalizing factor.

Substituting (5.9) into (5.8) yields

$$\underset{\sim}{\frac{\partial^2 U}{\partial p^2}} \; \underset{\sim}{\frac{dp}{d\lambda}} = \underset{\sim}{\bar{R}} \, . \tag{5.10}$$

This system is in the form of first order differential equations which can be solved by a Runge-Kutta scheme. This method has the advantage in that the absolute value of $\underset{\sim}{R}$ has little significance since a normalization process occurs. This procedure is similar to Stricklin and Haisler's self-correcting method (38). In its present form the self-correcting method is inaccurate and requires many expensive equilibrium correction steps.

Geometrically nonlinear problems generally deal with structural stability as either limit point analysis or bifurcation analysis. In both cases the calculation of the critical point is of utmost importance. The region near the critical point is very sensitive, for a small change in load may give a corresponding large change in deflection. Common within the solution scheme review is the fact that the process for calculating the critical point is based upon load incrementation. Using such a scheme, the process of choosing the load step is crucial. There are a multitude of such procedures, and the more important ones will be discussed in the following paragraphs.

The easiest procedure to implement and the least effective is the method using pre-established load increments or the constant load increment. There are three primary problems with this scheme: (1) the critical points

may be missed entirely, (2) a too large of a load step may cause the scheme to diverge, and (3) the method does not account for the degree of nonlinearity within the problem.

Mau and Gallagher (31) employed an extrapolation procedure to determine the load steps and to calculate the limit point. The loading parameter was represented as a polynomial where the value of the determinant was the independent variable. Knowing the value of the determinant and calculating the coefficients of the polynomial, the loading parameter could be calculated. At the critical point the determinant is zero, therefore, the loading parameter at that point can be determined. The method is effective for calculating the limit point.

The next two methods of load incrementation deserve more attention, for a numerical study was made to determine their effectiveness. The first of these two schemes was the Adaptive Step Size method developed by Schmidt (37). The scheme is based upon the Contractive Mapping Theorem which assures convergence and a computable error bound provided the contractive constant is known. With the use of the contractive constant two equations can be used to either increase or decrease the load step size, depending upon the degree of nonlinearity of the previous equilibrium configuration. This method was tested on a simple geometric nonlinear finite element problem and demonstrated some merit;

however, the scheme was extremely sensitive to the initial load step. Because of the high degree of sensitivity for such a simple problem, an effort to use it on a larger, more complex system appeared to be a risk.

The last load incrementation scheme to be discussed is the current Stiffness Parameter method developed by Bergan and Soreide (4). This method is based upon the stipulation that the change in the instantaneous stiffness parameter should be the same for all load steps. A detailed discussion on this method is given in Appendix F. The same problem tested using the Adaptive Step Size method was also tested with this method. The current stiffness parameter method appeared much more effective even with a linear extrapolation procedure. The procedure appears to have merit and may warrant the usage on a larger, more complex problem. The method was not used on the nonlinear arch problem in this work, for the procedure underwent many operations to obtain the next load step. For a very large and complex problem it would seem to add excessive computational expense.

An incrementing procedure that has not been discussed thus far is displacement incrementation. It is a common belief among finite element researchers that this process is expensive and, if used, should be used near the critical points for stability analysis. This was the case of Pian and Tang (33), Zienkiewicz (48), and Stricklin

(40) who used a load incrementation process until a region near the critical point was reached at which time a change was made to displacement incrementation.

After a thorough investigation of various solution schemes for geometrically nonlinear finite element problems very little mention was made of rate equations, except for Haisler and Stricklin's self-correcting method (38) and Richard and Blacklock's (36) solution scheme for inelastic problems both of which differentiated the displacement vector with respect to a normalized load parameter. DaDeppo and Schmidt (15) and Qaqish (35) used rate equations for nonlinear arch problems. The displacement vector was differentiated with respect to time, and incrementations were made with displacements rather than loads.

The nonlinear arch problems that are investigated in this work use a solution scheme that is a variation of the procedure used by DaDeppo and Schmidt (15). The actual method used is discussed step-by-step below:

The initial structural system of equations is

$$\underset{\sim}{K}(\underset{\sim}{p}_i)\dot{\underset{\sim}{p}}_1 = \dot{\underset{\sim}{R}} \quad , \tag{5.11}$$

where i indicates the step number, $\underset{\sim}{K}(\underset{\sim}{p}_i)$ is the instantaneous stiffness matrix, $\dot{\underset{\sim}{p}}_1$ is the nodal displacement rate, and $\dot{\underset{\sim}{R}}$ is the load rate.

These equations are solved using a fourth order Runge-Kutta scheme with Simpson's coefficients. The solution steps are numerically listed below:

1. The first step is to solve for $\dot{\underset{\sim}{p}}_1$ using a Gaussian elimination equation solver

$$\underset{\sim}{K}_1(\underset{\sim}{p}_i)\dot{\underset{\sim}{p}}_1 = \dot{\underset{\sim}{R}} \tag{5.12}$$

2. Once $\dot{p}_1$ is calculated an incremental time step is obtained. This time step is of vital importance, for it aids in the calculation of the displacement correction terms used in the Runge-Kutta scheme. The time step, δt, is determined by using the following equation

$$\delta t = \frac{\delta p_{max}}{|\dot{\underset{\sim}{p}}_1|} , \tag{5.13}$$

where δp_{max} is a scalar and a pre-established maximum displacement increment and $|\dot{\underset{\sim}{p}}_1|$ is the magnitude of the displacement rate calculated in (5.12).

3. After δt is obtained, the first displacement correction vector must be calculated using

$$\underset{\sim}{\delta p}_1 = \delta t \, \dot{\underset{\sim}{p}}_1 . \tag{5.14}$$

4. The next step is to form the stiffness matrix

$$\underset{\sim}{K}_2(\underset{\sim}{p}_i + \frac{1}{2}\,\underset{\sim}{\delta p}_1) \rightarrow \underset{\sim}{K}_2. \tag{5.15}$$

5. Now it is necessary to solve for $\dot{\underset{\sim}{p}}_2$ using

$$\underset{\sim}{K}_2 \dot{\underset{\sim}{p}}_2 = \dot{\underset{\sim}{R}} \quad . \tag{5.16}$$

6. Step six determines the second displacement correction, $\delta\underset{\sim}{p}_2$.

$$\delta\underset{\sim}{p}_2 = \delta t \, \dot{\underset{\sim}{p}}_2 \tag{5.17}$$

7. Step seven forms

$$\underset{\sim}{K}_3(\underset{\sim}{p}_i + \frac{1}{2} \delta\underset{\sim}{p}_2) \Rightarrow \underset{\sim}{K}_3 \quad . \tag{5.18}$$

8. The next step solves for $\dot{\underset{\sim}{p}}_3$,

$$\underset{\sim}{K}_3 \dot{\underset{\sim}{p}}_3 = \dot{\underset{\sim}{R}} \quad . \tag{5.19}$$

9. Step nine calculates the third displacement correction, $\delta\underset{\sim}{p}_3$, using

$$\delta\underset{\sim}{p}_3 = \delta t \, \dot{\underset{\sim}{p}}_3 \quad . \tag{5.20}$$

10. Step ten forms

$$\underset{\sim}{K}_4(\underset{\sim}{p}_i + \delta\underset{\sim}{p}_3) \Rightarrow \underset{\sim}{K}_4 \quad . \tag{5.21}$$

11. Step eleven solves for $\dot{p}_4$,

$$\underset{\sim}{K}_4 \dot{\underset{\sim}{p}}_4 = \dot{\underset{\sim}{R}} \tag{5.22}$$

12. The next step is to calculate the fourth displacement correction vector, $\delta\underset{\sim}{p}_4$.

$$\delta\underset{\sim}{p}_4 = \delta t \, \dot{\underset{\sim}{p}}_4 \tag{5.23}$$

13. At this point the next displacement vector is calculated from (fourth order Runge-Kutta scheme with Simpson's coefficients)

$$\underset{\sim}{p}_{i+1} = \underset{\sim}{p}_i + 1/6\ (\underset{\sim}{\delta p}_1 + 2\underset{\sim}{\delta p}_2 + 2\underset{\sim}{\delta p}_3 + \underset{\sim}{\delta p}_4)\ . \tag{5.24}$$

14. The next step is to apply the Newton-Raphson iteration scheme. The details of this process are stated below:

    a. The first step is to form the instantaneous stiffness matrix at the current displacement level,

$$\underset{\sim}{K}(\underset{\sim}{p}^j_{i+1})\ , \tag{5.25}$$

    where j is the iteration number.

    b. The next step is to calculate the load for this displacement step by this equation

$$\underset{\sim}{R} = t\,\dot{\underset{\sim}{R}}\ . \tag{5.26}$$

    c. The next step is to determine the residual or

$$\underset{\sim}{\delta} = \underset{\sim}{R} - \frac{\partial U}{\partial \underset{\sim}{p}}\ (\underset{\sim}{p}^j_{i+1}) \tag{5.27}$$

    where $\frac{\partial U}{\partial \underset{\sim}{p}}\ (\underset{\sim}{p}^j_{i+1})$ are the equilibrium equations at the current displacement.

d. At this point it becomes necessary to solve for the correction $\underset{\sim}{\Delta p}$ using the following system of equations:

$$\underset{\sim}{K}(\underset{\sim}{p}^{j}_{i+1})\ \underset{\sim}{\Delta p} = \underset{\sim}{\delta} \quad . \tag{5.28}$$

e. This step calculates the new displacement

$$\underset{\sim}{p}^{j+1}_{i+1} = \underset{\sim}{p}^{j}_{i+1} + \underset{\sim}{\Delta p} \tag{5.29}$$

f. Return to step c and recalculate $\underset{\sim}{\delta}$. If $\underset{\sim}{\delta}$ meets a pre-established convergence criteria, the iteration process is terminated and a return is made to step 1. If the convergence criteria is not satisfied, form the new instantaneous stiffness matrix and repeat steps d and e.

Since the Runge-Kutta scheme is a marching procedure, the solution will go through the entire cycle, steps 1-14, until the determinant of the instantaneous stiffness matrix goes to zero or goes from plus to minus.

CHAPTER 6

EXPLANATION OF THE COMPUTER PROGRAM

Because of the complexities of the geometrically nonlinear arch problem and the large number of mathematical operations to solve such a problem, a finite element computer program was written to analyze arches which undergo large deflections. The arches analyzed have various geometries, various loading conditions, and various constraints. An explanation of the program is given within this chapter. The description of the program includes a discussion of the main program and all major subroutines. Flow charts are given to represent the computer logic.

To begin, Fig. 6.1 gives a block diagram of the subroutines called from the main program. The main program performs two functions: (1) enters necessary data, and (2) calls the major subroutines. A brief description of the data entered is listed below.

Data Entered into Main Program

1. The number of interpolation points for spline curve fitting (NIPS).
2. The number of radii for an arch with segmentally circular geometry (NRAD).

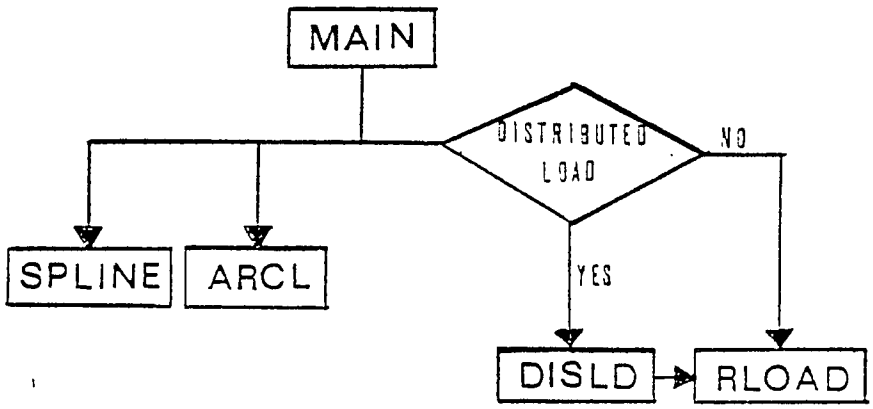

Fig. 6.1. General block diagram of program.

3. The total number of finite elements in the arch (NEL).
4. The total number of node points in the arch (NPTS).
5. Young's Modulus (EM).
6. The thickness of the arch element (TH).
7. The height of the arch element (Z2).
8. The subtending angle of the circular arch (AANG).
9. The X and Y coordinates of the interpolation points.
10. The nodal external load (the one dimensional array RL).
11. The constraint conditions (the one dimensional array NSP).

Description of Subroutines Called from Main Program

Subroutine SPLINE

If the arch being analyzed has an arbitrary geometry, i.e., the geometry is defined by data points, this subroutine enters the X and Y coordinates of the interpolation points, it calls SUBROUTINE SPLICO which calculates the cubic spline coefficients for each line segment, and places the X and Y coordinates into a master coordinate array. If the arch being analyzed has a circular geometry, this subroutine only places the X and Y coordinates into a master coordinate array.

Subroutine ARCL

This subroutine calculates the arc measurement, the value of the slope, the value of y", and the curvature at each nodal point. The flowchart for this subroutine is shown in Fig. 6.2.

Subroutine RLOAD

This subroutine enters all information either read into or calculated in the MAIN program and subroutines SPLINE and ARCL, it performs all operations discussed in Chapter 5, it calculates the rotation at each node point, and it calculates designated nodal moments and axial forces.

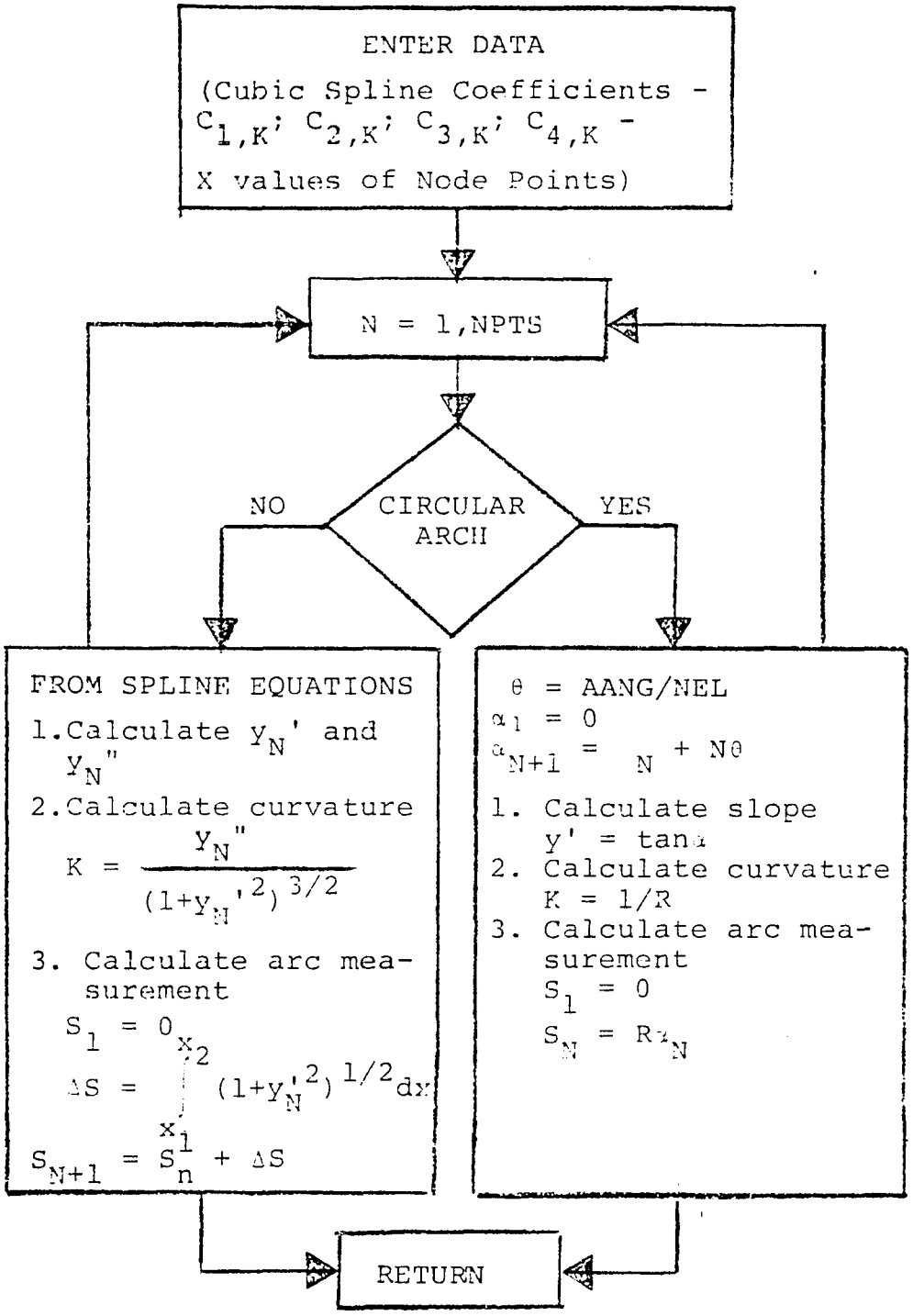

Fig. 6.2. Flow chart for SUBROUTINE ARCL.

The general flow chart is shown in Fig. 6.3. The displacement rates are obtained by using a banded Gaussian limination equation solver. This subroutine is called GAUSL. The displacement increments, $\Delta \underset{\sim}{p}$, are calculated using a banded Gaussian limination equation solver (SUBROUTINE SOLV). The rotations are calculated in SUBROUTINE ROTA, and the axial forces and moments are calculated in SUBROUTINE MOMENT. The determinant of the instantaneous stiffness matrix is calculated in SUBROUTINE STKK. This subroutine is in double precision and uses a Gaussian elimination scheme with pivoting. The matrix of $\frac{\partial U}{\partial \underset{\sim}{p}}$ is obtained by use of SUBROUTINES RESID and EQUIL. Finally, the instantaneous stiffness matrix is formed in SUBROUTINE ASSTIF. A detailed discussion of this subroutine and the various subroutines it calls is given in the following paragraphs.

SUBROUTINE ASSTIF calls SUBROUTINE SKARCH which forms the stiffness for each arch element and assembles each element into a banded master stiffness matrix. The block diagram for SUBROUTINE ASSTIF is shown in Fig. 6.4. A brief explanation of the subroutines called is discussed below.

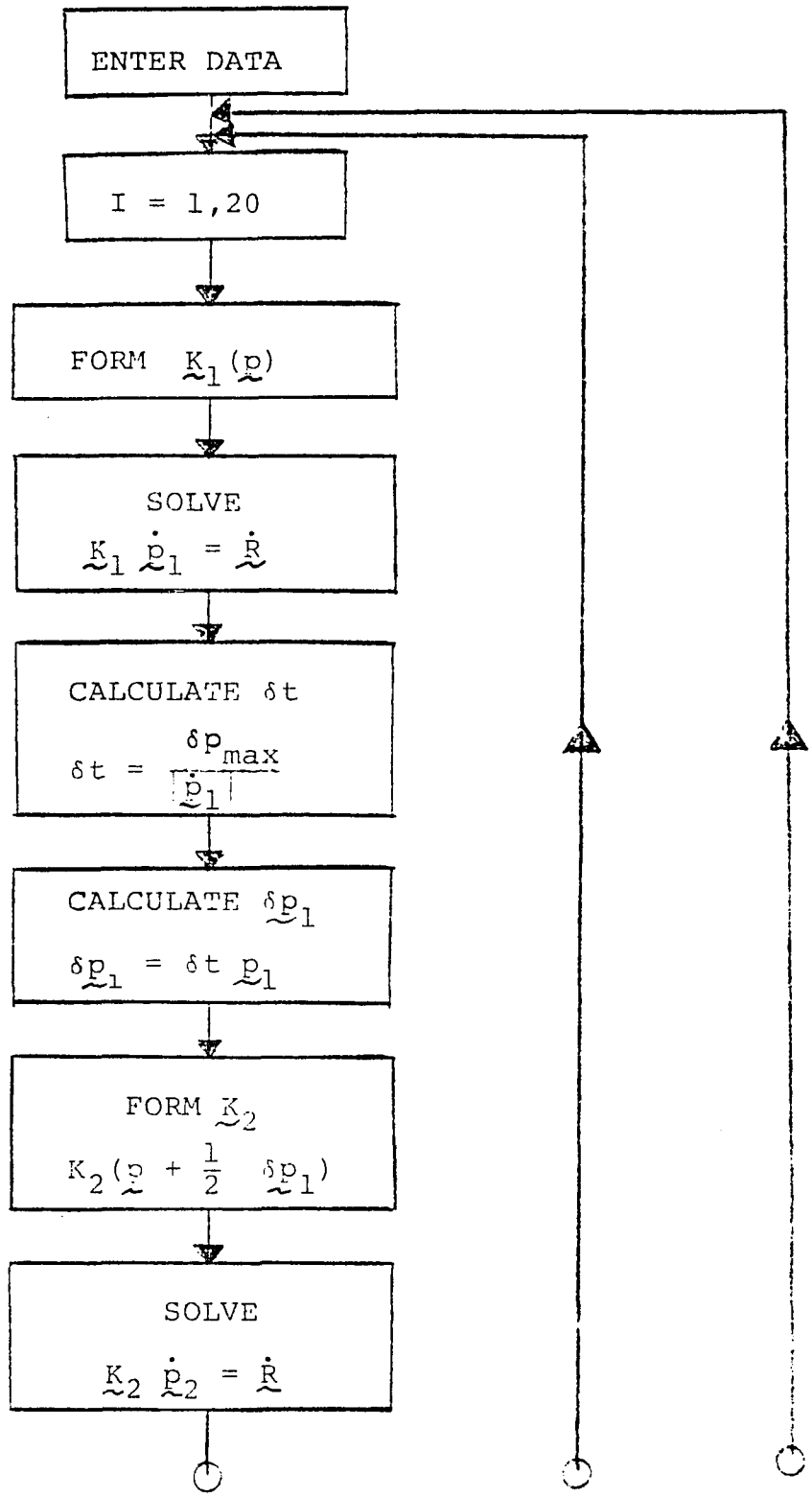

Fig. 6.3. Flow chart for SUBROUTINE RLOAD.

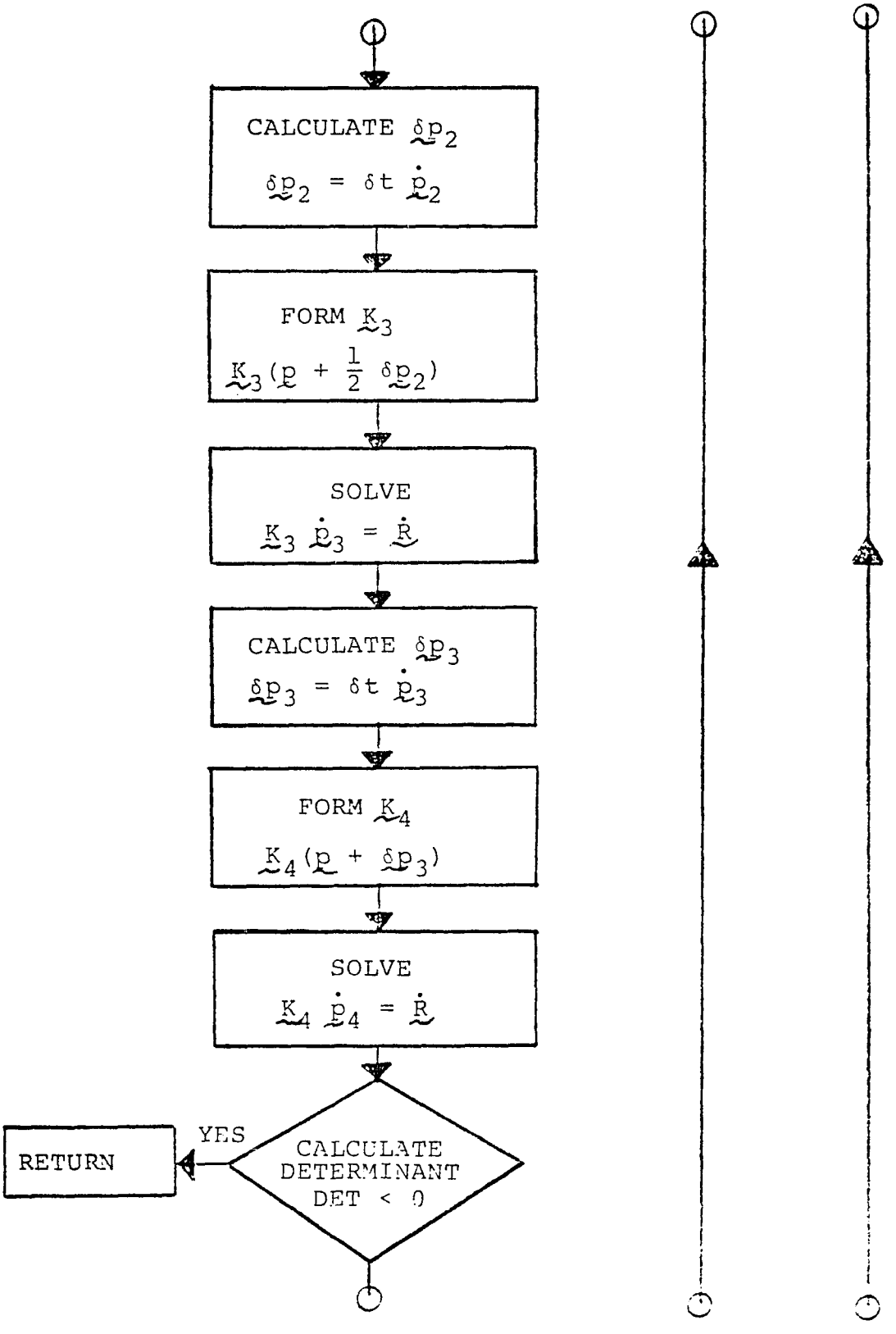

Fig. 6.3--Continued.

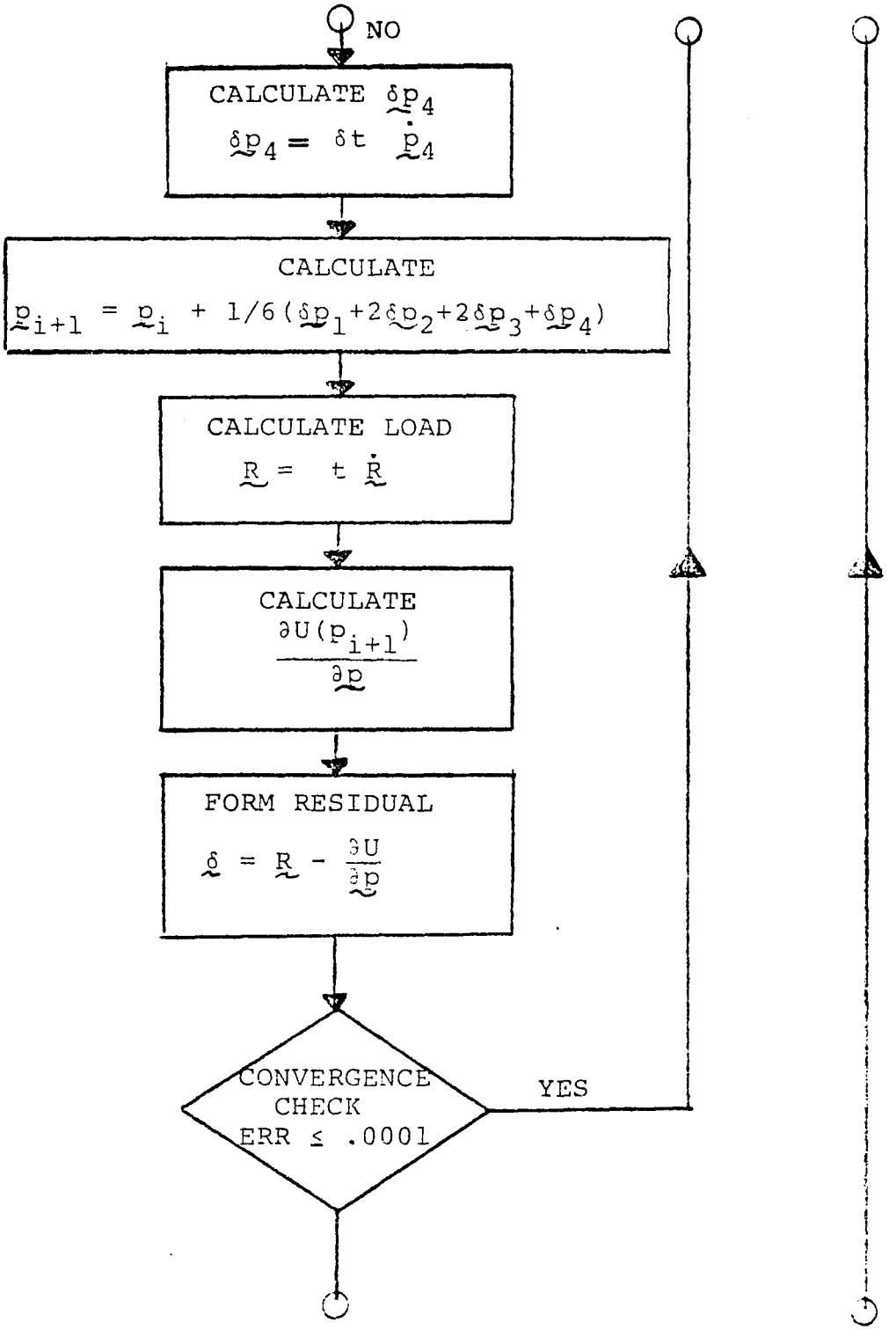

Fig. 6.3. Flow chart for SUBROUTINE RLOAD--Continued.

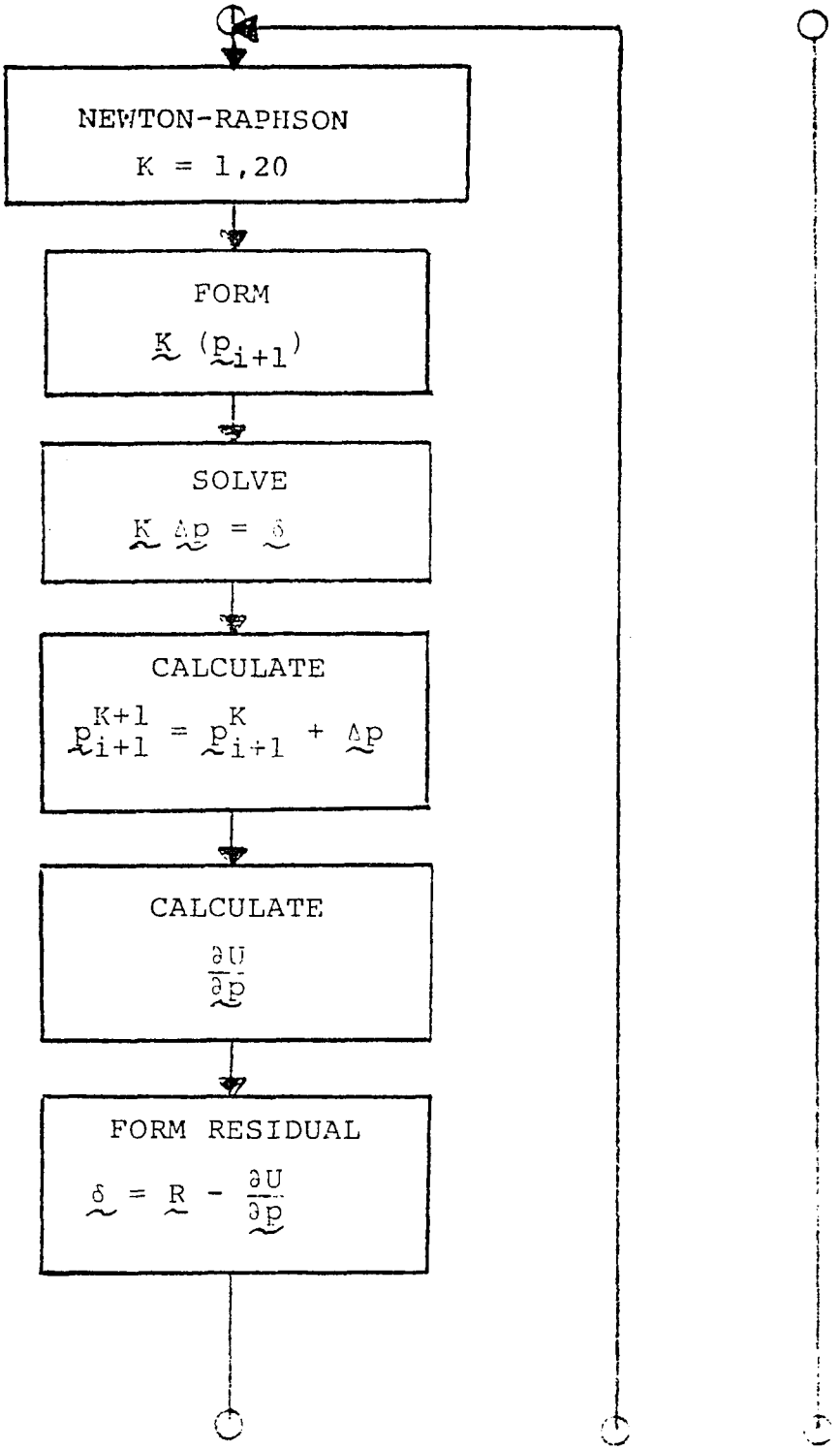

Fig. 6.3--Continued.

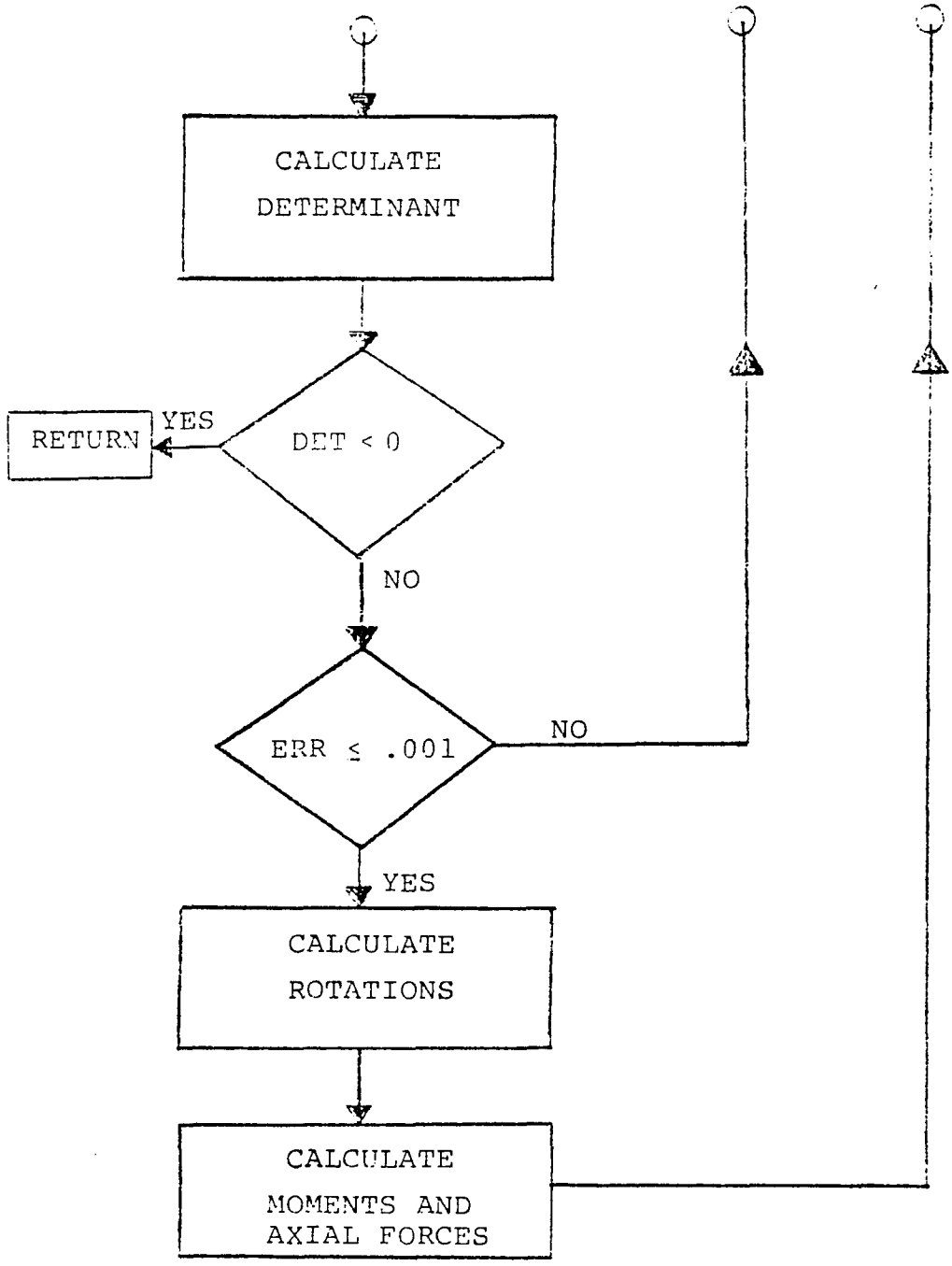

Fig. 6.3. Flow chart for SUBROUTINE RLOAD.

a. SUBROUTINE FORMB calculates matrix $\underset{\sim}{B}$ which is shown in Eq. (4.10).

b. SUBROUTINE XKPSUB calculates K' for arches with arbitrary geometries.

c. SUBROUTINE ECOMB calculates the various displacement components, U_N, U_N', U_N'', U_t, U_t', and U_t'', and their products.

d. SUBROUTINES UNS, UTS, DUTS, DUNS, and D2US calculate $\frac{\partial U_N}{\partial p}$, $\frac{\partial U_t}{\partial p}$, $\frac{\partial U_{N'}}{\partial p}$, $\frac{\partial U_{t'}}{\partial p}$, $\frac{\partial U_{N''}}{\partial p}$, and $\frac{\partial U_{t''}}{\partial p}$, respectively which are needed in SUBROUTINE ECOMB. These values are determined at the various Gauss sampling points which are used in the numerical integration scheme.

e. SUBROUTINE TRANS forms the element transformation matrix, $\underset{\sim}{T}$, which is shown in (4.43).

Subroutine DISLD

If the problem calls for distributed loading, this subroutine determines the nodal consistent loading vector. This formulation is discussed in Chapter 4. Matrix $\underset{\sim}{T}_{u,p}$ which is defined by Eq. (4.39) is formed in SUBROUTINE TRANL. The element consistent load vector is transformed

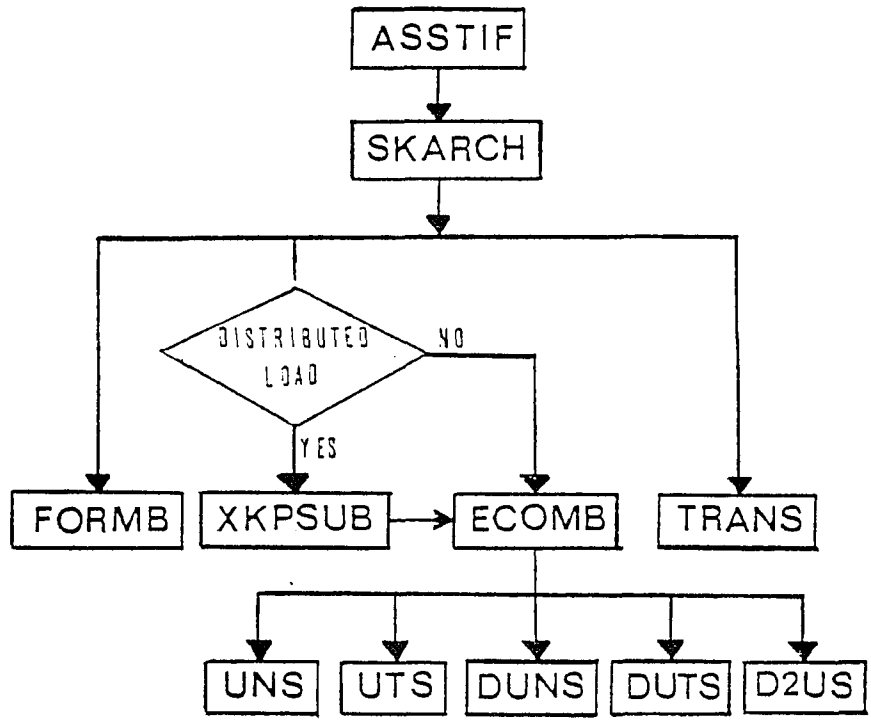

Fig. 6.4. Block diagram for SUBROUTINE ASSTIF.

into the global load vector by using the transformation matrix, $\underset{\sim}{T}$. The flow chart for this subroutine is shown in Fig. 6.5.

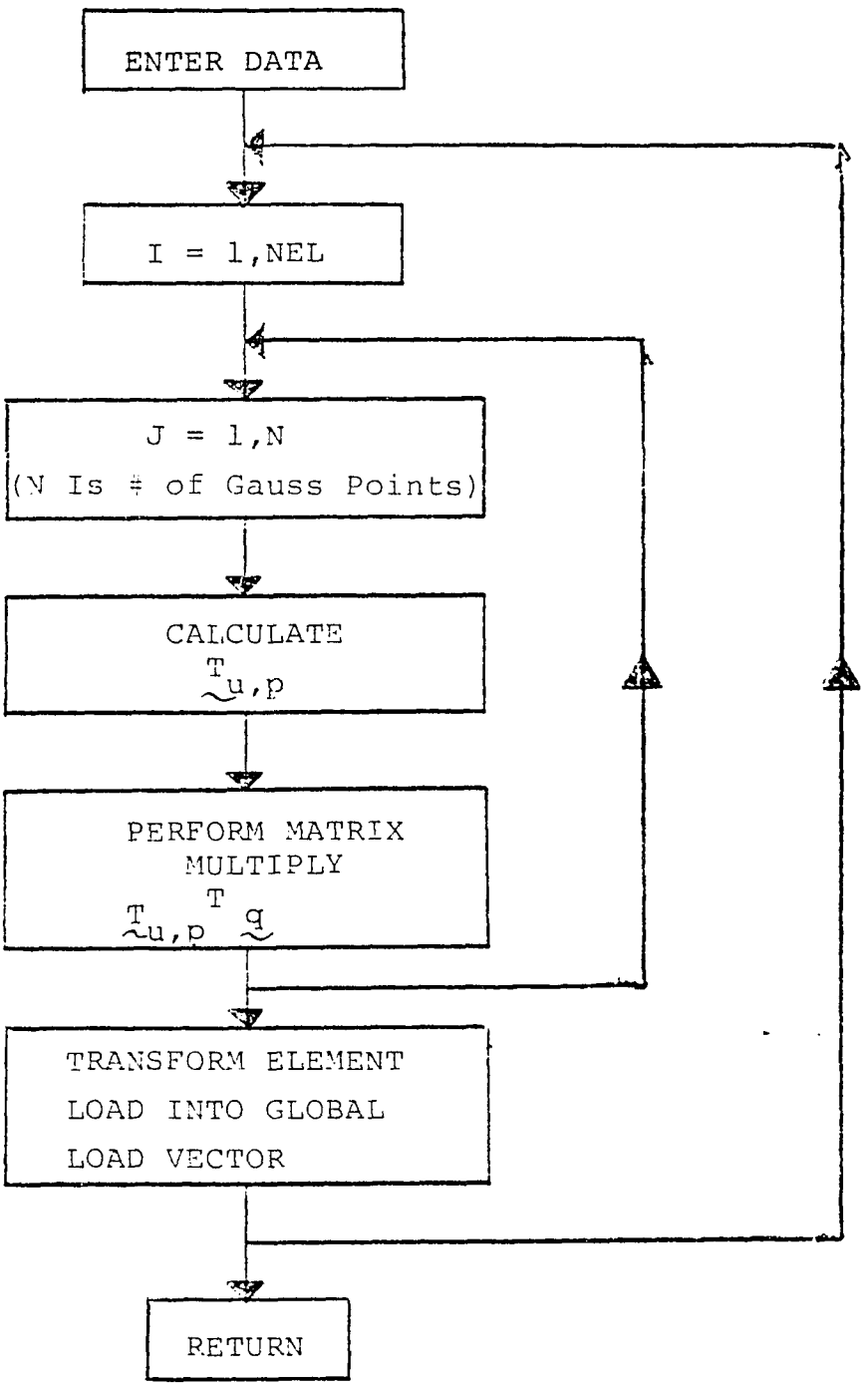

Fig. 6.5. Flow chart for SUBROUTINE DISLD.

CHAPTER 7

DISCUSSION OF PROGRAM RESULTS

Within this chapter a variety of structural problems are solved to study the accuracy, the cost, and the capabilities of the computer program which was explained in Chapter 6. Several structural problems with known solutions are used to test the accuracy, the cost, and the capabilities of the program. The remaining problems are used primarily to demonstrate the extended capabilities of the program. These test problems were run on both the DEC-10 system and the CDC SYBER 175 at The University of Arizona.

Application of the Boundary Conditions to a Fixed End Problem

The initial step in solving the fixed end problem is to apply the boundary conditions to the governing nonlinear differential equations of (3.23) and (3.25), which are

$$(1+\varepsilon_c)\ \cos\beta = (1 + U_t' - KU_N) \qquad (3.23)$$

and

$$(1+\varepsilon_c)\ \sin\beta = (U_N' + KU_t)\ . \qquad (3.25)$$

A general fixed end problem is shown in Fig. 7.1. The structure is fixed at point 1. The following

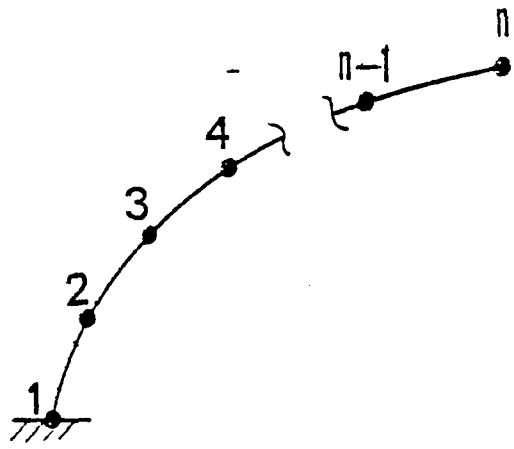

Fig. 7.1. General fixed end problem.

constraints must be applied at this point. The rotation, β_1, the normal displacement component, U_{N_1}, and the tangential displacement component, U_{t_1}, must all be equal to zero. Putting these conditions into (3.23) and (3.25) yields in terms of rates

$$U_{t_1}' = \varepsilon_{c_1} \tag{7.1}$$

and

$$U_{N_1}' = 0 \quad . \tag{7.2}$$

In order to solve the problem the necessary constraints must be inserted into the governing equations

$$\underset{\sim}{K}_{xy}\, \dot{\underset{\sim}{p}}_{xy} = \dot{\underset{\sim}{R}}_{xy} \tag{7.3}$$

where $\underset{\sim}{K}_{xy}$ is the global instantaneous stiffness matrix

$\dot{p}_{xy}$ is the matrix representation of the global degrees of freedom rate equations

$\dot{R}_{xy}$ is the global load rate vector.

The constrained system of equations will be solved using the procedure discussed in Chapter 5.

Nonlinear Cantilever Beam

The first test problem was that of a nonlinear cantilever beam. The cantilever beam is approximated using the nonlinear arch finite element with a radius of curvature equal to 1.E+04. The initial loading case studied was a vertical downward concentrated load, P, at the tip. This is shown in Fig. 7.2. The dimensions of the beam are L = 200 in., b = 2 in., and h = 2 in. A plot of the nondimensionalized deflection at the tip is also shown in Fig. 7.2. The nonlinear arch element solution is compared with that of an analytical solution calculated from the following set of equations

$$\frac{PL^2}{EI} = 2\alpha + \frac{11}{15}\alpha^3 + \frac{1481}{6300}\alpha^5 \tag{7.5}$$

$$\frac{U_c}{L} = \frac{2}{3}\alpha - \frac{19}{315}\alpha^3 + \frac{283}{69300}\alpha^5 \tag{7.6}$$

which were derived by DaDeppo and Schmidt (13).

As can be seen from the graph the results are initially identical and drift slightly with an increase in

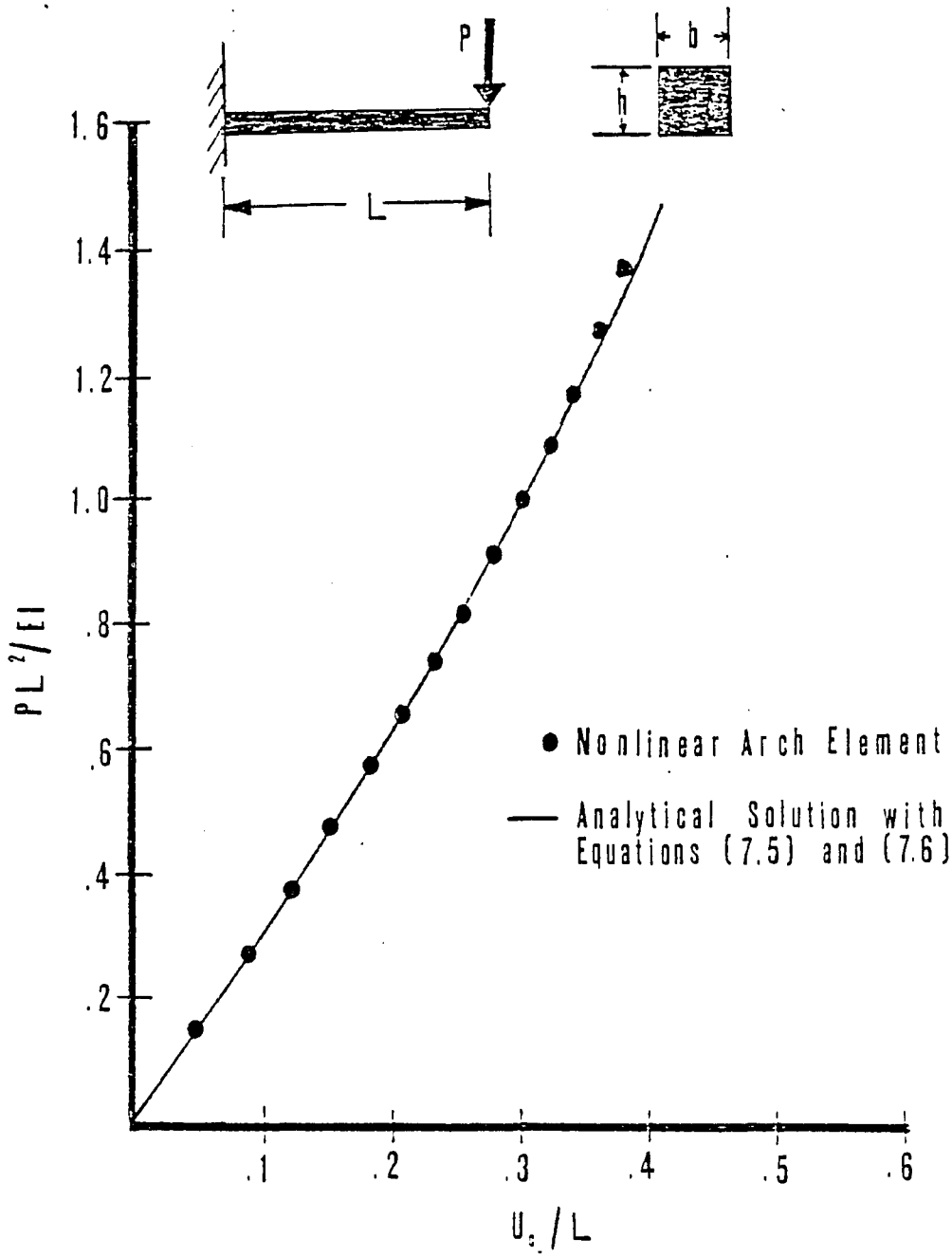

Fig. 7.2. Nondimensionalized load-deflection curve for nonlinear beam with a concentrated load at the tip.

load. The largest % error occurs at the final solution point, and it is equal to 1.274%. Both one and two element models of the beam were tested on this problem, and the results were identical for both models.

The second problem tested was the nonlinear cantilever beam with a uniformly distributed load applied over the entire length of the beam. The dimensions of the beam were the same as those for the first problem. The nonlinear arch element solution is compared to an analytical solution calculated by DaDeppo and Schmidt (13) using the following equations:

$$\frac{WL^3}{EI} = 6\alpha + \frac{41}{20}\alpha^3 + \frac{117039}{184800}\alpha^5 \qquad (7.7)$$

$$\frac{U_c}{L} = \frac{3}{4}\alpha - \frac{13}{160}\alpha^3 + \frac{7643}{739200}\alpha^5 \ . \qquad (7.8)$$

The uniformly distributed load was modeled using the finite element consistent load method explained in Chapter 4.

The results of the nonlinear beam problem with a uniformly distributed load are represented in Fig. 7.3. Similar to the first test problem the results of the nonlinear arch element and the analytical solution were initially the same; however, they drifted with an increase in the load intensity. The maximum % error occurred at the final solution point and was equal to 1.854%. The problem

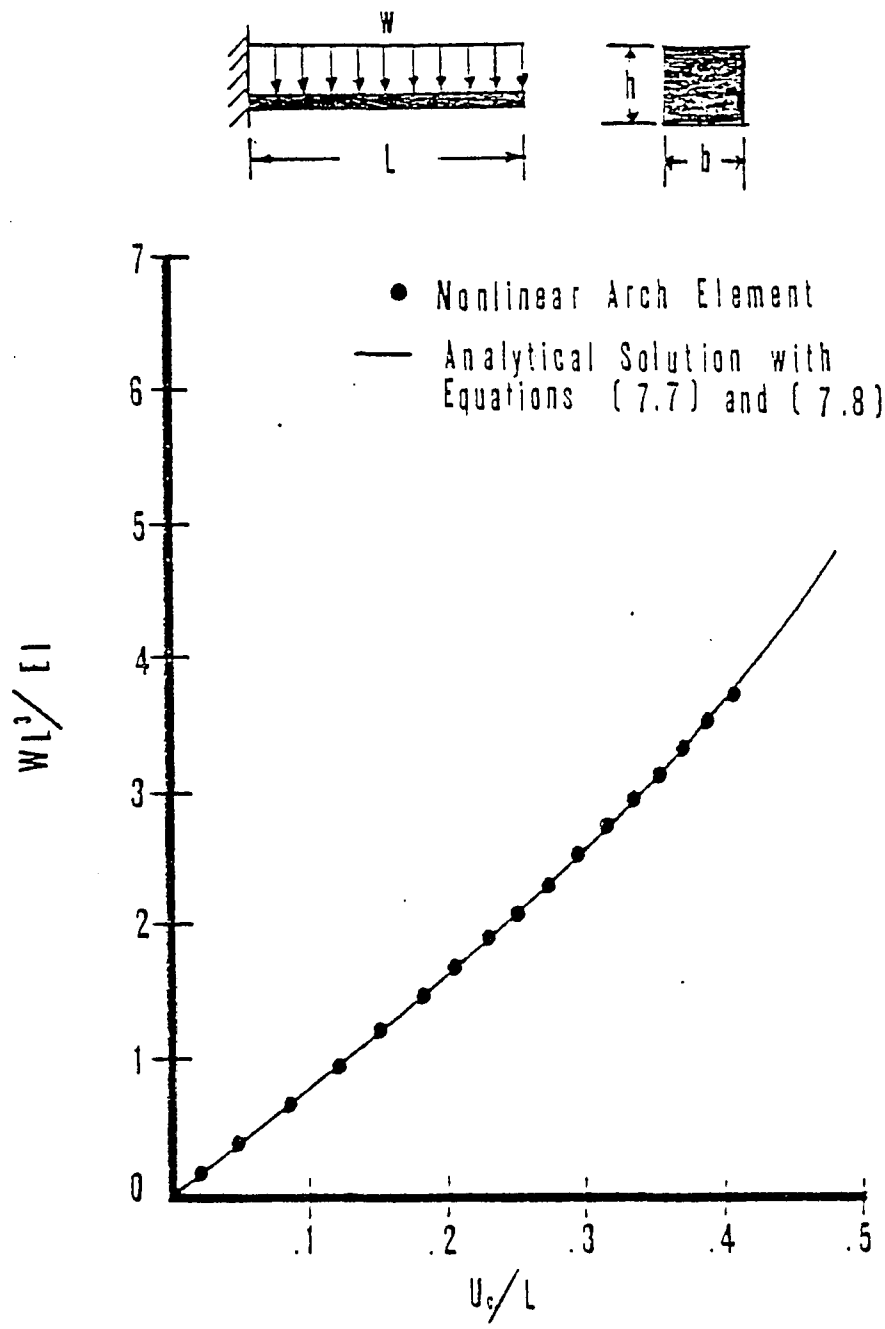

Fig. 7.3. Nondimensionalized load-deflection curve for a nonlinear beam with a uniformly distributed load.

was tested with both one and two element models, and the results were nearly identical.

Clamped Circular Arches

The problems that follow are the initial stability analysis test cases. The nonlinear arch problems investigated have some common characteristics which are:

1. All of the arches are circular and symmetric,
2. All of the arches have a subtending angle equal to 60° and a radius of 200 in.,
3. All of the arches have a rectangular cross section with a height of 2 in. and a base of 2 in.,
4. All of the arches are clamped at both ends,
5. All of the arches have a Young's modulus equal to 1.E+05, and
6. The plotted nondimensionalized deflection is 100 times the vertical deflection at the crown divided by the arch radius of curvature.

The first problem analyzed had a vertical downward concentrated load at the crown. Three tests were run using 4, 8, and 16 nonlinear arch elements. The results using 4 elements are shown in Fig. 7.4. The results using 8 and 16 elements are shown in Fig. 7.5. A comparison of the program results were made with the results obtained by DaDeppo and Schmidt (15) who determined that the critical

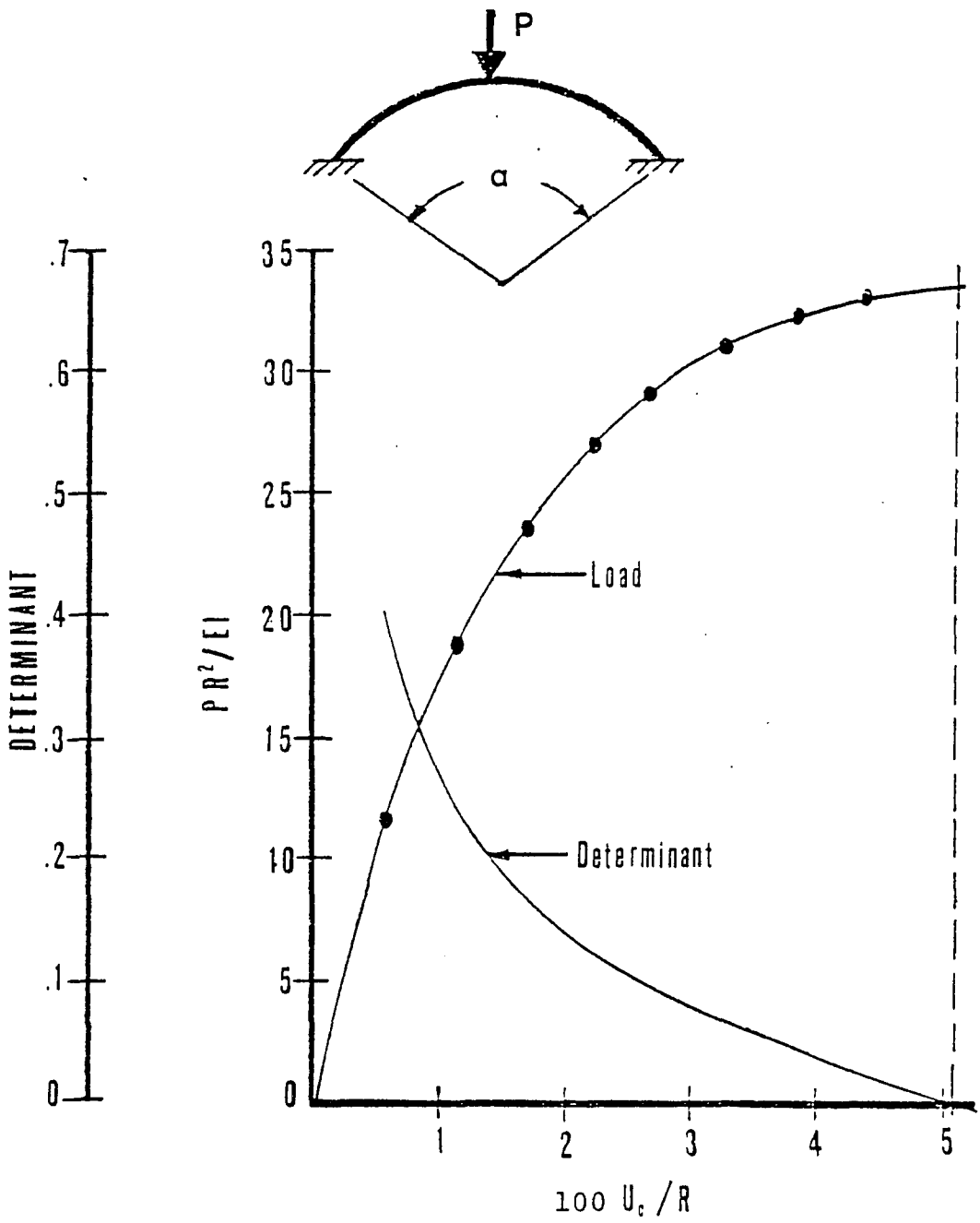

Fig. 7.4. Nondimensionalized load-deflection and determinant-deflection for clamped circular arch with a vertical downward concentrated load at the crown.

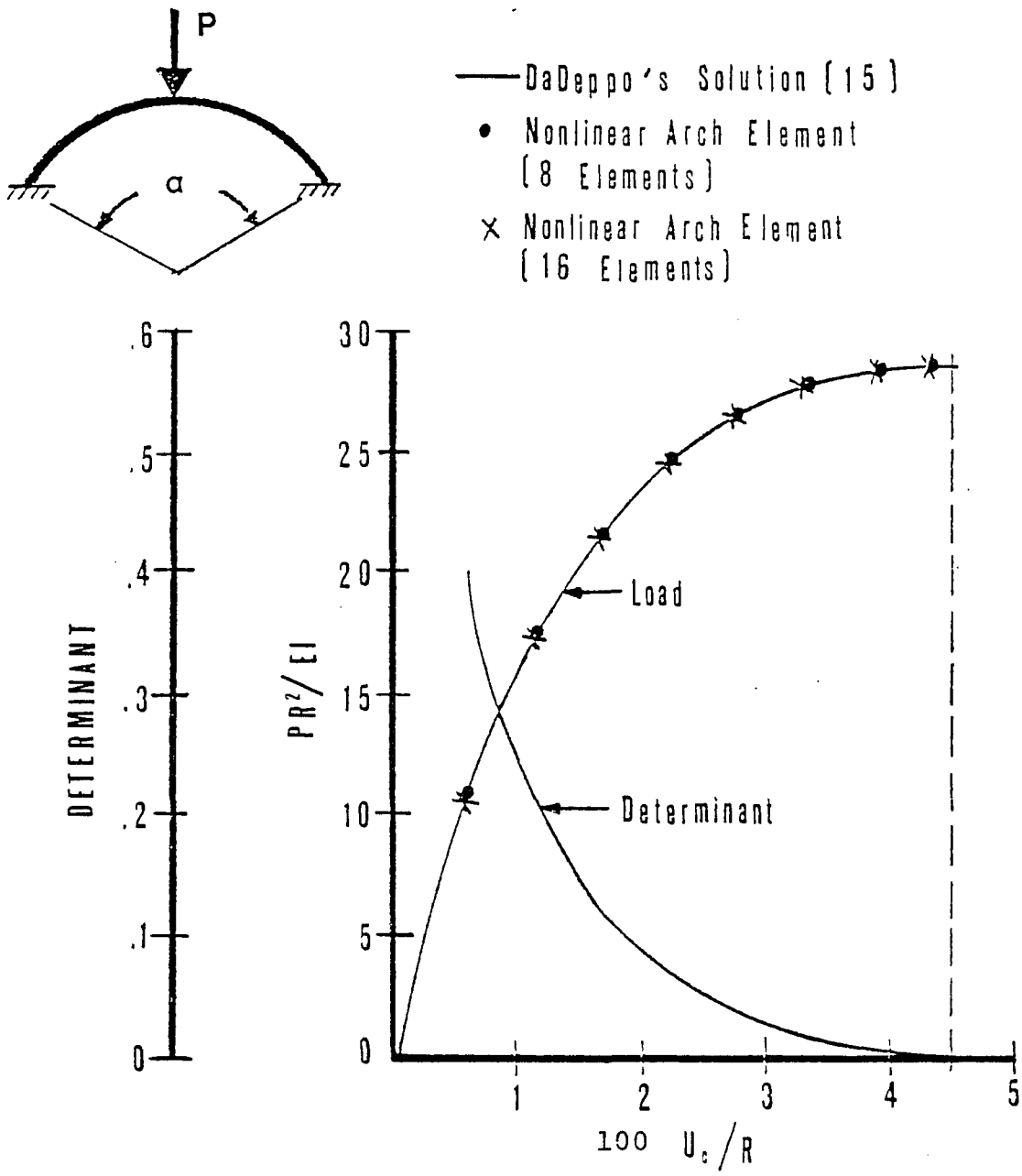

Fig. 7.5. Nondimensionalized load-deflection and determinant-deflection curves for a clamped arch with a vertical concentrated load at the crown.

nondimensionalized load for this problem was equal to 28.591 and the corresponding nondimensionalized deflection, U_c/R, was equal to 4.5. Various comparative calculations were made on this test problem and are shown in Table 7.1.

Table 7.1. Comparative results of clamped circular arch with a vertical downward concentrated load at the crown.

	4 ELEMENTS	8 ELEMENTS	16 ELEMENTS
Critical Load (P_cR^2/EI)	33.500	28.500	28.500
Vertical Crown Deflection (U_c/R)	5.140	4.51	4.51
Rotation at Crown (β)	0.0	0.0	0.0
% Error of P_c (Program vs. Analytical)	17.218	.318	.318
CPU Time/Step	2.305	4.903	10.896
Number of Steps to Reach P_c	9	9	9

In reviewing the literature most geometrically non-linear problems solved using finite element analysis assume symmetry in an effort to decrease the number of elements which decreases computer costs. In making such an assumption stability analysis is neglected, for the buckling mode is assumed not observed. In this work the entire arch was analyzed such that the buckling mode could be observed. This nearly doubles the computer costs, but is essential. For the clamped arch problems discussed in the previous paragraphs total symmetry for all degrees of freedom was observed, therefore, the buckling mode was a snap through type.

Considering I/O and miscellaneous costs, an average computer run for 4 elements would cost approximately $8. For 8 elements an average computer cost would be $16., and for 16 elements the cost would be $32.

In order to study the accuracy of the solution with reference to the number of elements a study was made comparing the moments and reactions for the arch using the non-linear arch element in the small deflection range with those calculated using the linear theory. The program's method for calculating the moment and axial forces is explained in Appendix H. The linear equations for the moment, M, and the horizontal reaction, H, were derived by Leontovich (27). Figure 7.6 is an element convergence graph comparing the

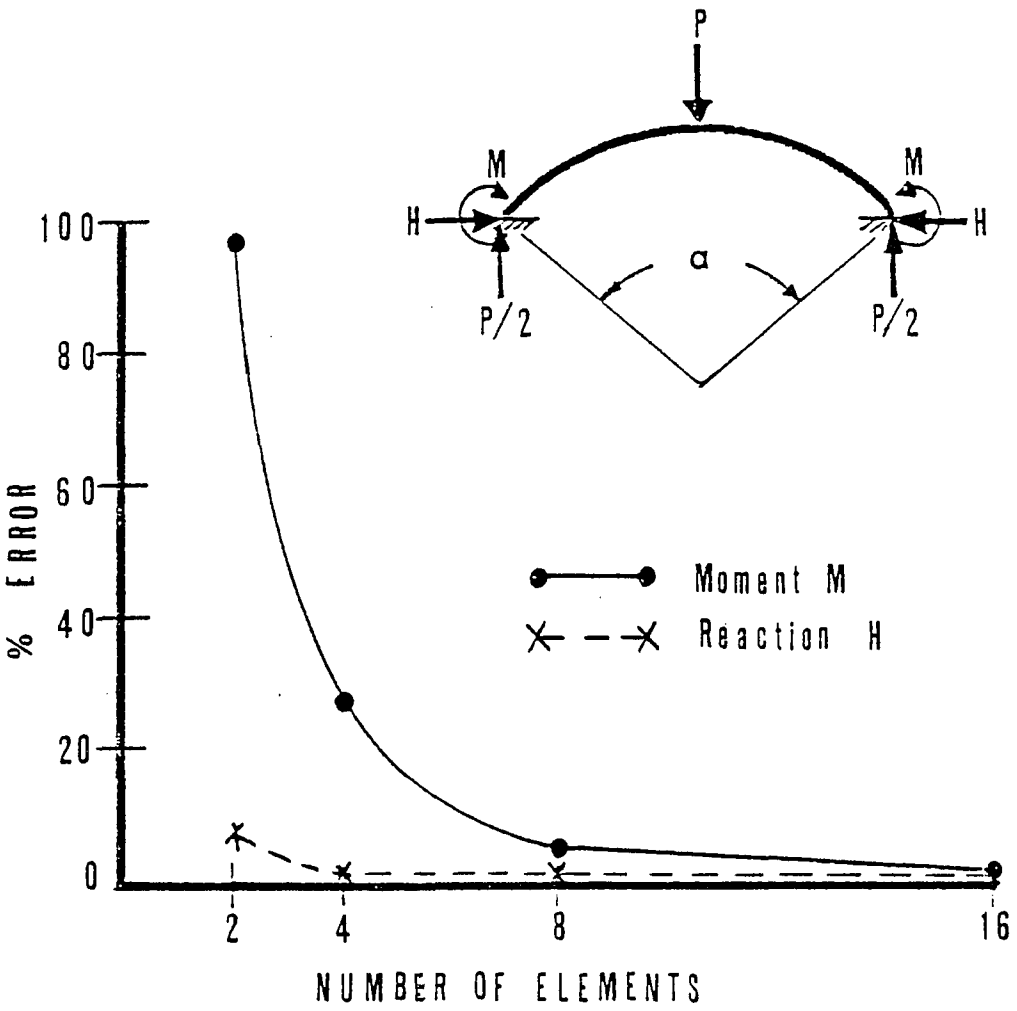

Fig. 7.6. Element convergence graph for a clamped arch with a vertical downward load at the crown.

nonlinear arch element calculations with those using the linear theory. A numerical summary of these results is shown in Table 7.2.

Table 7.2. % Difference between the calculation of moments and reactions using the nonlinear arch element and the linear theory.

	2 ELEMENTS	4 ELEMENTS	8 ELEMENTS	16 ELEMENTS
% ERROR M	97.781	27.056	4.233	1.691
% ERROR H	7.614	1.2928	.896	.896

As can be seen from this test the convergence for the horizontal reaction, H, is more rapid than the convergence for the moment, M. However, for 8 and 16 elements the error in the reactions and moments is within acceptable limits.

In summary the results using 8 and 16 elements were nearly the same for all tests. The computer cost for 16

elements was nearly twice that for 8 elements. Since the use of 8 elements was sufficiently accurate for all tests, it can be safely stated that the use of 8 nonlinear arch elements or 7.5°/ELEMENT gives accurate and inexpensive results for this nonlinear structural problem.

In reference to the same problem, a series of tests were run using 8 elements and various combinations of base, b, and height, h. All of the combinations of cross-sectional dimensions met the following criteria, $h/R < .01$. The load-deflection curves were identical to the curve shown in Fig. 7.5.

The second problem investigated had a uniformly distributed load over the arch. All other arch characteristics were identical to those of the first nonlinear arch problem. The nondimensionalized load-deflection and determinant-deflection curves are given in Fig. 7.7. The nondimensionalized critical load was equal to 75.00, and the nondimensionalized deflection at the crown was equal to .176. For the same problem DaDeppo and Schmidt (15) obtained values for the critical load equal to 74.77 and the corresponding deflection equal to .1766. The percentage error between the program's results and DaDeppo's results for $\frac{WR^3}{EI}$ is .31%. As expected the determinant of the stiffness matrix was negative for loads beyond the bifurcation point. The bifurcation point was obtained without the use of a

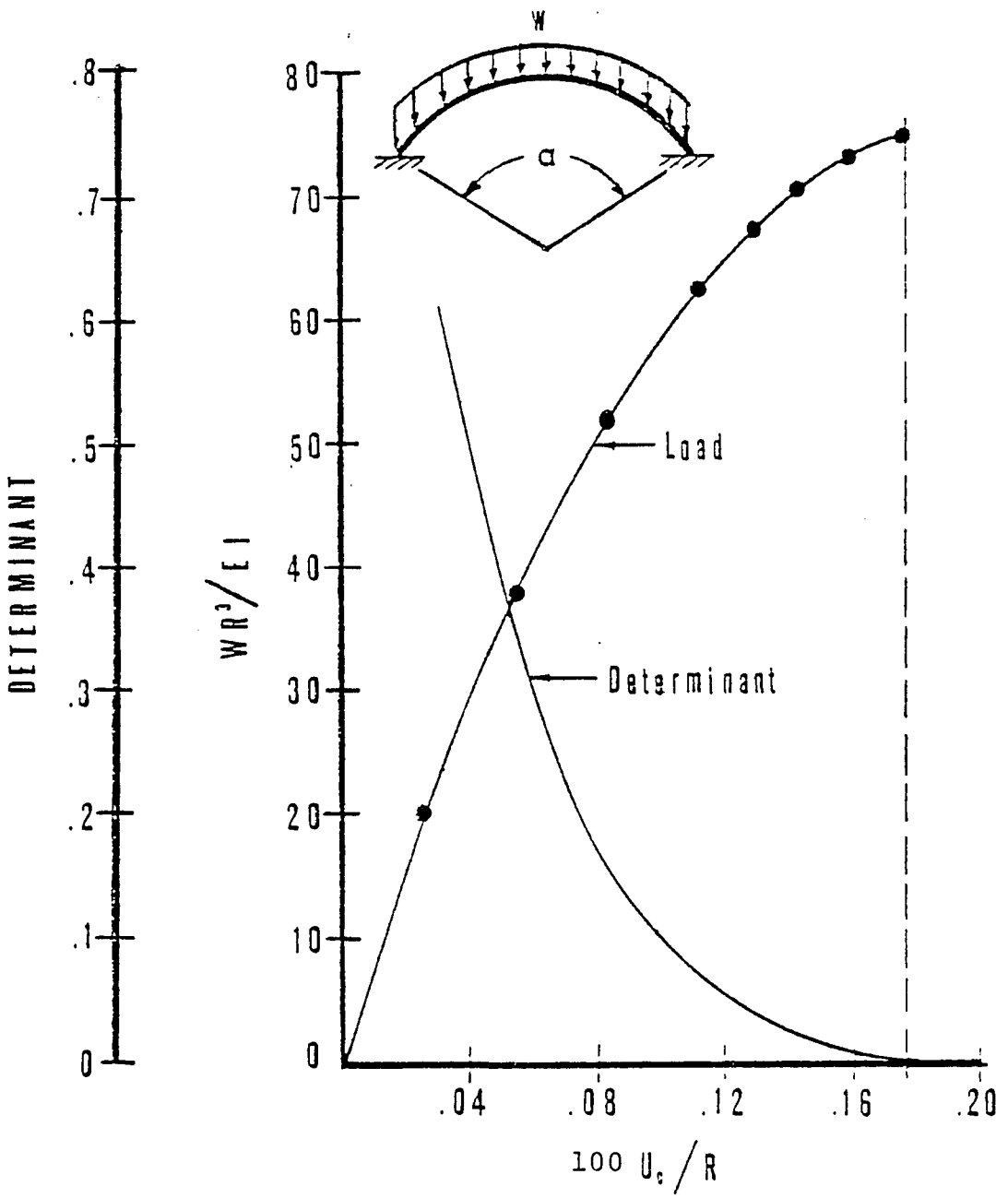

Fig. 7.7. Nondimensionalized load-deflection and determinant-deflection curves for a clamped circular arch with uniformly distributed load.

perturbing load which was not the case for Wood and Zienkiewicz (44) and Batoz, Chattopadhyay, and Dhatt (3). This is significant, for the antisymmetric buckling mode was observed without using additional and expensive schemes to find the bifurcation point.

The third test problem compared various combinations of a vertical downward concentrated load at the crown and a uniformly load over the arch. The arch characteristics are identical to the first two test problems. The various load-deflection curves are shown in Fig. 7.8. Table 7.3 represents the critical values and types of buckling modes where $\dot{P}$ is the concentrated load rate and $\dot{W}$ is the uniformly distributed load rate.

As the ratio of $\dot{P}/\dot{W}$ decreases the critical load and the critical deflection at the crown also decrease. At a specific loading combination the buckling mode changes from snap through to bifurcation. This is similar to the results obtained by DaDeppo and Schmidt (15).

Application of the Boundary Conditions to a Hinged End Problem

To solve a structural problem with a hinged end the following boundary conditions must be applied at the hinge point:

$$U_N = U_t = M = 0 \quad . \tag{7.9}$$

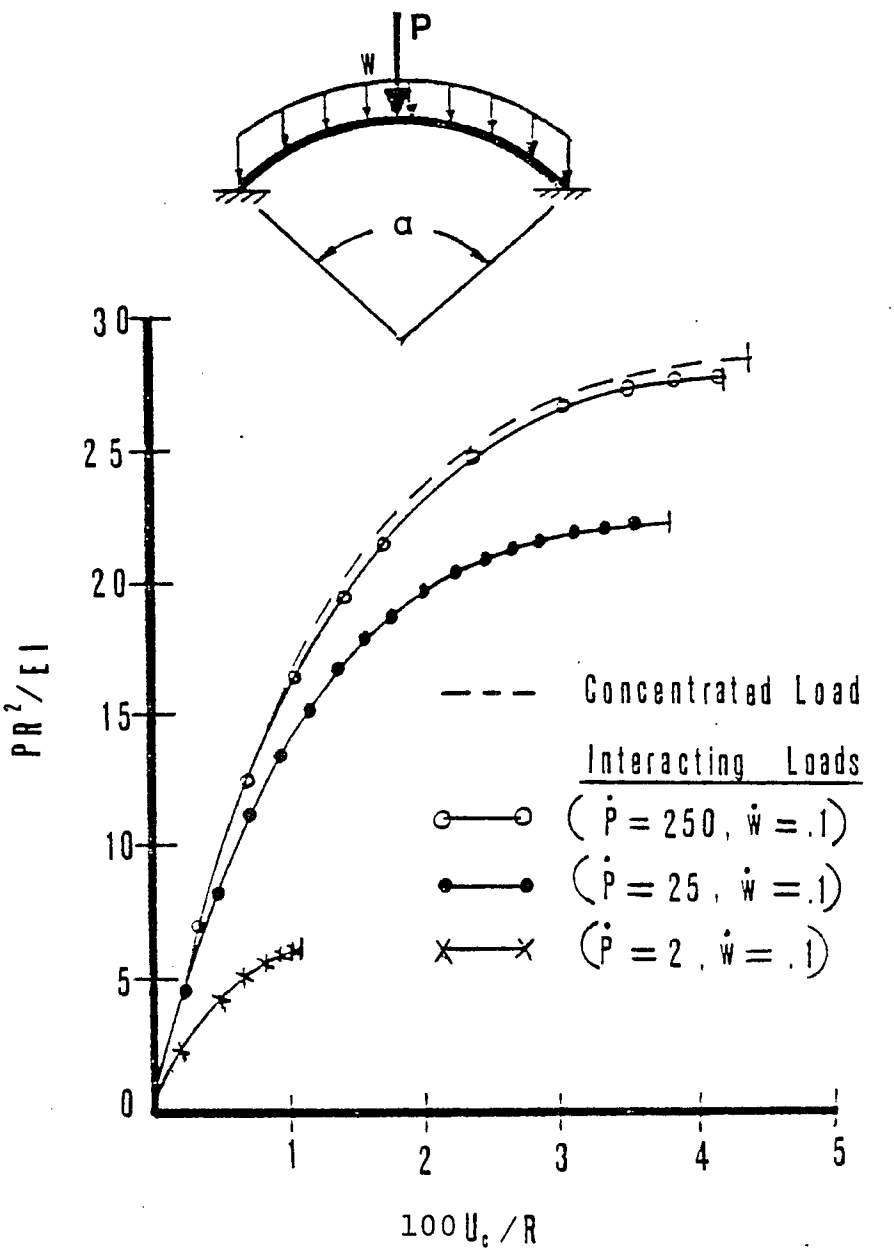

Fig. 7.8. Nondimensionalized load-deflection curve for interacting concentrated and distributed loads.

Table 7.3. Comparison of buckling modes for a clamped circular arch with interacting concentrated and distributed loads.

P	W	$\frac{P_c R^2}{EI}$	$\frac{W_c R^3}{EI}$	U_c/R	BUCKLING MODE
500.	0.	28.50	0.	4.51	Snap through
250.	.1	27.72	2.22	4.20	Snap through
25.	.1	22.35	17.88	3.81	Snap through
2.	.1	6.34	63.39	1.08	Bifurcation

Making the substitution of (7.9) into a global system, U_x and U_y are equal to zero; and U_x' and U_y' are unknown. In order to apply the boundary conditions $\dot{U}_x$ and $\dot{U}_y$ must be suppressed in the system of equations

$$K_{xy}\ \dot{p}_{xy} = \dot{R}_{xy} \tag{7.3}$$

whereas all other degrees of freedom are not suppressed.

Hinged End Circular Arches

The hinged end problems that follow have the same arch characteristics as the previous problems except that the arch is hinged rather than fixed at each end.

The first hinged arch to be investigated has a vertically upward concentrated load applied at the crown. The results of this test case are shown in Fig. 7.9. The program's results are compared with DaDeppo's (8) results. As can be seen, the results are initially the same; however, the results obtained from the program tend to drift from the analytical solution.

The second hinged arch problem considers a vertically downward concentrated load at the crown. The results of this problem are shown in Fig. 7.10, and are compared to the results obtained by DaDeppo and Schmidt (12,14). As can be seen from the load deflection curve the program results compare favorably with the results obtained by DaDeppo and Schmidt (12). However, the solution scheme was highly

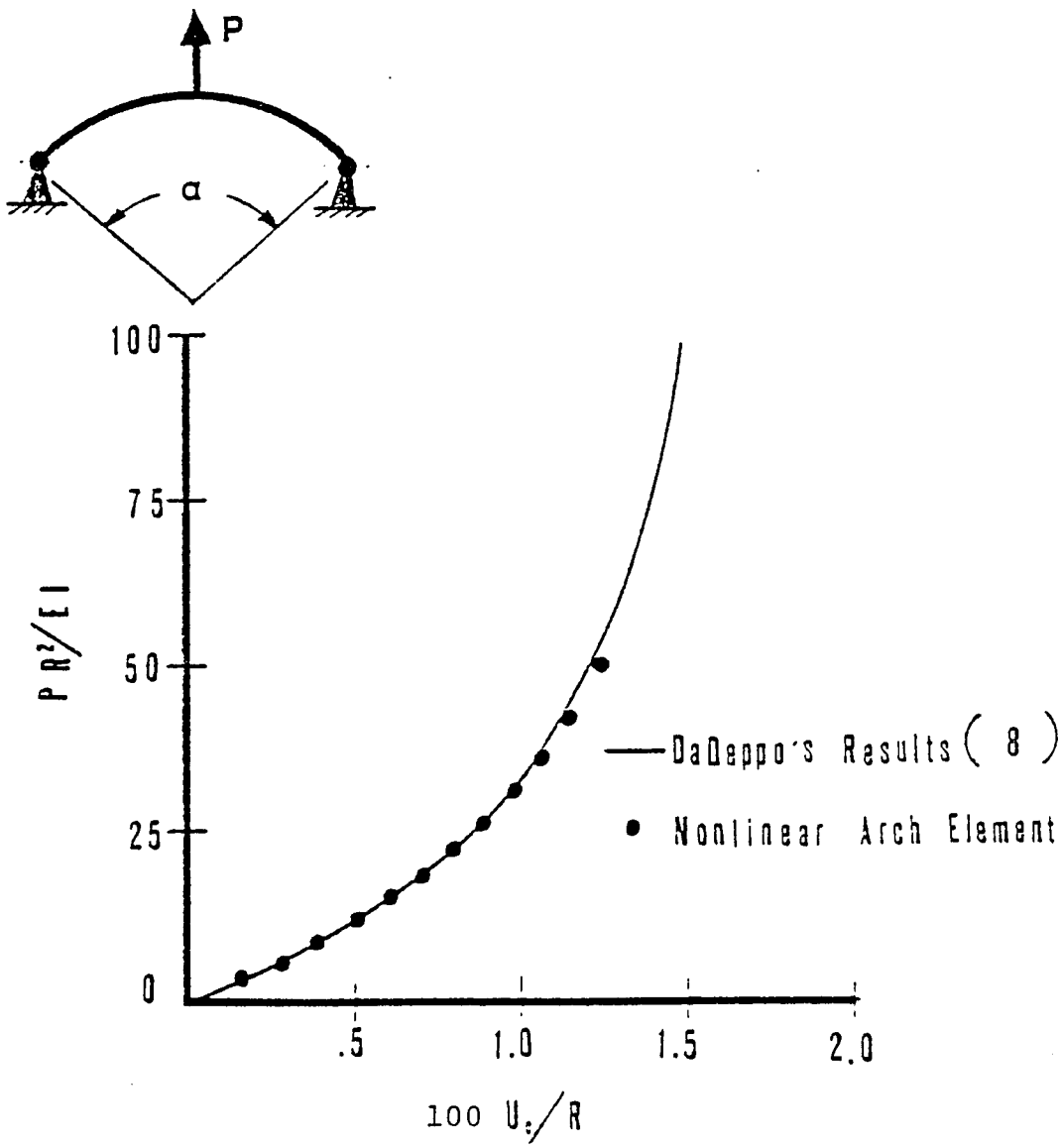

Fig. 7.9. Nondimensionalized load-deflection curve for a hinged circular arch with a vertical upward concentrated load at the crown.

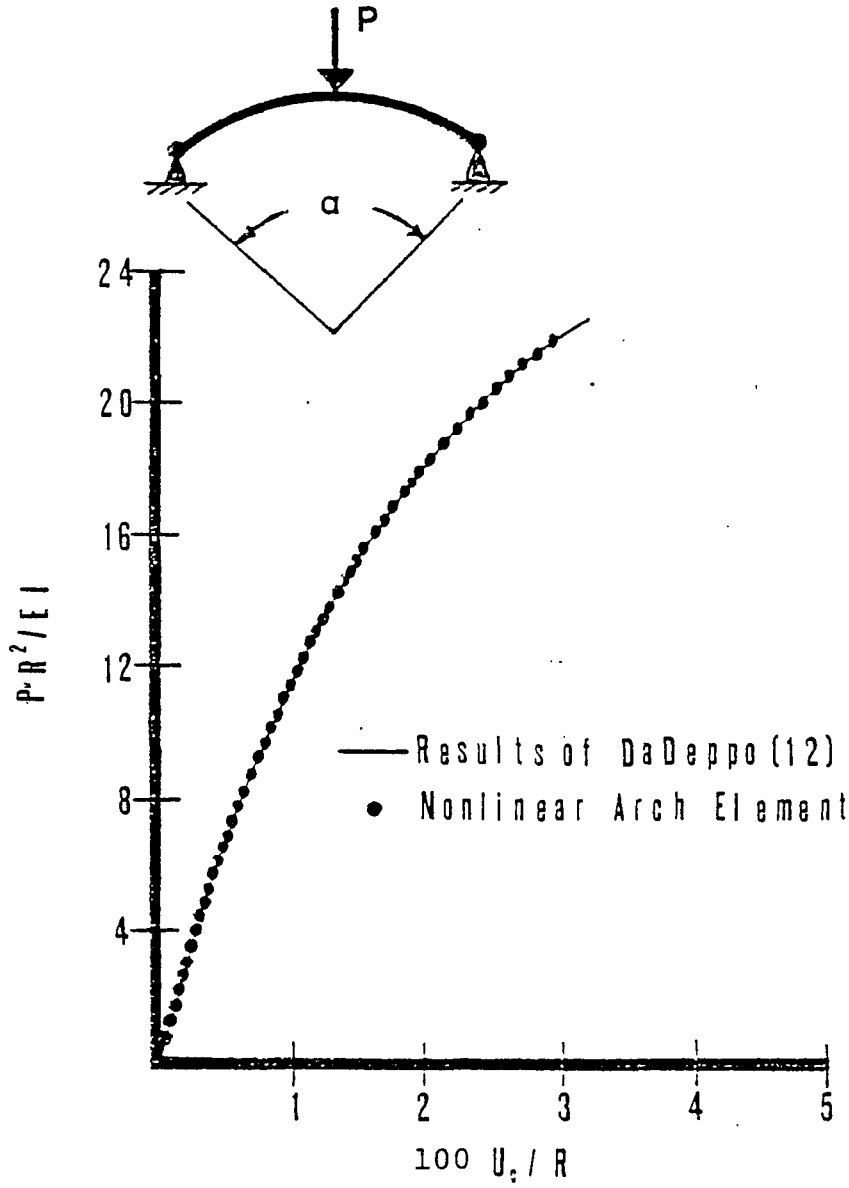

Fig. 7.10. Nondimensionalized load-deflection curve for a hinged circular arch with a vertical downward concentrated load at the crown.

sensitive to the magnitude of the initial displacement increment, δp_{max}. The maximum value which could be used in the nondimensionalized form, $\delta p_{max}/R$, was .0005. Therefore, to reach a value of $\frac{PR^2}{EI}$ equal to 22.5, which is near the bifurcation point, it took a total of 58 steps. The solution scheme took at least 4 iterations at each step. Therefore, to reach this point on the curve using 8 nonlinear arch elements the computer cost was approximately $133.00. Also the calculated value of the determinant at the various steps was erratic and did not represent a smooth determinant-deflection curve. Therefore, using this scheme, the bifurcation point could not be calculated.

This indicated two possible problem areas: (1) the numerical method of applying the boundary conditions was not appropriate, or (2) the numerical method for calculating the determinant was incorrect. The second area was initially investigated. Various methods for calculating the determinant were attempted, such as Gaussian elimination with pivoting. The program was converted into double precision which doubled the storage and increased each computer word to 64 significant figures. The structural system of equations was nondimensionalized such as to eliminate the large numbers associated with Young's modulus. All of these factors were employed together and the value of the determinant remained unchanged. This led to the

conclusion that the existing numerical instabilities were a result of the application of the boundary conditions.

In order to determine if the boundary conditions were being met correctly the problem was modified. The new problem introduced a free element extending from each hinge point as shown in Fig. 7.11.

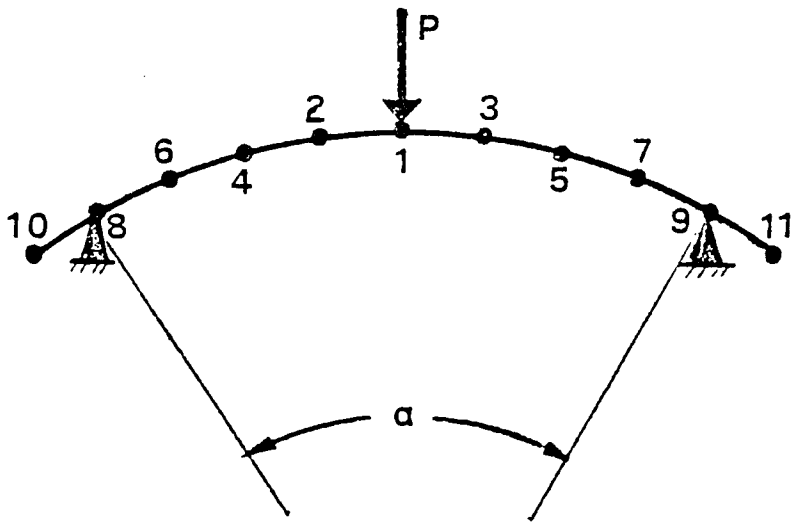

Fig. 7.11. Hinged arch with an extension of elements.

The modified problem improved the condition. Also the load-deflection curve was the same as that in Fig. 7.10. The solution scheme was again highly sensitive to the magnitude of the initial displacement increment. With the addition of two extra elements it increased the computer cost by nearly 25%. But even more important the value of the determinant was again erratic which revealed that this new approach would not overcome the problem.

A second alternative was attempted and that was to use a higher order element as discussed by Dawe (17, 18). A quintic-quintic element was formulated and introduced into the program. The general description of the element is given in Appendix G. The actual use of this element in the stability analysis of geometrically nonlinear problems was economically not feasible. The formulation of the element stiffness for both the cubic-cubic element and the quintic-quintic element required a double integration or a double summation using the Gauss Quadrature integration scheme. To achieve numerical stability for the problem using the quintic-quintic element the number of Gauss points was increased which caused the computer costs to increase considerably. Also the basic formulation included an extremely large number of terms. So using a higher order element only magnified the computer cost. One step cost approximately $60. So if it took over 50 steps to reach the bifurcation point, the problem would cost in excess of $3000.

Even though the quintic-quintic element is economically not feasible for stability analysis of nonlinear problems, it played an important role in this work. One step was run using the quintic-quintic element. The step was small, and the solution fell within the linear region. A similar small step was taken for both of the modified

problems which used the cubic-cubic interpolation functions. The centroidal strain, the moment at the hinge, and the axial force at the crown were calculated using the method described in Appendix H. The results are compared with the linear values derived by Leontovich (27), and are listed in Table 7.4. In this table M_1 and M_2 are the moments at points 1 and 2, respectively. The axial force at point 2 is represented as N_2, and the strain of the centroidal line at points 1 and 2 are ε_{c_1} and ε_{c_2}, respectively. The forces and moments being considered are shown in Fig. 7.12.

Table 7.4. Comparison of the application of the nonlinear arch element in the small deflection region with the linear theory.

		CUBIC ELEMENT	CUBIC ELEMENT (EXTENDED)	QUNITIC ELEMENT
ε_{c_1}		.19668 E-02	.1869 E-02	.2251 E-06
ε_{c_2}		.19668 E-02	.1869 E-02	.1088 E-05
LINEAR	M_1	0.	0.	0.
	M_2	3.08	3.08	3.08
	N_2	.416	.416	.416
NONLINEAR ARCH ELEMENT	M_1	.1343	.01	.26 E-03
	M_2	3.16	3.16	3.25
	N_2	.7857 E+03	.7466 E+03	.4188

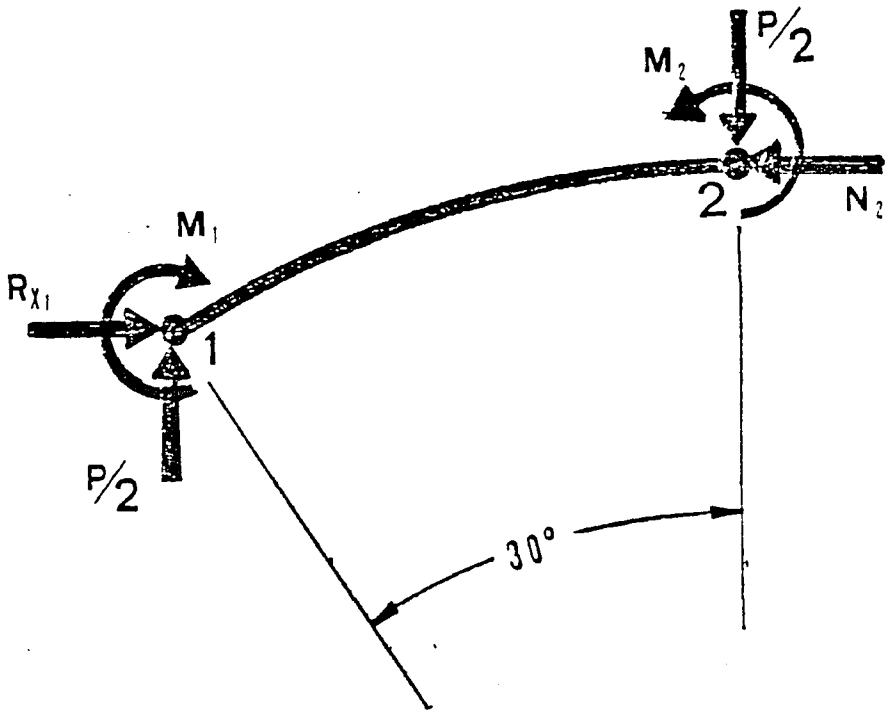

Fig. 7.12. Forces and moments on an arch segment.

For both methods which used the cubic-cubic shape function the strain of the centroidal line at points 1 and 2 were equal. This should not be true and reveals an inaccuracy within the solution. The moment at the hinge which should be zero decreased in value by the addition of the free element; however, the value is not sufficiently small to accurately indicate the proper application of the boundary conditions.

As for the quintic-quintic element, the value of of the centroidal strain changed from points 1 to 2 which should be the case. Also the moment at point 1 decreased

by nearly 10^{-2}. The value is sufficiently small without iterating; therefore, with a few iterations it would become even more accurate.

The most sensitive of all calculated values is the axial force; therefore, it is a good indicator as to the accuracy of the solution. As can be seen from Table 7.4, the value of the axial force was large and unacceptable for both cubic-cubic methods. Yet, for the quintic-quintic element the % error from the exact solution was .673% which is more than acceptable.

This test indicates that using the cubic-cubic element for the stability analysis of nonlinear hinged arches is not adequate. It can give an accurate load-deflection plot; however, it cannot be used for stability analysis. The quintic-quintic element is accurate but economically not feasible.

Capabilities of the Computer Program

The remaining structural problems demonstrate the extended capabilities of the program. All problems are clamped at each end and have a rectangular cross section with the base equal to 2 in. and the height equal to 2 in. In all problems Young's modulus is equal to 1.E+05.

The first problem to be examined is a circular arch with a radius of curvature of 200 in. A combined vertical and horizontal load is applied at the crown.

$\dot{P}_y$ = 500 lbs/unit of load time

$\dot{P}_x$ = 400 lbs/unit of load time

Therefore, the resultant load rate

$\dot{P}_{RESULTANT}$ = 640.312 lbs/unit of load time.

The nondimensionalized load-deflection curve is shown in Fig. 7.13. The nondimensional critical resultant load, $\frac{P_c R^2}{EI}$, is equal to 25.71, and the corresponding deflection, U_c/R, is equal to 4.395. The buckling mode is the snap through type.

The second problem analyzed combines a uniformly distributed load over the arch length from ±15° and a concentrated load at the crown with concentrated loads at ±15°. The arch is circular with the radius of curvature equal to 200 in., and the subtending angle equal to 60°. The concentrated load rate and the load intensity rate are

$\dot{P}$ = 250 lbs/unit of load time

$\dot{W}$ = .1 lbs/unit of load time, respectively.

The results are shown in Fig. 7.14. The critical load, $\frac{P_c R^2}{EI}$, is equal to 19.22, and the corresponding deflection is 4.40. The buckling mode is the bifurcation type.

The next problem studied has two different radii, R_1 = 200 in. and R_2 = 100 in. The two radii have a common tangent point at the crown of the arch. The arch has an angle of ±30° from the crown. Also a vertical downward

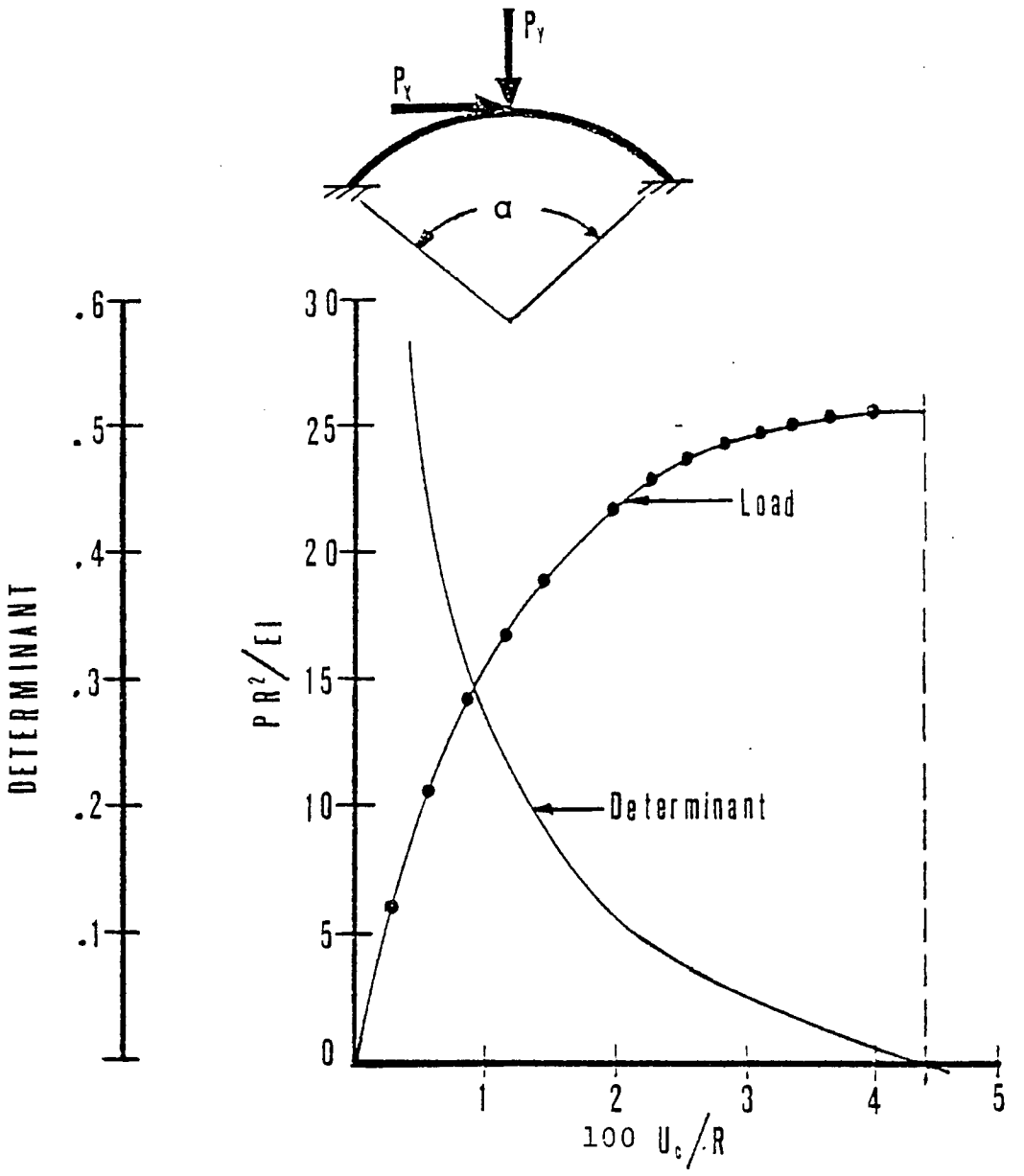

Fig. 7.13. Nondimensionalized load-deflection and determinant-deflection curves for a clamped circular arch with a resultant load at the crown.

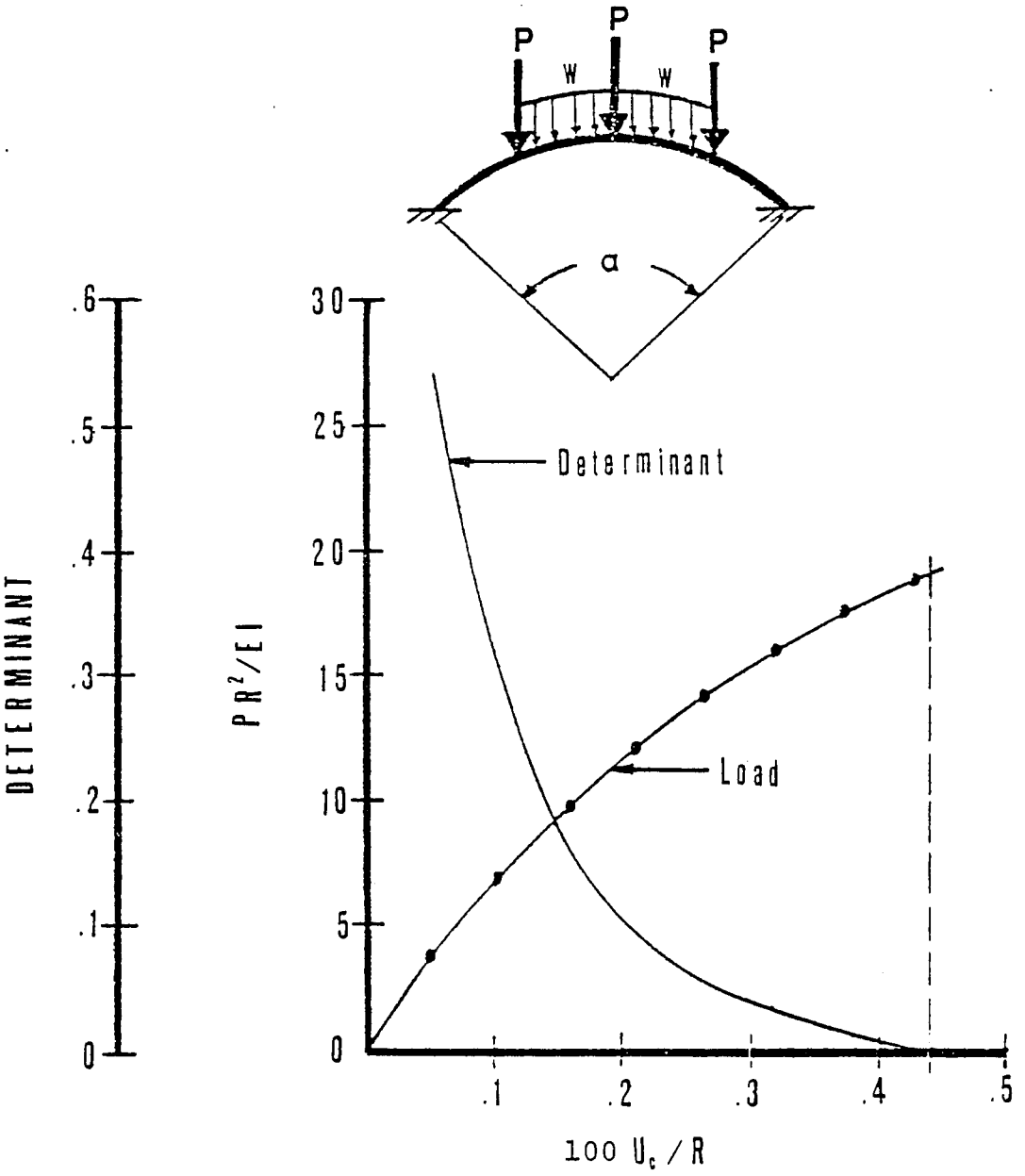

Fig. 7.14. Nondimensionalized load-deflection and determinant-deflection curves for a clamped arch with a combined loading condition.

concentrated load is applied at the crown. The results are shown in Fig. 7.15. The term R_m is the mean radius and is equal to

$$R_m = \frac{R_1 + R_2}{2} = 150 .$$

The critical load, $\frac{P_c R_m^2}{EI}$, is equal to 28.38, and the corresponding deflection, U_c/R_m, is equal to 6.38. The buckling mode is the snap through type.

The next problem demonstrates the capability of using the spline curve fitting on an arch with arbitrary geometry. The arch with its various interpolation points is shown in Fig. 7.16. The x and y values for the interpolation points are given in Table 7.5. The spline curve fitting is tested in Appendix I.

This particular arch is subject to a vertical concentrated load at the crown. The results for this structural problem are shown in Fig. 7.17. The critical load, $\frac{P_c L^2}{EI}$, is equal to 30.12, and the corresponding deflection, U_c/L, is equal to 4.178.

The final problem again demonstrates the spline curve fitting capabilities. The arch with its interpolation points is shown in Fig. 7.18. The nondimensionalized load-deflection curve is plotted in Fig. 7.19. The nondimensionalized critical load, $\frac{P_c L^2}{EI}$, is equal to 31.41, whereas the nondimensionalized deflection is equal to 7.85.

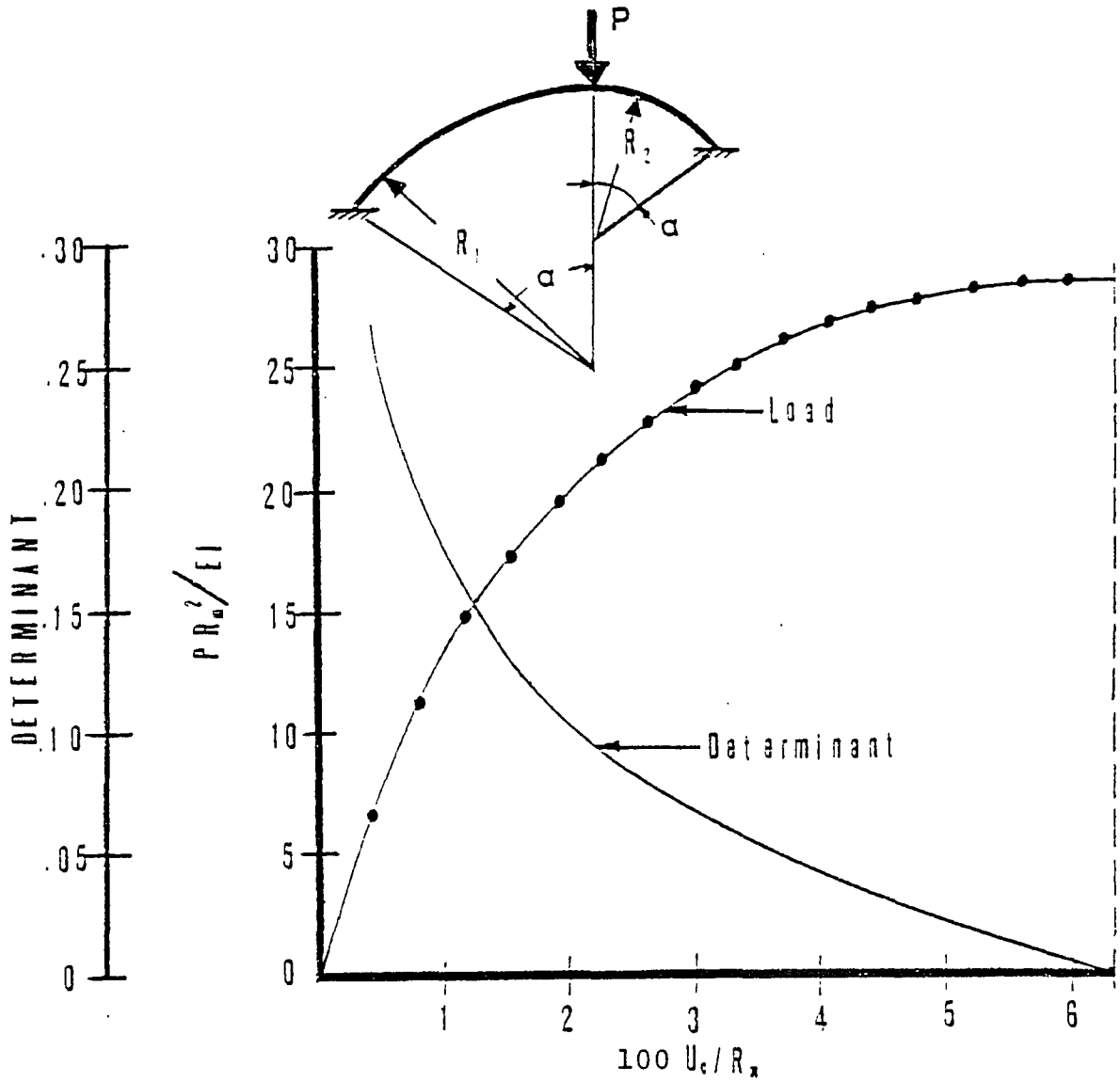

Fig. 7.15. Nondimensionalized load-deflection and determinant-deflection curves for a clamped arch with two radii and a vertical downward concentrated load at the crown.

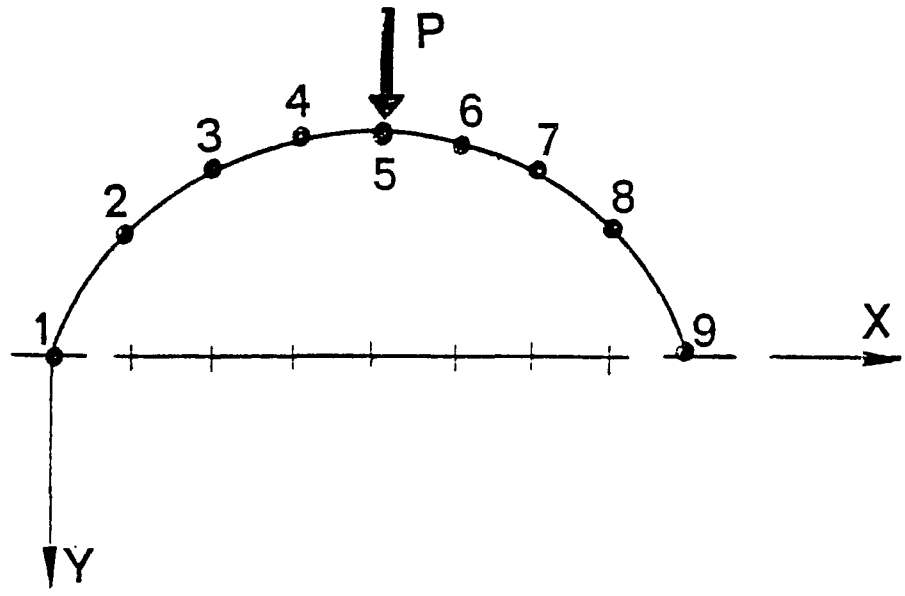

Fig. 7.16. Symmetric arch defined by data points.

Table 7.5. Coordinates of interpolation points.

INTERPOLATION POINT	X	Y
1	0.	0.
2	25.	-11.7206
3	50.	-20.0925
4	75.	-25.1156
5	100.	-26.7900
6	125.	-25.1156
7	150.	-20.0925
8	175.	-11.7206
9	200.	0.

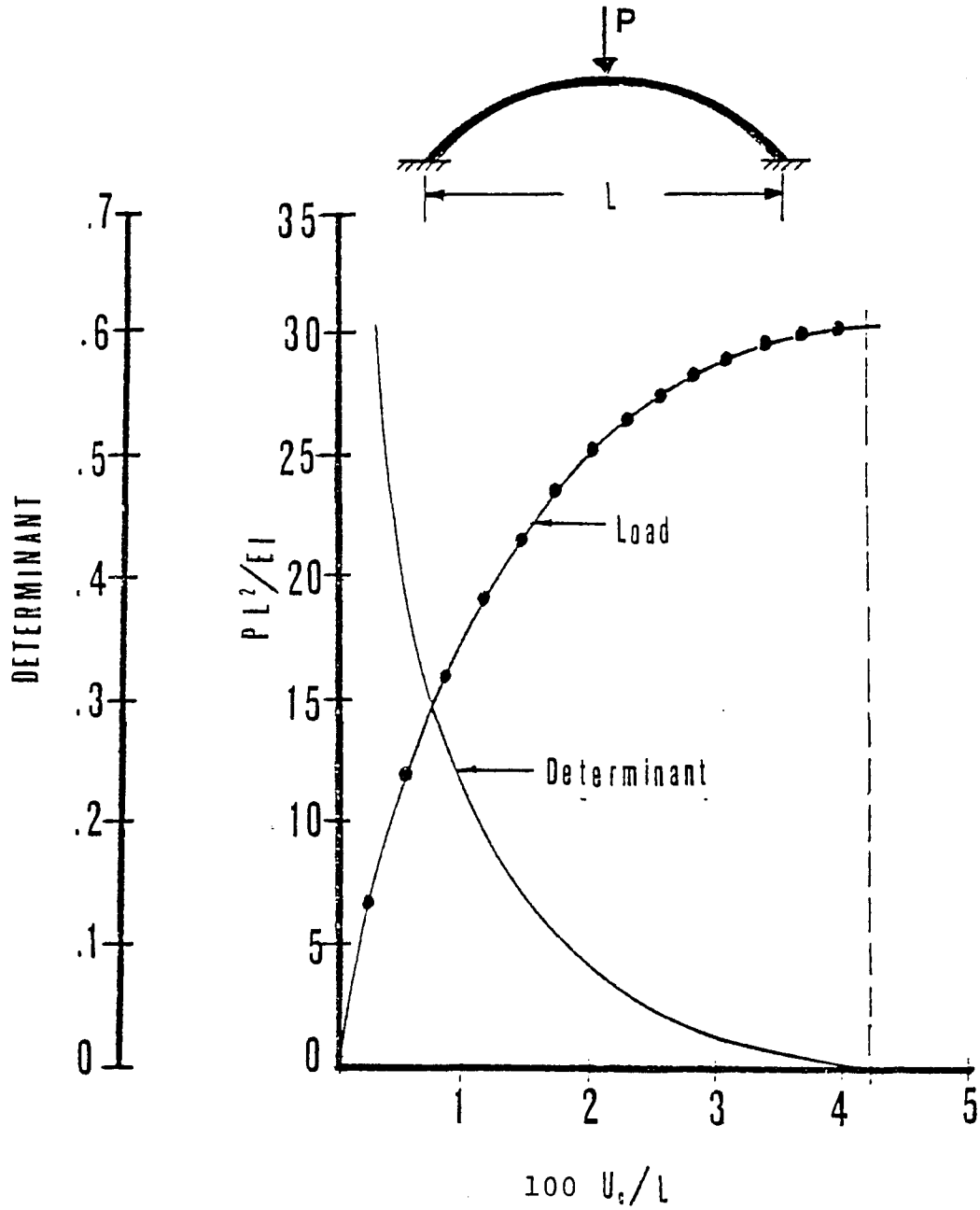

Fig. 7.17. Nondimensionalized load-deflection and determinant-deflection curves for a symmetric arbitrary clamped arch with a vertical downward concentrated load at the crown.

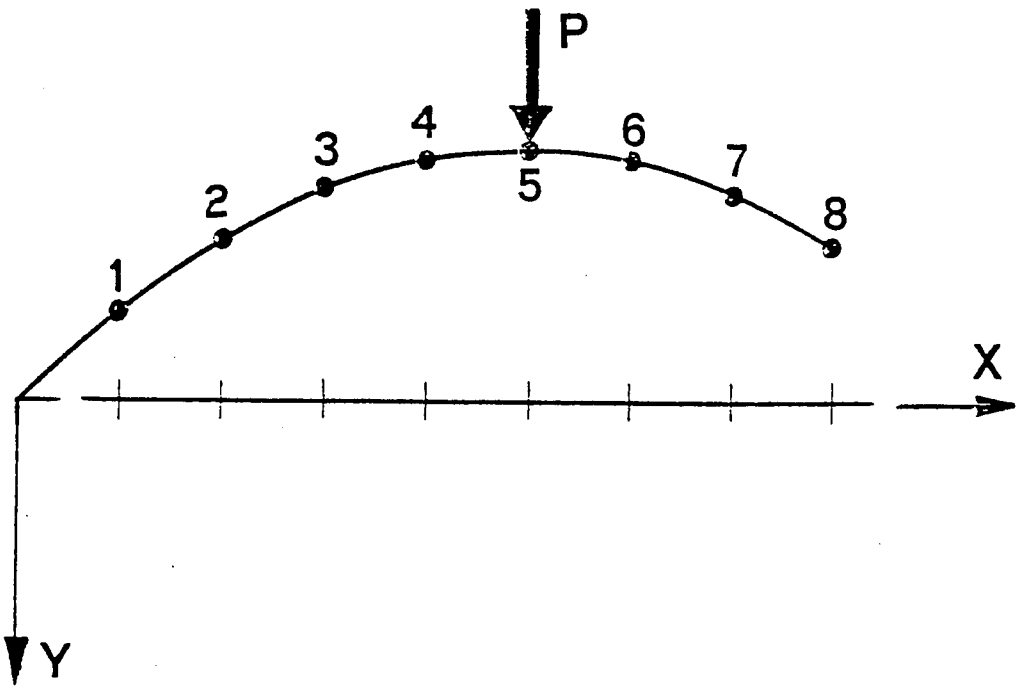

Fig. 7.18. Arch defined by data points.

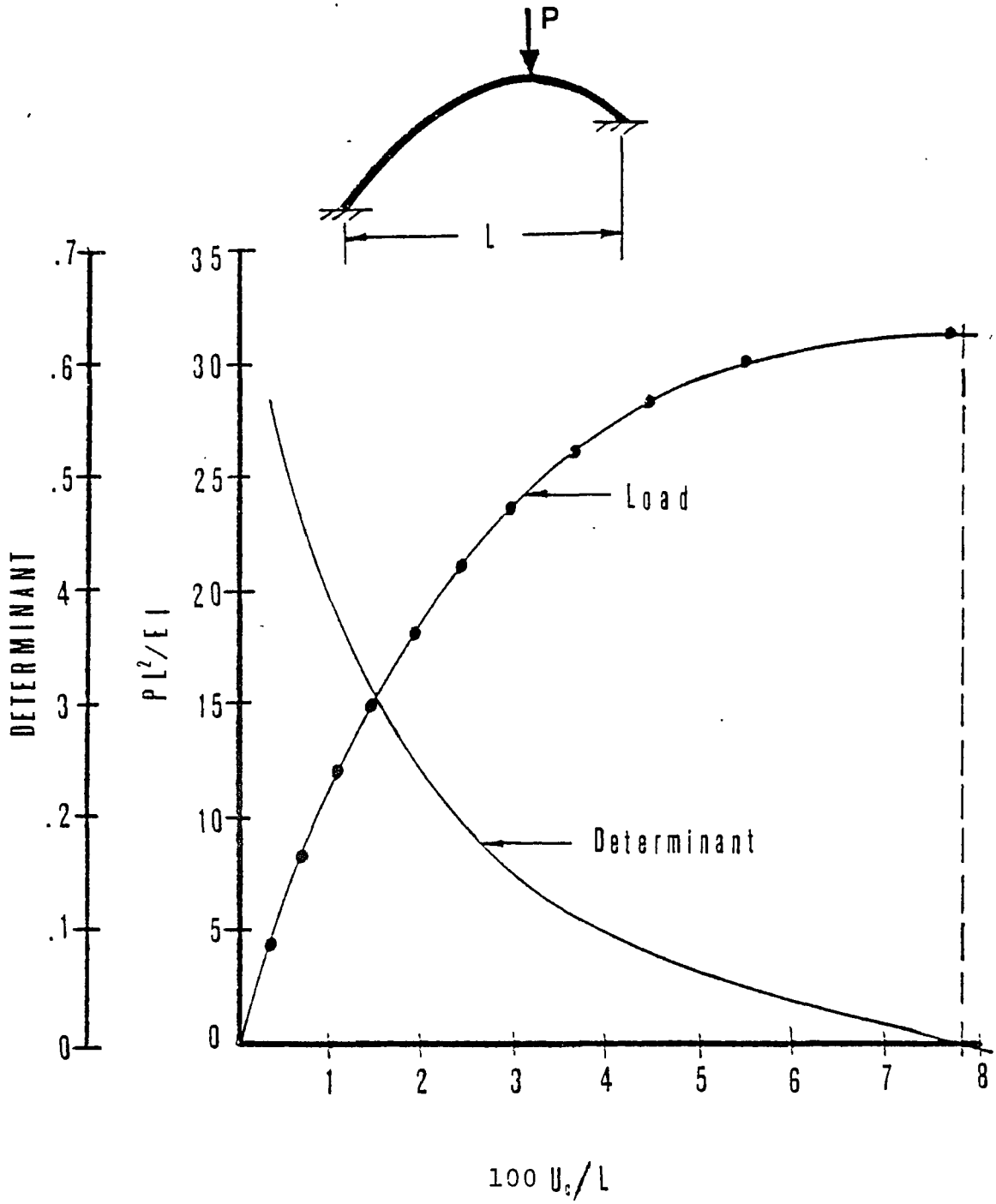

Fig. 7.19. Nondimensionalized load-deflection and determinant-deflection curves for arch of arbitrary geometry with a vertical downward concentrated load at the crown.

CHAPTER 8

SUMMARY AND RECOMMENDATIONS

A curved nonlinear finite element has been presented to observe the instability modes for geometrically nonlinear arch problems. The element was formulated using Euler's extensional theory of curved structural members. The strain equation was derived using the Winkler-Bach hypothesis and the reasonable assumption of small strain and finite rotations. No terms within the strain equation were neglected during the finite element formulation nor during the solution of any arch problem. The geometry of the arch was represented by exact equations in the case of the circular arch and by approximate equations in the case of the arch with arbitrary geometry of the centroidal axis. A spline curve fitting procedure was used in determining the approximate equation for the arch of arbitrary geometry. The governing differential equations were differentiated with respect to time to give a system of rate equations. By the use of these equations the original nonlinear differential equations were solved using the Runge-Kutta method with Simpson's coefficients. If the solution drifted, a Newton-Raphson iteration scheme was used to return the solution to the equilibrium path.

Two curved nonlinear finite elements were developed. The first element had eight degrees of freedom and used cubic Hermite polynomials to represent both the normal and tangential displacement fields. The second element had twelve degrees of freedom and used quintic Hermite polynomials to represent the normal and tangential displacement fields. The element with eight degrees of freedom was used for every nonlinear arch problem in this study. The element with twelve degrees of freedom was used only for the hinged arch problem which had a vertical downward concentrated load at the crown.

A computer program was written to test the curved nonlinear element developed in this work on various deep arch problems. These tests had three purposes: (1) to prove the validity of the element, (2) to check the accuracy of the solutions of the arch problems tested (a comparison was made with known and accepted solutions) and (3) to evaluate the computer costs of the various arch problems.

For all test cases on clamped circular arches the results using the curved nonlinear element were nearly identical with the results of DaDeppo and Schmidt. The values of the nondimensionalized buckling loads were within .32% of the buckling loads calculated by DaDeppo and Schmidt for the same problems. The computer costs on these

stability problems using eight curved nonlinear elements ranged from $16 to $20. Snap through buckling was observed for all arch problems with concentrated loads, and bifurcation buckling was observed for all arch problems with distributed loading. The bifurcation points were met without using additional schemes to find the secondary equilibrium path.

Two hinged end circular arch problems were tested. The first had a vertical upward concentrated load at the crown. This was not a buckling problem; however, the load-deflection results compared favorably with the results by DaDeppo (8) for the same problem. The second problem had a vertical downward concentrated load at the crown. The results using the curved nonlinear finite element with eight degrees of freedom gave accurate load-deflection results, however, no buckling could be observed. It was discovered by using the curved nonlinear element with twelve degrees of freedom that the first element which uses cubic-cubic interpolation functions was not accurate enough to correctly satisfy the boundary conditions. Also the computer costs for solving the hinged end problem using the curved nonlinear element were so large that its use for such problems was economically not feasible.

Additional problems were run to demonstrate the extended capabilities of the program. A brief description

of the problems and the buckling modes is shown below:

1. A clamped circular arch with both vertical and horizontal concentrated loads at the crown--the buckling mode was snap through.
2. A clamped circular arch with a combination of concentrated loads and uniformly distributed load over a segment of the arch--the buckling mode was bifurcation.
3. A clamped arch with two radii of curvature with a downward concentrated load at the crown--the buckling mode was snap through.
4. A clamped symmetric arch in which the geometry of the centroidal axis is defined by data points and has a downward concentrated load at the crown--the buckling mode was snap through.
5. A clamped arch in which the geometry of the centroidal axis is defined by data points and has a downward concentrated load at the crown--the buckling mode was snap through.

In general, it can be stated that for fixed end nonlinear arch problems, the curved nonlinear finite element developed in this work demonstrated a high degree of accuracy, gave correct buckling modes, and exhibited low computational expense for all problems tested.

Recommendations for Future Research

The following recommendations for future research can be both a challenge and an extension of this work.

1. To investigate the stability at large deflections of arches with arbitrary geometry of the centroidal axis and variable thicknesses under a combination of loads with various boundary conditions.
2. To investigate the stability at large deflections of frames with curved members under a combination of loads with various boundary conditions.

APPENDIX A

TWO-DIMENSIONAL GAUSS QUADRATURE INTEGRATION SCHEME FOR THE NONLINEAR FINITE ELEMENT ARCH PROBLEM

The integral in question is

$$I = \frac{tE}{2} \int_{Z_1}^{Z_2} \int_{S_1}^{S_2} f(S,Z)\, dSdZ \qquad (A.1)$$

With reference to Fig. A.1 the integral can be transformed into a two-dimensional Gauss Quadrature scheme.

$$I = \frac{tE(Z_2-Z_1)(S_2-S_1)}{4} \sum_{i=1}^{n} \sum_{j=1}^{m} W_i W_j\, f(z_j,s_i) \qquad (A.2)$$

where

$$z_j = \frac{1}{2}\left(Z_2+Z_1 + (Z_2-Z_1)\xi_j\right) , \qquad (A.3)$$

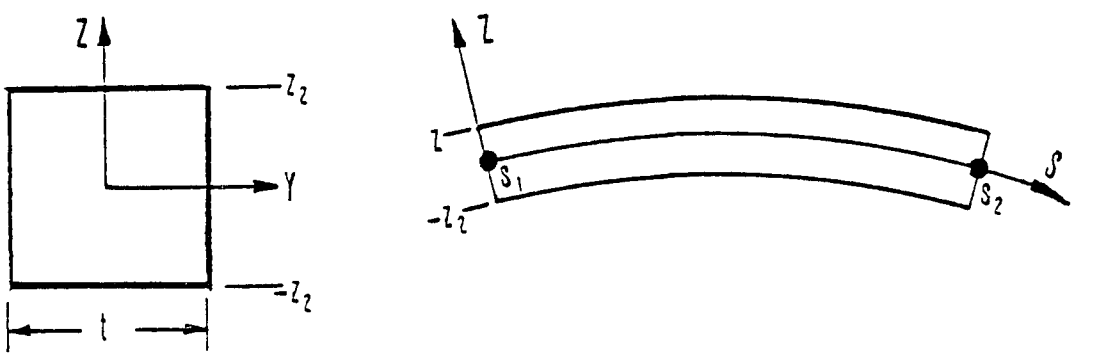

Fig. A.1. Dimensions of arch element.

and

$$s_i = \frac{1}{2}\left(S_2+S_1 + (S_2-S_1)\xi_i\right) . \qquad (A.4)$$

W's are the weighting factors.

ξ's are the sampling points.

From the dimensions given in Fig. A.1,

$$I = \frac{tE\ Z_2(S_2-S_1)}{4} \sum_{i=1}^{n} \sum_{j=1}^{m} W_i W_j\ f(z_i,s_i) \qquad (A.5)$$

where

$$z_i = Z_2\xi_j \qquad (A.6)$$

$$s_i = \frac{1}{2}\left(S_2+S_1 + (S_2-S_1)\xi_i\right) . \qquad (A.7)$$

APPENDIX B

CALCULATION OF A PORTION OF THE ELEMENT STIFFNESS

Since the strain energy is a function of U_N, U_N', U_N'', U_t, U_t', and U_t'' and since the stiffness matrix is formed by taking the second partial derivative of the strain energy with respect to the nodal degrees of freedom, the following matrices are needed in determining the element stiffness matrix.

$$\frac{\partial U_N}{\partial \underset{\sim}{p}} = \left[\, 1 \mid S \mid S^2 \mid S^3 \mid 0 \mid 0 \mid 0 \mid 0 \,\right] \underset{\sim}{B}\,\underset{\sim}{I} \qquad \text{(B.1)}$$

$$\frac{\partial U_N'}{\partial \underset{\sim}{p}} \left[\, 0 \mid 1 \mid 2S \mid 3S^2 \mid 0 \mid 0 \mid 0 \mid 0 \,\right] \underset{\sim}{B}\,\underset{\sim}{I} \qquad \text{(B.2)}$$

$$\frac{\partial U_N''}{\partial \underset{\sim}{p}} \left[\, 0 \mid 0 \mid 2 \mid 6S \mid 0 \mid 0 \mid 0 \mid 0 \,\right] \underset{\sim}{B}\,\underset{\sim}{I} \qquad \text{(B.3)}$$

$$\frac{\partial U_t}{\partial \underset{\sim}{p}} \left[\, 0 \mid 0 \mid 0 \mid 0 \mid 1 \mid S \mid S^2 \mid S^3 \,\right] \underset{\sim}{B}\,\underset{\sim}{I} \qquad \text{(B.4)}$$

$$\frac{\partial U_t'}{\partial \underset{\sim}{p}} \left[\, 0 \mid 0 \mid 0 \mid 0 \mid 0 \mid 1 \mid 2S \mid 3S^2 \,\right] \underset{\sim}{B}\,\underset{\sim}{I} \qquad \text{(B.5)}$$

$$\frac{\partial U_t''}{\partial \underset{\sim}{p}} \left[\, 0 \mid 0 \mid 0 \mid 0 \mid 0 \mid 0 \mid 2 \mid 6S \,\right] \underset{\sim}{B}\,\underset{\sim}{I} \qquad \text{(B.6)}$$

From the first integral of (4.22) and Eq. (4.24), it is apparent that the second partial derative of $\varepsilon_c{}^2$

with respect to p must be determined to obtain a portion of the element stiffness matrix.

$$\varepsilon_c = \frac{1}{2}\left(U_t'^2 + U_N'^2 + K^2U_N^2 + K^2U_t^2 + 2U_t' - 2KU_N - 2KU_NU_t' + 2KU_tU_N'\right) \tag{B.7}$$

Therefore, in terms of matrices

$$\underset{8x8}{\frac{\partial^2\varepsilon_c}{\partial\underset{\sim}{p}^2}} = \left(\frac{\partial U_t'^T}{\partial\underset{\sim}{p}}\frac{\partial U_t'}{\partial\underset{\sim}{p}} + \frac{\partial U_N'^T}{\partial\underset{\sim}{p}}\frac{\partial U_N'}{\partial\underset{\sim}{p}} + K^2\frac{\partial U_N^T}{\partial\underset{\sim}{p}}\frac{U_N}{\partial\underset{\sim}{p}} + K^2\frac{\partial U_t^T}{\partial\underset{\sim}{p}}\frac{\partial U_t}{\partial\underset{\sim}{p}} - K\frac{\partial U_T'^T}{\partial\underset{\sim}{p}}\frac{\partial U_N}{\partial\underset{\sim}{p}} - K\frac{\partial U_N^T}{\partial\underset{\sim}{p}}\frac{\partial U_t'}{\partial\underset{\sim}{p}} + K\frac{\partial U_N'^T}{\partial\underset{\sim}{p}}\frac{\partial U_t}{\partial\underset{\sim}{p}} + K\frac{\partial U_t^T}{\partial\underset{\sim}{p}}\frac{\partial U_N'}{\partial\underset{\sim}{p}}\right) \tag{B.8}$$

and

$$\underset{1x8}{\frac{\partial\varepsilon_c}{\partial\underset{\sim}{p}}} = \left(U_t'\frac{\partial U_t'}{\partial\underset{\sim}{p}} + U_N'\frac{\partial U_N'}{\partial\underset{\sim}{p}} + K\,U_N\frac{\partial U_N}{\partial\underset{\sim}{p}} + K^2\,U_t\frac{\partial U_t}{\partial\underset{\sim}{p}} + \frac{\partial U_t'}{\partial\underset{\sim}{p}} + K\frac{\partial U_N}{\partial\underset{\sim}{p}} - K\,U_N\frac{\partial U_t'}{\partial\underset{\sim}{p}} - K\,U_t'\frac{\partial U_N}{\partial\underset{\sim}{p}} + K\,U_t\frac{\partial U_N'}{\partial\underset{\sim}{p}} + K\,U_N'\frac{\partial U_t}{\partial\underset{\sim}{p}}\right) \tag{B.9}$$

Performing the matrix multiplication of $\frac{\partial\varepsilon_c}{\partial\underset{\sim}{p}}^T\frac{\partial\varepsilon_c}{\partial\underset{\sim}{p}}$ will give another component of the stiffness matrix. All components of the stiffness matrix can be

calculated in a similar fashion. Because of the extraordinarily large number of matrix operations to be performed, the instantaneous stiffness must be formed by use of a digital computer.

APPENDIX C

DERIVATION OF THE SINθ AND COSθ IN TERMS OF y'

To begin the following trigonometric identity is used.

$$\cos^2\theta + \sin^2\theta = 1 \qquad \text{(C.1)}$$

Dividing (C.1) by $\sin^2\theta$ and rearranging yields

$$\sin^2\theta = \frac{\tan^2\theta}{1 + \tan^2\theta} \qquad \text{(C.2)}$$

Taking the square root of (C.2) gives

$$\sin\theta = \pm\left(\frac{\tan^2\theta}{1 + \tan^2\theta}\right)^{1/2} \qquad \text{(C.3)}$$

A similar operation yields an expression for $\cos\theta$. Thus,

$$\cos\theta = \pm\left(\frac{1}{1 + \tan^2\theta}\right)^{1/2} . \qquad \text{(C.4)}$$

Since $y' = \tan\theta$, (C.3) and (C.4) can be expressed as

$$\sin\theta = \pm\left(\frac{y'^2}{1 + y'^2}\right)^{1/2}$$

$$\cos\theta = \pm\left(\frac{1}{1 + y'^2}\right)^{1/2} , \text{ respectively.}$$

APPENDIX D

EXAMPLE USING SPLINE CURVE FITTING

With reference to the curve shown in Fig. D.1, there are 6 interpolation points approximating this curve, and their X and Y values are listed in Table D.1

Using the general equation for the cubic spline, (4.50), and letting K = 3, the equation for line segment 3 can be written as

$$y = C_{1,3}\,(x_4-x)^3 + C_{2,3}\,(x-x_3)^3 + C_{3,3}\,(x_4-x) + C_{4,3}(x-x_3)\ , \qquad (D.1)$$

or

$$y = C_{1,3}\,(4-x)^3 + C_{2,3}\,(x-3)^3 + C_{3,3}\,(4-x) + C_{4,3}\,(x-3)\ . \qquad (D.2)$$

The X and Y values shown in Table D.1 can be placed into one dimensional arrays and used in SUBROUTINE SPLICO. This subroutine calculates the cubic spline coefficients for each line segment. Having obtained these values, any Y value can be calculated if the corresponding X value and line segment number are known.

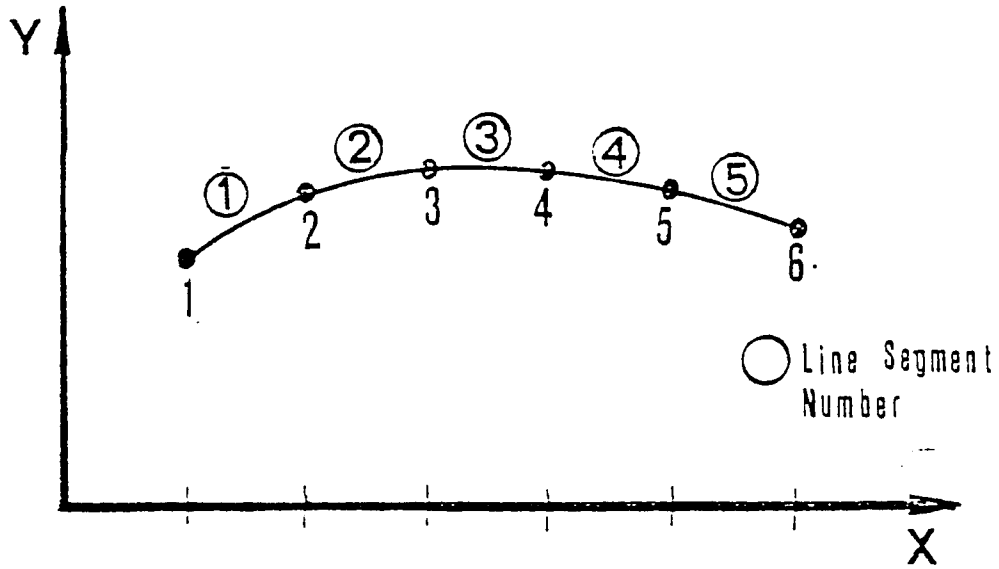

Fig. D.1. Curve represented by six interpolation points.

Table D.1. Coordinates of interpolation points.

INTERPOLATION POINT	X	Y
1	1.	2.
2	2.	3.25
3	3.	3.7
4	4.	3.8
5	5.	3.5
6	6.	3.1

APPENDIX E

DERIVATION OF K AND K'

The definition of curvature is

$$K = \frac{d\theta}{dS} \quad . \tag{E.1}$$

With reference to Fig. E.1,

$$\tan\theta = \frac{dy}{dx} \tag{E.2}$$

$$\cos\theta = \frac{dx}{dS} \quad . \tag{E.3}$$

Taking the derivative of (E.2),

$$\sec^2\theta \frac{d\theta}{dx} = \frac{d^2y}{dx^2} \quad . \tag{E.4}$$

An alternative form of (E.4) is

$$\sec^2\theta \frac{d\theta}{dS} = \frac{d^2y}{dx^2} \tag{E.5}$$

Rearranging (E.5) and substituting (E.2) gives an expression for K

$$K = \frac{y''}{(1 + y'^2)^{3/2}} \tag{E.6}$$

For the derivation of the curvature we have an expression for K'

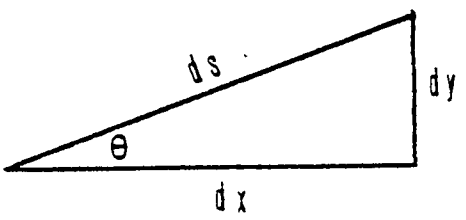

Fig. E.1. Approximate differential arc length.

$$K' = \frac{dK}{dS} = \frac{d^2\theta}{dS^2} \tag{E.7}$$

Taking the derivative of (E.5) with respect to x gives

$$y''' = 3 \sec^2\theta \sec\theta \tan\theta \frac{d}{dx}\frac{d}{dS} + \sec^2\theta \frac{d}{dx}\frac{d\theta}{dS} \quad . \tag{E.8}$$

Making use of the identities:

$$\frac{d\theta}{dx} = \frac{d\theta}{dS}\frac{dS}{dx}$$

$$\frac{dS}{dx} = \sec\theta$$

$$\frac{d}{dx}\left(\frac{d}{dS}\right) = \sec\theta \frac{d^2\theta}{dS^2}$$

and substituting them into (E.8) yields

$$y''' = 3 \sec^4\theta \tan\theta K^2 + \sec^4 \frac{d^2\theta}{dS^2} \quad . \tag{E.9}$$

An alternative form of (E.9) is

$$y''' = 3K^2 (1 + y'^2)^2 y' + (1+y'^2)^2 K' . \qquad (E.10)$$

Rearranging (E.10) gives

$$K' = \frac{(y''' - 3K^2(1+y'^2)^2 y')}{(1+y'^2)^2} \qquad (E.11)$$

APPENDIX F

CURRENT STIFFNESS PARAMETER METHOD

This is a brief explanation of the CURRENT STIFFNESS PARAMETER method developed by Bergan and Soreide (4).

At increment i there is a load step $\underset{\sim}{\Delta R}_i$ and an incremental displacement $\underset{\sim}{\Delta p}_i$. The Euclidean norm of the load step can be represented as $|| \underset{\sim}{\Delta R}_i ||$. Therefore, a normalized load vector is

$$\underset{\sim}{\Delta R}_i^{*} = \frac{\underset{\sim}{\Delta R}_i}{|| \underset{\sim}{\Delta R}_i ||} \tag{F.1}$$

and the normalized displacement vector is

$$\underset{\sim}{\Delta p}_i^{*} = \frac{\underset{\sim}{\Delta p}_i}{|| \underset{\sim}{\Delta R}_i ||} \tag{F.2}$$

With a unit of incremental load, $\underset{\sim}{\Delta R}_i^{*}$, produces $\underset{\sim}{\Delta p}_i^{*}$. The resultant work is

$$\Delta W^{*} = \underset{\sim}{\Delta p}_i^{*T} \underset{\sim}{\Delta R}_i^{*} . \tag{F.3}$$

The current stiffness parameter of the structure is measured as the reciprocal of the incremental work. This is written as

$$S_{p_i}^{*} = \frac{1}{\Delta W_i^{*}} = \frac{|| \underset{\sim}{\Delta R}_i ||}{\underset{\sim}{\Delta p}_i^{T} \underset{\sim}{\Delta R}_i} . \tag{F.4}$$

The stiffness parameter can be scaled with reference to the undeformed state.

$$S_{p_i} = \frac{\Delta p_1^T \Delta R_1}{\Delta p_i^T \Delta R_i} \frac{\|\Delta R_i\|^2}{\|\Delta R_1\|^2} \tag{F.5}$$

In this form S_p will have an initial value of one. For proportional loading

$$R = \lambda R_{REF} \tag{F.6}$$

where λ is the loading parameter.

The new form of the stiffness parameter is

$$S_{p_i} = \frac{\Delta \lambda_i}{\Delta \lambda_1} \frac{\Delta p_1^T R_{REF}}{\Delta p_i^T R_{REF}} . \tag{F.7}$$

Introducing the instantaneous stiffness, K, and using Eq. (F.5),

$$S_{p_i} = \left(\frac{\Delta \lambda_i}{\Delta \lambda_1}\right)^2 \frac{\Delta p_1^T K \Delta p_1}{\Delta p_i^T K \Delta p_i} . \tag{F.8}$$

The difference in successive stiffness parameters is represented as ΔS_{p_i}.

In its present form the change in the current stiffness parameter ($\Delta \tilde{S}_p$) should be nearly the same for all load steps. It is initially input into the program with a value between .05 and .1. The smaller the value of $\Delta \tilde{S}_p$, the smaller the load step will be. Figure F.1

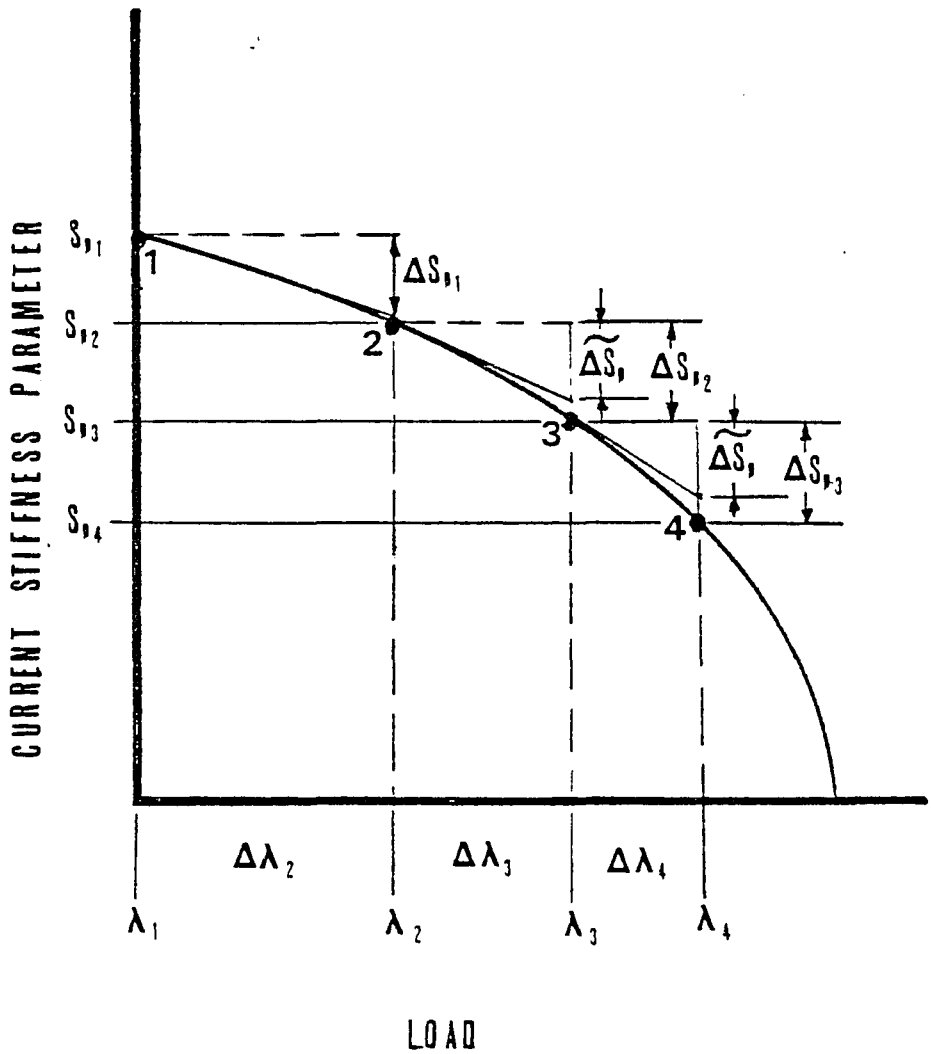

Fig. F.1. S_p vs. λ curve.

graphically represents the procedure. The various steps are listed below:

1. An initial load is prescribed, that is $\Delta\lambda_1 = R_1 - 0$. The initial displacement increment, $\underset{\sim}{\Delta p}_1$, can be calculated. From Eq. (F.8) it can be seen that $S_{p_1} = 1$.
2. For the second step another load is prescribed, that is $\Delta\lambda_2 = \Delta\lambda_1$. Using the Newton-Raphson iteration scheme, $\underset{\sim}{\Delta p}_2$ is calculated. Using Eq. (F.8), S_{p_2} is determined.
3. Extrapolating through 1 and 2, the next load increment, $\Delta\lambda_3$, is determined. This is accomplished by using the following expression:

$$\Delta\lambda_{i+1} = \Delta\lambda_i \frac{\Delta\tilde{S}_p}{|\Delta S_{p_i}|} \qquad \text{(F.8)}$$

4. Once $\Delta\lambda_3$ is known, Δp_3 and S_{p_3} can be calculated ($\Delta S_{p_2} = S_{p_3} - S_{p_2}$).
5. The process will continue until the value of S_p goes to zero or from positive to negative. The point at which S_p is equal to zero is the buckling load.

APPENDIX G

FORMULATION OF THE QUINTIC-QUINTIC INTERPOLATION FUNCTION

The independent-interpolating functions used for both the normal displacement field, U_N, and the tangential displacement field, U_t, are shown below:

$$U_N = A_1 + A_2S + A_3S^2 + A_4S^3 + A_5S^4 + A_6S^5 \quad (G.1)$$

$$U_t = A_7 + A_8S + A_9S^2 + A_{10}S^3 + A_{11}S^4 + A_{12}S^5 \quad (G.2)$$

where S (the distance along the arc length) is the independent variable.

In matrix form (G.1) and (G.2) become

$$\begin{bmatrix} U_N \\ U_t \end{bmatrix} = \left[\begin{array}{c|c|c|c|c|c|c|c|c|c|c|c} 1 & S & S^2 & S^3 & S^4 & S^5 & 0 & 0 & 0 & 0 & 0 & 0 \\ 0 & 0 & 0 & 0 & 0 & 0 & 1 & S & S^2 & S^3 & S^4 & S^5 \end{array}\right] \begin{bmatrix} A_1 \\ A_2 \\ A_3 \\ A_4 \\ A_5 \\ A_6 \\ A_7 \\ A_8 \\ A_9 \\ A_{10} \\ A_{11} \\ A_{12} \end{bmatrix}$$

or

$$\underset{\sim}{U}_{2x1} = \underset{\sim}{S}_{2x12}\ \underset{\sim}{A}_{12x1} \quad . \quad (G.3)$$

The finite element model has six degrees of freedom at each node. This is shown in Fig. G.1.

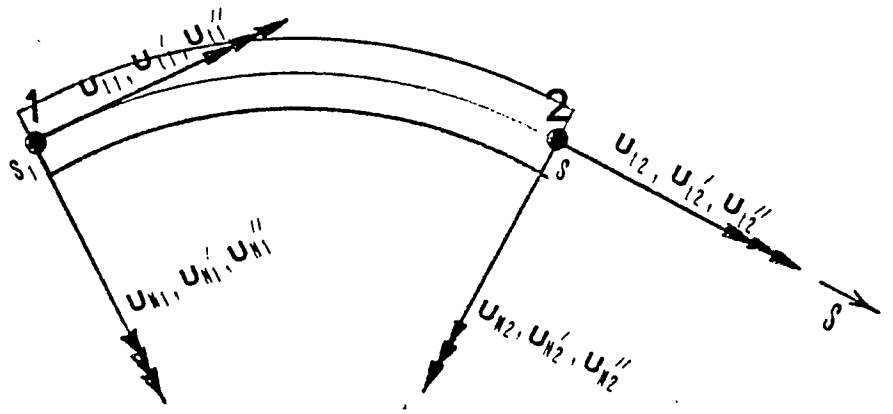

Fig. G.1. Nonlinear arch finite element.

A procedure similar to (4.6) to (4.29) must be performed such that

$$\underset{2x1}{\underset{\sim}{U}} = \underset{2x12}{\underset{\sim}{S}} \; \underset{12x12}{\underset{\sim}{B}} \; \underset{12x1}{\underset{\sim}{p}} \tag{G.4}$$

where p represents the nodal degrees of freedom and

$$\underset{12x12}{\underset{\sim}{B}} = \underset{12x12}{\underset{\sim}{C}^{-1}}$$

where

$$\underset{12\times12}{\underset{\sim}{C}} = \left[\begin{array}{c|c|c|c|c|c|c|c|c|c|c|c}
1 & s & s_1^2 & s_1^3 & s_1^4 & s_1^5 & 0 & 0 & 0 & 0 & 0 & 0 \\
0 & 1 & 2s & 3s_1^2 & 4s_1^3 & 5s_1^4 & 0 & 0 & 0 & 0 & 0 & 0 \\
0 & 0 & 2 & 6s_1 & 12s_1^2 & 20s_1^3 & 0 & 0 & 0 & 0 & 0 & 0 \\
0 & 0 & 0 & 0 & 0 & 0 & 1 & s_1 & s_1^2 & s_1^3 & s_1^4 & s_1^5 \\
0 & 0 & 0 & 0 & 0 & 0 & 0 & 1 & 2s_1 & 3s_1^2 & 4s_1^3 & 5s_1^4 \\
0 & 0 & 0 & 0 & 0 & 0 & 0 & 0 & 2 & 6s_1 & 12s_1^2 & 20s_1^3 \\
1 & s_2 & s_2^2 & s_2^3 & s_2^4 & s_2^5 & 0 & 0 & 0 & 0 & 0 & 0 \\
0 & 1 & 2s_2 & 3s_2^2 & 4s_2^3 & 5s_2^4 & 0 & 0 & 0 & 0 & 0 & 0 \\
0 & 0 & 2 & 6s_2 & 12s_2^2 & 20s_2^3 & 0 & 0 & 0 & 0 & 0 & 0 \\
0 & 0 & 0 & 0 & 0 & 0 & 1 & s_2 & s_2^2 & s_2^3 & s_2^4 & s_2^5 \\
0 & 0 & 0 & 0 & 0 & 0 & 0 & 1 & 2s_2 & 3s_2^2 & 4s_2^3 & 5s_2^4 \\
0 & 0 & 0 & 0 & 0 & 0 & 0 & 0 & 2 & 6s_2 & 12s_2^2 & 20s_2^3
\end{array}\right]$$

The strain components for this element are

$$U_N = \left[\begin{array}{c|c|c|c|c|c|c|c|c|c|c|c} 1 & s & s^2 & s^3 & s^4 & s^5 & 0 & 0 & 0 & 0 & 0 & 0 \end{array}\right] \underset{\sim}{B}\,\underset{\sim}{p} \qquad \text{(G.5)}$$

$$U_N' = \left[\begin{array}{c|c|c|c|c|c|c|c|c|c|c|c} 0 & 1 & 2s & 3s^2 & 4s^3 & 5s^4 & 0 & 0 & 0 & 0 & 0 & 0 \end{array}\right] \underset{\sim}{B}\,\underset{\sim}{p} \qquad \text{(G.6)}$$

$$U_N'' = \left[\begin{array}{c|c|c|c|c|c|c|c|c|c|c|c} 0 & 0 & 2 & 6s & 12s^2 & 20s^3 & 0 & 0 & 0 & 0 & 0 & 0 \end{array}\right] \underset{\sim}{B}\,\underset{\sim}{p} \qquad \text{(G.7)}$$

$$U_t = \left[\begin{array}{c|c|c|c|c|c|c|c|c|c|c|c} 0 & 0 & 0 & 0 & 0 & 0 & 1 & s & s^2 & s^3 & s^4 & s^5 \end{array}\right] \underset{\sim}{B}\,\underset{\sim}{p} \qquad \text{(G.8)}$$

$$U_t' = \left[\begin{array}{c|c|c|c|c|c|c|c|c|c|c|c} 0 & 0 & 0 & 0 & 0 & 0 & 0 & 1 & 2s & 3s^2 & 4s^3 & 5s^4 \end{array}\right] \underset{\sim}{B}\,\underset{\sim}{p} \qquad \text{(G.9)}$$

$$U_t'' = \left[\begin{array}{c|c|c|c|c|c|c|c|c|c|c|c} 0 & 0 & 0 & 0 & 0 & 0 & 0 & 0 & 2 & 6s & 12s^2 & 20s^3 \end{array}\right] \underset{\sim}{B}\,\underset{\sim}{p} \qquad \text{(G.10)}$$

The transformation matrix T can be written in block matrix form as

$$\underset{12\times12}{\tilde{T}} = \left[\begin{array}{c|c} \underset{6\times6}{\tilde{T}_1} & \underset{6\times6}{\tilde{0}} \\ \hline \underset{6\times6}{\tilde{0}} & \underset{6\times6}{\tilde{T}_2} \end{array}\right]$$

where

$$\underset{6\times6}{\tilde{T}_1} = \left[\begin{array}{c|c|c|c|c|c} -\sin\theta_1 & 0 & 0 & \cos\theta_1 & 0 & 0 \\ -K_1\cos\theta_1 & -\sin\theta_1 & 0 & -K_1\sin\theta_1 & \cos\theta_1 & 0 \\ K_1{}^2\sin\theta_1 & & & -K_1{}^2\cos\theta_1 & & \\ -K_1{}^1\cos\theta_1 & -2K_1\cos\theta_1 & -\sin\theta_1 & -K_1{}^1\sin\theta_1 & -2K_1\sin\theta_1 & \cos\theta_1 \\ \cos\theta_1 & 0 & 0 & \sin\theta_1 & 0 & 0 \\ -K_1\sin\theta_1 & \cos\theta_1 & 0 & K_1\cos\theta_1 & \sin\theta_1 & 0 \\ -K_1{}^2\cos\theta_1 & & & -K\ \sin\theta_1 & & \\ -K_1{}^1\sin\theta_1 & -2K_1\sin\theta_1 & \cos\theta_1 & +K_1{}^1\cos\theta_1 & 2K_1\cos\theta_1 & \sin\theta_1 \end{array}\right]$$

$$\underset{6\times6}{\tilde{T}_2} = \left[\begin{array}{c|c|c|c|c|c} -\sin\theta_2 & 0 & 0 & \cos\theta_2 & 0 & 0 \\ -K_2\cos\theta_2 & -\sin\theta_2 & 0 & -K_2\sin\theta_2 & \cos\theta_2 & 0 \\ K_2{}^2\sin\theta_2 & & & -K_2{}^2\cos\theta_2 & & \\ -K_2'\cos\theta_2 & -2K_1\cos\theta_2 & -\sin\theta_2 & -K_2'\sin\theta_2 & -2K_2\sin\theta_2 & \cos\theta_2 \\ \cos\theta_2 & 0 & 0 & \sin\theta_2 & 0 & 0 \\ -K_2\sin\theta_2 & \cos\theta_2 & 0 & K_2\cos\theta_2 & \sin\theta_2 & 0 \\ -K_2{}^2\cos\theta_2 & & & -K_2{}^2\sin\theta_2 & & \\ -K_2'\sin\theta_2 & -2K_2\sin\theta_2 & \cos\theta_2 & +K_2'\cos\theta_2 & 2K_2\cos\theta_2 & \sin\theta_2 \end{array}\right]$$

APPENDIX H

CALCULATING MOMENTS AND AXIAL FORCES AT NODAL POINTS

Qaqish (34) derived equations for the moment and axial forces at any point on the nonlinear arch. These equations are written below where M and N represent the moment and axial force respectively.

$$M = -\frac{EAZ}{K}\varepsilon_c + \frac{EAZ}{K^2}\beta' \qquad (H.1)$$

$$N = EA(1+Z)\varepsilon_c - \frac{EAZ}{K}\beta' \qquad (H.2)$$

ε_c = strain of centroidal line

A = cross sectional area

K = arch curvature

$\beta' = \frac{d\beta}{dS}$

and

$$Z = \frac{1}{A}\iint_A \frac{Z}{R - Z}\,dA \qquad (H.3)$$

where

R = the radius of curvature of the arch

Z = measured distance from the centroidal axis

These equations can be implemented to calculate the moments and axial forces at the nodal points using the

nonlinear finite element solution. With reference to Fig. H.1, the centroidal strain, ε_c, and β' at point 3 can be determined using these functions,

$$\varepsilon_{c_3} = f(U_{N_3}, U_{N_3}', U_{t_3}, U_{t_3}') \qquad (H.4)$$

$$\beta_3' = g(U_{N_3}, U_{N_3}', U_{N_3}'', U_{t_3}, U_{t_3}', U_{t_3}''). \qquad (H.5)$$

The arc measurement at point 3 on the general arch is represented as S_3.

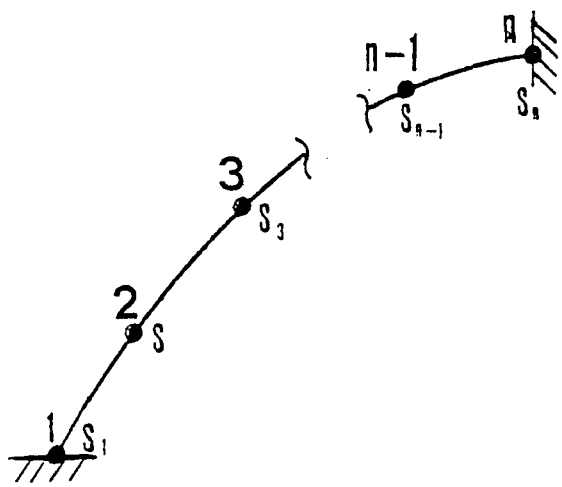

Fig. H.1. General arch with nonlinear finite elements.

To calculate the moment and axial force at point 3 the following quantities must be known or calculated,

$$U_{N_3} = \left\lfloor 1 \mid S_3 \mid S_3^2 \mid S_3^3 \mid 0 \mid 0 \mid 0 \mid 0 \right\rfloor \underset{\sim}{B}\,\underset{\sim}{p} \qquad \text{(H.6)}$$

$$U_{N_3}' = \left\lfloor 0 \mid 1 \mid 2S_3 \mid 3S_3^2 \mid 0 \mid 0 \mid 0 \mid 0 \right\rfloor \underset{\sim}{B}\,\underset{\sim}{p} \qquad \text{(H.7)}$$

$$U_{N_3}'' = \left\lfloor 0 \mid 0 \mid 2 \mid 6S_3 \mid 0 \mid 0 \mid 0 \mid 0 \right\rfloor \underset{\sim}{B}\,\underset{\sim}{p} \qquad \text{(H.8)}$$

$$U_{t_3} = \left\lfloor 0 \mid 0 \mid 0 \mid 0 \mid 1 \mid S_3 \mid S_3^2 \mid S_3^3 \right\rfloor \underset{\sim}{B}\,\underset{\sim}{p} \qquad \text{(H.9)}$$

$$U_{t_3}' = \left\lfloor 0 \mid 0 \mid 0 \mid 0 \mid 0 \mid 1 \mid 2S_3 \mid 3S_3^2 \right\rfloor \underset{\sim}{B}\,\underset{\sim}{p} \qquad \text{(H.10)}$$

$$U_{t_3}'' = \left\lfloor 0 \mid 0 \mid 0 \mid 0 \mid 0 \mid 0 \mid 2 \mid 6S_3 \right\rfloor \underset{\sim}{B}\,\underset{\sim}{p} \qquad \text{(H.11)}$$

Also A, K, Z, R, and z must all be known or calculated at point 3.

APPENDIX I

TEST ON USE OF CUBIC SPLINE INTERPOLATION FUNCTION TO REPRESENT ARCH GEOMETRY

Test

Using the equation of a circle with the radius equal to 3 units, fifteen points were generated with $\Delta x = .1$. The X and Y values represented fifteen interpolation points which were to be used as the X and Y arrays in SUBROUTINE SPLICO. The purpose of the test was to see if by using the spline Eq. (4.50) and the radius of curvature equation of (4.54), the same value of the radius could be calculated as was input as data into the equation of a circle.

Two points were tested and the results are shown in Table I.1.

Table I.1. Calculated radii at various points on a circle.

POINT	1	2
Arc Measurement S_1	.52360	1.0472
X Value	.52093	1.02528
Calculated Radius	3.0000	3.0000

LIST OF REFERENCES

1. Ashwell, D. G., and A. B. Sabir, "Limitations of Certain Curved Finite Elements when Applied to Arches," Int. J. Mech. Sci., Vol. 13, 1971, pp 133-139.

2. Bathe, K. J., and S. Boulourchi, "Large Displacement Analysis of Three-dimensional Beam Structures," Int. J. for Num. Methods in Eng., Vol. 14, 1979, pp 961-986.

3. Batoz, J. L., A Chattopadhyay, and G. Dhatt, "Finite Element Large Deflection Analysis of Shallow Shells," Int. J. of Num. Meth. Engns., Vol. 10, 1976, pp 35-38.

4. Bergan, P. G., and T. H. Soreide, "Solutions of Large Displacement and Instability Problems Using the Current Stiffness Parameter," Int. Conf. on Finite Elements in Nonlinear Solid and Structural Mechanics, Geilo, 1977.

5. Cantin, G., and R. W. Clough, "A Curved, Cylindrical-shell, Finite Element," AIAA J., Vol. 6, 1968, pp 1057-1062.

6. Connor, J. J., and N. Morin, "Perturbation Techniques in the Analysis of Nonlinear Shells," Proc. of Symp. on High Speed Computing of Elastic Structures, Liege, 1970.

7. Cook, R. D., Concepts and Applications of Finite Element Analyses, John Wiley and Sons, Inc., New York, 1974.

8. DaDeppo, D. A., "Finite Deflections of Inverted Circular Arches," Industrial Mathematics, J. Ind. Math. Soc., Vol. 19, Part 2, 1969, pp 89-109.

9. DaDeppo, D. A., and R. Schmidt, "Nonlinear Analysis of Buckling and Postbuckling Behavior of Circular Arches," Zeitschrift für angewandte Mathematik und Physik, Vol. 20, No. 6, 1969, pp 847-857.

10. DaDeppo, D. A., and R. Schmidt, "Side Sway Buckling of Deep Circular Arches under a Concentrated Load," J. App. Mech., Vol. 36, 1969, pp 325-327.

11. DaDeppo, D. A., and R. Schmidt, "Stability of an Arch under Combined Loads; Bibliography on Stability of Arches," Ind. Math., Vol. 20, Part 2, 1970, pp 71-89.

12. DaDeppo, D. A., and R. Schmidt, "Large Deflections of Eccentrically Loaded Arches," Zeitschrift für angewandte Mathematik and Physik, Vol. 21, No. 6, 1970, pp 991-1004.

13. DaDeppo, D. A., and R. Schmidt, "Analysis of Nonlinear Deflections of Fibers," Textile Research Journal, Vol. 41, No. 11, 1971, pp 911-915.

14. DaDeppo, D. A., and R. Schmidt, "Stability of Heavy Circular Arches with Hinged Ends," AIAA J., Vol. 9, No. 6, 1971, pp 1200-1201.

15. DaDeppo, D. A., and R. Schmidt, "Large Deflections and Stability of Hingeless Circular Arches under Interacting Loads," J. App. Mech., Vol. 41, No. 4, 1974, pp 989-994.

16. DaDeppo, D. A., and R. Schmidt, "Instability of Clamped-hinged Circular Arches Subjected to a Point Load," J. Eng. for Ind., Trans. ASME 1975, pp 894-896.

17. Dawe, D. J., "Curved Finite Elements for Analysis of Shallow and Deep Arches," Computers and Structures, Vol. 4, 1974, pp 559-580.

18. Dawe, D. J., "Numerical Studies Using Circular Arch Finite Elements," Computers and Structures, Vol. 4, 1974, pp 729-740.

19. Fung, Y. C., and A. Kaplan, "Buckling of Low Arches or Curved Beams of Small Curvature," NACA Technical Note Z840, 1952.

20. Fried, I., "Basic Computational Problems in the Finite Element Analysis of Shells," Int. J. Solids Struct., Vol. 7, 1971, pp 1705-1715.

21. Fried, I., "Shape Functions and the Accuracy of Arch Finite Elements," AIAA J., Vol. 11, 1973, pp. 287-291.

22. Gallagher, R. H., "Finite Element Analysis of Geometrically Nonlinear Problems," Proc. of 1973 Tokyo Seminar on Finite Element Analysis, Tokyo, 1973.

23. Gallagher, R. H., Finite Element Analysis Fundamentals, Prentice-Hall, Inc., 1975.

24. Haisler, W. E., and J. A. Stricklin, "Rigid-body Displacements of Curved Elements in the Analysis of Shells by the Matrix-displacement Method," AIAA J., Vol. 5, 1967, pp 1525-1527.

25. Huddleston, J. V., "Finite Deflection and Snap Through of High Circular Arches," J. App. Mech, Vol. 35, 1968, pp 763-769.

26. Langhaar, H. L., A. P. Boresi, and D. R. Carver, "Energy Theory of Buckling of Circular Elastic Rings and Arches," Proc. of the Second U. S. Natl. Cong. of App. Mech., 1954, pp 437-443.

27. Leontovich, Frames and Arches, McGraw-Hill, Princeton, N. J., 1971.

28. Lind, N. C., "Elastic Buckling of Symmetrical Arches," University of Illinois Engineering Experiment Station Technical Report No. 3, 1962.

29. Liu, D., "Finite Element Analysis of Arbitrary Shells," Ph. D. dissertation, The University of Arizona, Tucson, 1978.

30. Matsui, T., and O. Matsuoka, "A New Finite Element Scheme for Instability Analysis of Thin Shells," Int. J. of Num. Meth. Eng., Vol. 10, 1976, pp. 145-170.

31. Mau, S., and R. H. Gallagher, "A Finite Element Procedure for Nonlinear Prebuckling and Initial Postbuckling Analysis," NASA CR-1936, 1972.

32. Mebane, P. M., and J. A. Stricklin, "Implicit Rigid Body Motion in Curved Finite Elements," AIAA J., Vol. 9, pp. 344-345.

33. Pian, T. H., and P. Tang, "Variational Formulation of Finite Displacement Analysis," Proc. of IUTAM Sump. High Speed Computing of Elastic Struct., Liege, 1970.

34. Pennington, R. H., Introductory Computer Methods and Numerical Analysis, MacMillan Co., Toronto, 1965.

35. Qaqish, S., "Buckling Behavior of Symmetric Arches," Ph. D. dissertation, The University of Arizona, Tucson, 1977.

36. Richard, R. M., and J. R. Blacklock, "Finite Element Analysis of Inelastic Structures," AIAA Journal, Vol. 7, No. 3, 1969, pp 432-438.

37. Schmidt, W. F., "Adaptive Step Size Selection for Use of the Continuation Method," Int. J. of Num. Meth. Engng., Vol. 12, 1978, pp. 677-694.

38. Stricklin, J. A., W. E. Haisler, and W. A. Von Riesemann, "Self-correcting Initial Value Formulations in Nonlinear Structural Mechanics," AIAA J., Vol. 9, No. 10, 1971, pp 2066-2067.

39. Stricklin, J. A.,W. E. Haisler, and W. A. Von Riesemann, "Geometrically Nonlinear Structural Analyses by the Direct Stiffness Method," Trans. of ASCE, J. of Struct. Div., Vol. 97, No. ST9, 1971, pp 2299-2314.

40. Stricklin, J. A., "Self-correcting Method Using Incremental Displacements," Int. J. for Num. Meth. in Eng., Vol. 13, 1978, pp 432-439.

41. Walker, A. C., "A Nonlinear Finite Element Analysis of Shallow Circular Arches," Int. J. of Solids and Struct., Vol. 5, 1969, pp. 97-107.

42. Wempner, G. A., and N. E. Kesti, "On the Buckling of Circular Arches and Rings," Proc. of the Fourth U. S. Natl. Cong. of App. Mech., Vol. 2, 1962, pp 843-849.

43. Wempner, G. A., and G. E. Patrick, "Finite Deflections, Buckling and Postbuckling of an Arch," Proc. of the 11th Midwestern Mech. Conf., 1969, pp.439-450.

44. Wood, R. D., and O. C. Zienkiewicz, "Geometrically Nonlinear Finite Element Analysis of Beams, Frames, Arches and Axisymmetric Shells," Computers and Structures, Vol. 7, 1977, pp 725-735.

45. Yamada, Y., and Y. Ezawa, "On Curved Finite Elements for the Analysis of Circular Arches," Int. J. for Num. Meth. in Eng., Vol. 11, 1977, pp 1635-1651.

46. Yokoo, Y., T. Nakamura, and K. Uetani, "The Incremental Perturbation Method for Large Displacement Analysis of Elastic-Plastic Structure," Int. J. for Num. Meth. in Eng., Vol. 10, 1976, pp 503-525.

47. Zienkiewicz, O. C., The Finite Element in Engineering Science, 2nd Ed., McGraw-Hill, London, 1971.

48. Zienkiewicz, O. C., "Incremental Displacement in Nonlinear Analysis," Int. J.for Num. Meth. in Eng., Vol. 3, 1971, pp 587-588.